

OPTIMAL DESIGN AND DISPATCH OF HYBRID
CO-GENERATION MICROGRID SYSTEMS
WITH RESILIENCE CONSIDERATIONS

by
James C. Grymes

© Copyright by James C. Grymes, 2023

All Rights Reserved

A thesis submitted to the Faculty and the Board of Trustees of the Colorado School of Mines in partial fulfillment of the requirements for the degree of Doctor of Philosophy (Operations Research with Engineering).

Golden, Colorado

Date _____

Signed: _____

James C. Grymes

Signed: _____

Dr. Alexandra Newman
Thesis Advisor

Golden, Colorado

Date _____

Signed: _____

Dr. Alexandra Newman
Director, Operations Research with Engineering
Department of Mechanical Engineering

ABSTRACT

The decision to supplement conventional energy generation with an on-site microgrid consisting of a mix of distributed generation resources and energy storage devices is motivated by several factors, including reducing costs, increasing sustainability, and improving the resilience and reliability of an energy system. The procurement and operational costs of installing distributed generation are traditionally the impetus behind long-term decisions. While costs remain a key component, decision-makers are now interested in other benefits such as improved resilience and reliability, reduction in emissions, and public sentiment.

An open-sourced webtool, REopt[®], is a mixed-integer linear program that exists to provide users the ability to conduct parametric analysis under many scenarios. Often commercial optimization software struggles to obtain fast and reliable solutions. Therefore we develop a *Matheuristic* that yields objective function values within 5% of an exogenously produced optimal in fewer than 30 seconds for 90% of test cases compared to only 10% by a traditional optimization solver.

We then embellish REopt[®], to explore the tradeoffs between cost and resilience for a coastal wastewater treatment facility. We find that the facility can reduce life-cycle energy costs by 3.1% through the installation of a hybrid combined-heat-and-power, photovoltaic, and storage system. Furthermore, when paired with existing diesel generators, this system can sustain full load for seven days while saving \$664,000 over 25 years and reducing diesel fuel use by 48% compared to the diesel-only solution.

Finally, we extend the concepts of the first two works by incorporating emerging technologies (fuel cells) into a distributed generation multi-objective model that simultaneously minimizes costs while ensuring a communities' critical load is satisfied during a utility service disruption. This extension requires the incorporation of challenging non-linear constraints that inhibit state-of-the-art optimization software from finding solutions within 15%, on average, after two hours for realistic instances encompassing five technologies and a year-long time horizon at hourly fidelity. We devise a multi-stage methodology resulting in, on average, an 8% decrease in objective function value. Additionally, solutions obtained using our methodology result in fuel cell

utilization three times more often than solutions obtained with commercial solvers.

TABLE OF CONTENTS

ABSTRACT	iii
LIST OF FIGURES	x
LIST OF TABLES	xiii
LIST OF ABBREVIATIONS	xv
ACKNOWLEDGMENTS	xvi
CHAPTER 1 INTRODUCTION	1
1.1 Sets and Parameters	4
1.2 Variables	7
1.3 Objective Function	9
1.4 Constraints	10
1.4.1 Fuel Consumption	10
1.4.2 Thermal Production	10
1.4.3 Storage System	11
1.4.4 Production	13
1.4.5 Production Incentives	13
1.4.6 Power Rating	13
1.4.7 Load Balancing and Grid Sales	14
1.4.8 Rate Tariff Constraints	15
1.4.9 Minimum Utility Charge	17
1.4.10 Non-negativity	17
1.4.11 Integrality	18

CHAPTER 2	A MATHEURISTIC FOR DESIGN AND DISPATCH OF A UTILITY-CONNECTED DISTRIBUTED ENERGY SYSTEM	19
2.1	Abstract	19
2.2	Introduction	19
2.2.1	Motivation	20
2.2.2	Literature Review	21
2.3	Modeling the System	24
2.3.1	Model Overview	24
2.3.2	Model Contribution to Solution Latency	26
2.3.2.1	Design and Dispatch	27
2.3.2.2	Binary Variables for CHP Scheduling	27
2.3.2.3	Peak Demand Charges and Battery Energy Storage Systems	28
2.4	Method	29
2.4.1	A Genetic Algorithm for Candidate Design Selection	29
2.4.2	Energy Dispatch	34
2.4.2.1	CHP Scheduling	35
2.4.2.2	Economic Dispatch	38
2.5	Results	43
2.5.1	Inputs	43
2.5.2	Genetic Algorithm	44
2.5.3	Solution Quality	45
2.6	Conclusion	51
2.7	Acknowledgements	52
CHAPTER 3	NORTH CAROLINA WATER UTILITY BUILDS RESILIENCE WITH DISTRIBUTED ENERGY RESOURCES	53

3.1	Abstract	53
3.2	Introduction	53
3.3	Literature Review	56
3.4	Site Description	58
3.5	Methodology	60
3.5.1	Resilience Modifications	63
3.5.2	Utility Rate Tariff Modifications	64
3.5.3	Scenarios	65
3.6	Results	66
3.7	Conclusion	71
3.8	Acknowledgements	72
CHAPTER 4 OPTIMIZING MICROGRID DEPLOYMENT FOR COMMUNITY RESILIENCE		73
4.1	Abstract	73
4.2	Introduction and Background	73
4.3	Literature Review	77
4.4	Modeling the Energy System	80
4.4.1	Mathematical Formulation	81
4.4.2	Discussion of Formulation	85
4.4.2.1	Objective function	85
4.4.2.2	Load Balancing	86
4.4.2.3	Utility Operations	87
4.4.2.4	Power Capacity	87
4.4.2.5	Electrical Efficiency	87
4.4.2.6	Fuel Consumption	87

4.4.2.7	Start-up	88
4.4.2.8	Power Storage	88
4.4.2.9	Heat Capacity	88
4.4.2.10	Heat Storage	89
4.5	Solution Methodology	89
4.5.1	Linear Reformulation (Phase 1)	91
4.5.2	Transform Solution (Phase 2)	94
4.5.3	Return of the Original Formulation (P^0) (Phase 3)	96
4.6	Inputs and Results	97
4.6.1	General Inputs	97
4.6.2	Solid Oxide Fuel Cell Inputs	100
4.6.3	Model Inputs from Solution-Expediting Methodologies	101
4.6.4	Solution Quality	102
4.6.5	Solution Implications	103
4.7	Conclusion	107
4.8	Acknowledgments	107
CHAPTER 5 CONCLUSION		108
REFERENCES		110
APPENDIX A CHAPTER 2		124
A.1	Dynamic Programming Formulation and Algorithm	124
APPENDIX B CHAPTER 3		127
B.1	Technical and Economic Parameters	127
B.2	Utility Rate	129
B.3	Pricing	130

B.4 Renewable Energy Resource	131
B.5 Model Performance	132
APPENDIX C CHAPTER 4	134
C.1 Disaster Cost Components	134
C.2 Taxonomy Feeders	135
C.3 Additional Solid Oxide Fuel Cell Costs	136
APPENDIX D COPYRIGHT AND PERMISSIONS	139

LIST OF FIGURES

Figure 2.1	An example of a utility-connected microgrid showing design (yellow) and dispatch (blue arrows) components.	21
Figure 2.2	A categorical overview of the decision variables, objective function, and constraints that comprise the REopt [®] optimization model, (\mathcal{P}), where SOC denotes state of charge	25
Figure 2.3	An example of a 24-hour load profile with unmanaged demand peaks.	28
Figure 2.4	Heuristic methodology (M^H), including parallelization of dispatch subroutine. n : Number of parallel processes; CO_k : CHP operations for process k ; LP_k : Linear program for remaining dispatch for process k ; F_k : Feasibility step for process k	30
Figure 2.5	Genetic algorithm mutation example	32
Figure 2.6	REopt [®] System and Dependencies. Green, orange, and blue arrows represent electrical, hot-thermal, and cold-thermal flows, respectively.	34
Figure 2.7	Genetic algorithm progress for which x is the wall-clock elapsed time, $G(c; x) = \frac{L_{cx} - L_c}{L_{cx}}$, L_x is the objective function value associated with the best-found design for case c at time x , and L_c is the lowest overall objective function value found by (M^H) for case c	45
Figure 2.8	Performance plot comparison of objective function values returned by (M^H) and (M^O), measuring the proportion of cases ($p_m^g(x)$) using method m that are below the optimality threshold x after two minutes using method m	46
Figure 2.9	Performance plot comparison of solutions returned by (M^H) and (M^O), measuring the proportion of cases ($p_m^s(x)$) using method m that are below 5% optimality gap after x seconds using method m	47
Figure 2.10	Microgrid configuration comparison of all 12 cases. Radial length reflects the installed capacity of the technology.	50
Figure 3.1	2019 Northside wastewater treatment plant electric demand	59
Figure 3.2	2019 Northside wastewater treatment plant biogas production and use	59
Figure 3.3	Northside wastewater treatment plan anaerobic digestion system. Source: CFPUA	60

Figure 3.4	The REopt Lite model inputs include renewable energy, combined heat and power, and energy storage technology options (in red), and loads, utility costs, and technology costs (in blue). Outputs (in green) encompass recommended technology sizes, operations strategy, and project economics.	61
Figure 3.5	If load can be reduced during the outage by storing and deferring wastewater treatment, required system sizes and costs decrease	68
Figure 3.6	Peak loads are shed to reduce the required combined-heat-and-power and generator sizes, resulting in reduced life cycle cost, for the <i>All Technologies</i> seven-day outage case.	69
Figure 3.7	A hybrid combined-heat-and-power system in the <i>All Technologies</i> seven-day outage case reduces diesel consumption by 50% relative to the <i>Business-as-Usual</i> scenario when meeting the full load. Diesel consumption can be further reduced in the <i>Business-as-Usual</i> , <i>CHP Only</i> , and <i>All Technologies</i> scenarios by shedding load.	70
Figure 4.1	Climate-related disaster costs	74
Figure 4.2	Power outages in 2020	75
Figure 4.3	A representative microgrid and energy system.	77
Figure 4.4	Distributed Energy System modified from Pruitt et al.	80
Figure 4.5	Three-phase methodology to generate feasible solutions to (P^d) with improved solutions and optimality gaps.	91
Figure 4.6	Comparison of piece-wise linear and non-linear fuel consumption of a representative solid oxide fuel cell with two segments.	92
Figure 4.7	R1-12.47-2 Taxonomy Feeder. Magenta represents the slack bus (the power source of the distribution network), while dark red depicts the loads that require power. Green links are transformers; orange links are switches; and gray links and nodes are triplex lines and connections, respectively.	98
Figure 4.8	Example load profile	99
Figure 4.9	Hot thermal load profile derived from the EnergyPlus [®] simulation software, representing a collection of building types, including a hospital, hotel, apartment, large office, and supermarket.	99
Figure 4.10	Estimated electricity production of a grid-connected roof- or ground-mounted photovoltaic system installed in Richmond, CA. The arrow shows the approximate timeframe of the modeled utility service disruption.	100

Figure 4.11	Improvement from bound-tightening procedure for the auxiliary, bi-linear variable \hat{X}_{j_t} X_t^\dagger reduces the magnitude between the upper and lower bound by 57%, as an example.	102
Figure 4.12	Power output by technology type from a combination of microgrid and utility. Dashed lines show the start and end of the utility service disruption.	106
Figure A.1	An illustrative example of the discretized state of charge and associated possible moves from hour h to hour $h + 1$	126
Figure B.1	Real-time price for 2019	130
Figure B.2	Northside wastewater treatment plant solar production factor for a representative year.	131
Figure C.1	Levelized Cost of Energy for Solid Oxide Fuel Cells	138

LIST OF TABLES

Table 2.1	A selection of notation from model (P)	26
Table 2.2	Notation used for the Genetic Algorithm.	31
Table 2.3	Additional notation for CHP scheduling.	36
Table 2.5	Salient features of the 12 cases.	44
Table 2.6	Solving (P) using (M^O) and (M^H) after a two-minute time limit. Microgrid capacity is the sum of that generated by all technologies, including the power rating of the electrical storage system.	48
Table 3.1	System Sizes and Economics for No-Outage Case	67
Table 3.2	System Sizes and Economics for Seven-Day Outage Case	67
Table 4.1	Type and quantity of non-linear terms in the constraint set and how they are modified after performing standard linearization techniques . †: The case of the product of a continuous and an <i>integer</i> (vice binary) variable requires additional model elements for its linearization, and testing yields unfavorable results.	90
Table 4.2	Size of (P^b) in terms of set cardinality.	90
Table 4.3	Constraint numbers with associated quantities required to transform (P^b) into (P^c). The constraints in each of the rows corresponding to a particular model are mutually exclusive.	94
Table 4.4	Technology input values (not including solid oxide fuel cells). The lithium-ion battery has a two-hour power rating.	97
Table 4.5	Values used for power-only and combined-heat-and-power solid oxide fuel cells.	101
Table 4.6	Average size and structure of models (P^b) and (P^c). The (P^c) column shows the percent increase or decrease in size relative to (P^b).	102
Table 4.7	Comparison of solutions solving (P^b) with and without the solution obtained from (P^c). Objective function values and optimality gap after two hours of run time, and time until the first feasible solution is obtained. Δ : Reduction between methods (M^b) and (M^c)	103
Table 4.8	Solution comparison between purchasing all electricity from the utility versus installing a microgrid that is capable of meeting a 48-hour outage occurring during the highest electrical demand period.	104

Table 4.9	Percent of total power consumed during the year by each type of installed technology in the microgrid. No solution includes the diesel generator. CHP: combined heat and power; SOFC: solid oxide fuel cell; PV: photovoltaics	105
Table B.1	Combined-Heat-and-Power Parameters	127
Table B.2	Photovoltaic Parameters	127
Table B.3	Storage Parameters	128
Table B.4	System-wide General Economic Parameters	128
Table B.5	Duke Energy Progress Large General Service Real Time Pricing Rate	129
Table B.6	Solver Settings	133
Table B.7	Average Solve Times in Seconds	133
Table C.1	Summary of distribution feeders used to create electrical load profile. Data obtained from the Open Energy Data Initiative https://openenergydata.org/datasets/files/968/pub/individual_files/ and sourced from work by Schneider et al.	135
Table C.2	Projected costs of solid oxide fuel cells.	137

LIST OF ABBREVIATIONS

Colorado School of Mines	CSM
Combined Heat and Power	CHP
Department of Energy	DoE
Distributed Energy Resources	DER
National Renewable Energy Lab	NREL
Photovoltaic	PV
Renewable Energy Integration and Optimization	REopt

ACKNOWLEDGMENTS

I would like to express my deepest gratitude to my esteemed advisor, Professor Alexandra Newman, for her guidance, support, and invaluable mentorship throughout my doctoral journey. Without her expertise, dedication, and belief in my potential, this accomplishment would not have been possible. Professor Newman, your profound knowledge in the optimization field has been an endless source of inspiration for me. Your passion for research, commitment to excellence, and meticulous attention to detail have shaped me into a more critical thinker and a better researcher. Your unwavering enthusiasm and ability to challenge my ideas and push me beyond my comfort zone have significantly contributed to the growth of my academic and professional abilities. I am truly grateful for the countless hours you have invested in providing constructive feedback on my work, helping me refine my research questions, and offering invaluable insights into the complexities of the field. Your ability to ask probing questions and offer alternative perspectives has broadened my understanding and has been instrumental in shaping the direction of my research.

I am also indebted to you for creating a nurturing and collaborative environment within our research group. The opportunities to engage in stimulating discussions, attend conferences, and collaborate on projects have been invaluable experiences that have enriched my academic journey. Your commitment to fostering a supportive and inclusive community has created an environment where ideas flourish, and I have grown intellectually and personally.

I would also like to extend my appreciation to the members of my dissertation committee for their valuable input, constructive criticism, and guidance throughout the various stages of my research. Their expertise and diverse perspectives have been instrumental in shaping the trajectory of my work.

Additionally, I would like to acknowledge the support and encouragement I received from my colleagues and fellow researchers in the department. The exchange of ideas, collaborations, and shared experiences have enriched my understanding of the field and have made this journey all the more rewarding. I honestly could not have done it without you. Specifically, I am immensely grateful for the countless hours Dr. Alexander Zolan dedicated to mentoring and advising me.

Your patience, encouragement, and willingness to share your wisdom have ushered me through the various stages of my research. Your guidance in refining research questions and analyzing results has been invaluable in shaping the direction and outcomes of my work.

Last but certainly not least, I would like to express my heartfelt gratitude to my family and friends for their unwavering support, understanding, and love. Their encouragement, patience, and belief in my abilities have been my strength throughout this challenging yet fulfilling endeavor.

To my loving wife Paige, and our cherished children Jackson, Hudson, and Pierson. Your unwavering support, understanding, and encouragement have been the foundation for this journey. Your love has been my greatest inspiration, and your belief in me has propelled me forward, even during the most challenging moments. Paige, you have been my rock throughout this entire process. Your boundless patience, understanding, and empathy have sustained me during the long hours and countless late nights. Your constant encouragement, whether through a warm embrace or a simple word of reassurance, has given me the strength to overcome any obstacles that crossed my path. Your unwavering faith in my abilities has been the driving force behind my success. I am forever grateful to have you by my side.

Jackson, Hudson, and Pierson, you are the light of my life. Your smiles, laughter, and playful energy, have filled my heart with immeasurable joy. You have taught me the true meaning of perseverance, as I have witnessed your determination and curiosity in everything you do. Your innocence and love have reminded me of what truly matters in life, motivating me to push through the challenges and strive for excellence. Each of you holds a special place in my heart, and I am immensely proud to be your parent.

To my beautiful family, thank you for your sacrifices and understanding during the countless hours I spent immersed in research and writing. Your willingness to adapt to the demanding schedule and your ability to create a nurturing and loving home environment amidst the chaos has been nothing short of extraordinary. I am honored to have you as my family, and I am grateful for the love and support you have shown me every step of the way.

To all those who have supported me on this academic odyssey, I extend my deepest appreciation. Your guidance, mentorship, and encouragement have left an indelible mark on my professional and personal growth. I am honored and privileged to have had the opportunity to

work with you, and I am forever grateful for your contributions to my journey.

CHAPTER 1

INTRODUCTION

Effectively deploying sustainable and alternative energy sources is becoming more feasible and prevalent. Furthermore, the interest to acquire and operate the corresponding systems at minimal cost is a primary focus for a diverse set of decision-makers. This interest is motivated by several factors, including reducing costs, increasing sustainability, and improving the resilience and reliability of an energy system, and is prompted by many factors, including increasing energy dependence and climate-related natural disasters that contribute to or cause energy service disruptions.

The societal shift from analog to digital technologies in almost every arena has led to the energy system becoming a single point of failure. Communities rely on several critical services and, in almost all instances, depend on readily available electric and thermal energy. Communities across the United States and worldwide have experienced increased widespread natural disaster-related energy disruptions, degrading or eliminating these critical services [4]. Additionally, climate change considerations require a more concerted investigation of non-traditional types of energy generation to limit their impact on the future. The increased frequency of energy system outages due to an array of natural disasters is not a novel consideration by the research community; however, the over-dependency on electricity requires immediate solutions [5, 6].

An important qualification of an energy system is its resilience, defined as how quickly a system can restore its function after a disturbance [7]. Resilience in an energy system is necessary to ensure critical functions of society are minimally impacted in the case of a disaster-induced utility disruption. Traditional methods for reducing the impact of these outages require on-site backup power, such as a diesel-powered generator. While backup generators are practical solutions, they have several drawbacks. Traditional backup power generation typically requires either a large storage tank for fuel and means for resupply if necessary or access to a fuel pipeline that has not been compromised. Natural disasters often result in supply chain failures and infrastructure damage, limiting or eliminating access to the necessary fuel source. Additionally,

traditional backup power generators require routine maintenance, which is costly and often overlooked, leading to failures during outages. Power companies frequently levy restrictions that preclude the operation of these systems during non-outage times and, therefore, they often sit idle. Lastly, these fossil fuel-burning systems contribute higher amounts of undesired emissions per unit of energy output.

This work intends to address the gap between modeling microgrids for a single outcome, such as economic improvements or emissions reductions, and improving the overall resilience of an energy system. A multi-objective approach can inform decision-makers of possible solutions using a Pareto frontier that balances economics and resilience. Techno-economic microgrid optimization models assist in exploring energy-sourcing alternatives and informing long-term courses of action. However, these models rarely examine the additional benefits that accompany on-site systems. This work utilizes and modifies these models to investigate alternative energy sources while considering cost, baseline requirements, and disaster-related disruptions.

The first two chapters of this work begin with a pre-established model, Renewable Energy Integration and Optimization (REopt[®]), that originated at the National Renewable Energy Lab (NREL) and was documented by Anderson et al. [8] and re-formulated by Hirwa et al. [9]. We present the full model in below and discuss solution strategies and modifications in Chapters 2 and 3, respectively. REopt[®] is a large mixed integer linear program with hundreds of thousands of variables and constraints. The model often requires significant time to generate “good” solutions, which is problematic for the end user. The contributions of the dissertation writer to Chapter 3 include optimization modeling efforts, utility tariff inputs, outputs, and analysis of results.

Chapter 2 designs a *Matheuristic* for REopt[®] that returns a solution within 5% of optimality in fewer than two minutes for our test cases. The heuristic output can then be implemented directly or used as starting point in an optimizer. Our tool allows the practitioner to incorporate into REopt[®] more complicated system components, such as incorporating technologies, non-linearities, and multi-objectives with few capitulations. We then modify REopt[®] in Chapter 3 to analyze the resilience and cost benefits of an on-site distributed energy microgrid for a coastal wastewater treatment plant.

We extend this body of work in Chapter 4 to generalize the concepts explored in Chapters 2 and 3. We incorporate more complex technologies into our optimization model while producing good, feasible solutions. This affords the community with the ability to extend current models beyond simple applications. Specifically, we seek to combine the salient features of Chapter 3 with previous work by Pruitt et al. [2] who model the non-linearities of solid oxide fuel cells in a hybrid microgrid. Our work adds resilience to a specific site; the work in this dissertation, instead, generalizes resilience to communities by connecting to loads through the distribution network. The optimization model is a mixed-integer non-linear program that fails to achieve better than a 15% optimality gap after a multi-day time limit for our tested cases. We create a three-phase methodology and model modifications to induce feasible solutions. Our procedure results in 8% improvement, on average, in the objective function value and over a 50% improvement in the optimality gap after a two-hour solve time limit. Additionally, our method leverages the available co-generational fuel cells by providing approximately 58% of demanded annual power, a 100% increase over solutions returned by traditional methods.

Here, we introduce the monolith mixed-integer linear programming formulation of their design and dispatch problem from Ogunmodede et al. [10] and Hirwa et al. [9]. Specifically, the model we present here introduces combined heat and power into the system. We define, in alphabetic order within a group, indices and sets, parameters, and variables, in that order, and then state the objective function and the constraints. We choose as our naming convention calligraphic capital letters to represent sets, lower-case letters to represent parameters, and upper-case letters to represent variables; in the latter case, Z -variables are binary. X -variables represent continuous decisions, e.g., quantities of energy. All subscripts denote indices. Names with the same “stem” are related, and superscripts and “decorations” (e.g., hats, tildes) differentiate the names with respect to, e.g., various indices included in the name or maximum and minimum values for the same parameter.

1.1 Sets and Parameters

Sets

B	Storage systems
C	Technology classes
D	Time-of-use demand periods
E	Electrical time-of-use demand tiers
F	Fuel types
H	Time steps
K	Subdivisions of power rating
M	Months of the year
N	Monthly peak demand tiers
S	Power rating segments
T	Technologies
U	Total electrical energy pricing tiers
V	Net metering regimes

Subsets and Indexed Sets

B^c	B^{th}	Cold thermal energy storage systems
B^e	B	Electrical storage systems
B^h	B^{th}	Hot thermal energy storage systems
B^{th}	B	Thermal energy storage systems
H^g	H	Time steps in which grid purchasing is available
H_m	H	Time steps within a given month m
H_d	H	Time steps within electrical power time-of-use demand tier d
K_t	K	Subdivisions applied to technology t
K^c	K	Capital cost subdivisions
M^{lb}		Look-back months considered for peak pricing
S_{tk}	S	Power rating segments from subdivision k applied to technology t
T_b	T	Technologies that can charge storage system b
T_c	T	Technologies in class c
T_f	T	Technologies that burn fuel type f
T_u	T	Technologies that may access electrical energy sales pricing tier u
T_v	T	Technologies that may access net-metering regime v
T^{ac}	T^{cl}	Absorption chillers
T^{CHP}	T^{f}	CHP technologies
T^{cl}	T	Cooling technologies
T^e	T	Electricity-producing technologies
T^{ec}	T^{cl}	Electric chillers
T^{f}	T^e	Fuel-burning, electricity-producing technologies
T^{ht}	T	Heating technologies

T^{td}	T	Technologies that cannot turn down, i.e., PV and wind
U^c	U^s	Electrical energy curtailment pricing tiers
U^{nm}	U^s	Electrical energy sales pricing tiers used in net metering
U^p	U	Electrical energy purchase pricing tiers
U^s	U	Electrical energy sales pricing tiers
U_t^s	U^s	Electrical energy sales pricing tiers accessible by technology t
U^{sb}	U^s	Electrical energy sales pricing tiers accessible by storage

Scaling Parameters

Γ	Number of time periods within a day	[-]
Δ	Time step scaling	[h]
Θ	Peak load oversizing factor	[-]
M	Sufficiently large number	[various]

Parameters for Costs and their Functional Forms

c^{afc}	Utility annual fixed charge	[\$]
c^{amc}	Utility annual minimum charge	[\$]
c_{ts}^{cb}	y -intercept of capital cost curve for technology t in segment s	[\$]
c_{ts}^{cm}	Slope of capital cost curve for technology t in segment s	[\$/kW]
c_{uh}^e	Export rate for energy in energy demand tier u in time step h	[\$/kWh]
c_{uh}^g	Grid energy cost in energy demand tier u during time step h	[\$/kWh]
c_b^{kW}	Capital cost of power capacity for storage system b	[\$/kW]
c_b^{kWh}	Capital cost of energy capacity for storage system b	[\$/kWh]
c_b^{omb}	Operation and maintenance cost of storage system b per unit of energy rating	[\$/kWh]
c_t^{omp}	Operation and maintenance cost of technology t per unit of production	[\$/kWh]
c_t^{om}	Operation and maintenance cost of technology t per unit of power rating, including standby charges	[\$/kW]
c_{de}^r	Cost per unit peak demand in time-of-use demand period d and tier e	[\$/kW]
c_{mn}^{rm}	Cost per unit peak demand in tier n during month m	[\$/kW]
c_f^u	Unit cost of fuel type f	[\$/MMBTU]

Demand Parameters

c_h	Cooling load in time step h	[kW]
d_h	Electrical load in time step h	[kW]
gs_u	Maximum allowable sales in electrical energy demand tier u	[kWh]
h	Heating load in time step h	[kW]
lp	Look-back proportion for ratchet charges	[fraction]
mt_n	Maximum monthly electrical power demand in peak pricing tier n	[kW]
t_e	Maximum power demand in time-of-use demand tier e	[kW]
tu_u	Maximum monthly electrical energy demand in tier u	[kWh]

Incentive Parameters

ζ_t	Upper incentive limit for technology t	[\$]
i_v^n	Net metering limits in net metering regime v	[kW]
i_t^r	Incentive rate for technology t	[\$/kWh]
ζ_t	Maximum power rating for obtaining production incentive for technology t	[kW]

Technology-Specific Time-Series Factor Parameters

f_{th}^{ed}	Electrical power de-rate factor of technology t at time step h	[unitless]
f_{th}^{fa}	Fuel burn ambient correction factor of technology t at time step h	[unitless]
f_{th}^{ha}	Hot water ambient correction factor of technology t at time step h	[unitless]
f_{th}^{ht}	Hot water thermal grade correction factor of technology t at time step h	[unitless]
f_{th}^p	Production factor of technology t during time step h	[unitless]

Technology-Specific Factor Parameters

f_t^d	Derate factor for turbine technology t	[unitless]
f_t^l	Levelization factor of technology t	[fraction]
f_t^{li}	Levelization factor of production incentive for technology t	[fraction]
f_t^{pf}	Present worth factor for fuel for technology t	[unitless]
f_t^{pi}	Present worth factor for incentives for technology t	[unitless]
f_t^{td}	Minimum turn down for technology t	[unitless]

Generic Factor Parameters

f^e	Energy present worth factor	[unitless]
f^{om}	Operations and maintenance present worth factor	[unitless]
f^{tot}	Tax rate factor for off-taker	[fraction]

f^{tow}	Tax rate factor for owner	[fraction]
------------------	---------------------------	------------

Power Rating and Fuel Limit Parameters

b_f^a	Amount of available fuel for fuel type f	[MMBTU]
\underline{b}_c	Minimum power rating for technology class c	[kW]
\bar{b}_t	Maximum power rating for technology t	[kW]
\underline{b}_{tkS}^s	Minimum power rating for technology t , subdivision k , segment s	[kW]
\bar{b}_{tkS}^s	Maximum power rating for technology t , subdivision k , segment s	[kW]

Efficiency Parameters

bt^+	Efficiency of charging storage system b using technology t	[fraction]
b^-	Efficiency of discharging storage system b	[fraction]
ac	Absorption chiller efficiency	[fraction]
b	Boiler efficiency	[fraction]
ec	Electric chiller efficiency	[fraction]
g^+	Efficiency of charging electrical storage using grid power	[fraction]

Storage Parameters

\bar{w}_b^{bKW}	Maximum power output of storage system b	[kW]
$\underline{w}_b^{\text{bKW}}$	Minimum power output of storage system b	[kW]
\bar{w}_b^{bKWh}	Maximum energy capacity of storage system b	[kWh]
$\underline{w}_b^{\text{bKWh}}$	Minimum energy capacity of storage system b	[kWh]
w_b^d	Decay rate of storage system b	[1/h]
$\underline{w}_b^{\text{mcp}}$	Minimum percent state of charge of storage system b	[fraction]
w_b^0	Initial percent state of charge of storage system b	[fraction]

Fuel Burn Parameters

m_t^{tp}	y -intercept of the fuel rate curve for technology t	[MMBTU/h]
m_t^{fbm}	Fuel burn rate y -intercept per unit size for technology t	[MMBTU/kWh]
m_t^{fm}	Slope of the fuel rate curve for technology t	[MMBTU/kWh]

CHP Thermal Performance Parameters

k_t^{te}	Thermal energy production of CHP technology t per unit electrical output	[unitless]
k_t^{tp}	Thermal power production of CHP technology t per unit power rating	[unitless]

1.2 Variables

Boundary Conditions

$X_{b,0}^{se}$	Initial state of charge for storage system b	[kWh]
----------------	--	-------

Continuous Variables

X_b^{kW}	Power rating for storage system b	[kW]
X_b^{kWh}	Energy rating for storage system b	[kWh]
X_{de}^{de}	Peak electrical power demand allocated to tier e and time-of-use demand period d	[kW]
X_{bh}^{dfs}	Power discharged from storage system b during time step h	[kW]
X_{mn}^{dn}	Peak electrical power demand allocated to tier n during month m	[kW]
X^{fth}	Fuel burned by technology t in time step h	[MMBTU/h]
X_{th}^{fb}	y -intercept of fuel burned by technology t in time step h	[MMBTU/h]
X_{uh}^g	Power purchased from the grid for electrical load in demand tier u	
	during time step h	[kW]
X_h^{gts}	Electrical power delivered to storage by the grid in time step h	[kW]
X^{mc}	Annual utility minimum charge adder	[\$]
X_t^{pi}	Production incentive collected for technology t	[\$]
X^{plb}	Peak electrical demand during look back periods	[kW]
X_{tuh}^{ptg}	Exports from production to the grid by technology t in demand tier u	
	during time step h	[kW]
X_{bth}^{pts}	Power from technology t used to charge storage system b during time step h	[kW]
X_{th}^{ptw}	Thermal power from technology t sent to waste or curtailed during time step h	[kW]
X_{th}^{rp}	Rated production of technology t during time step h	[kW]
X_t	Power rating of technology t	[kW]
X_{tks}^s	Power rating of technology t allocated to subdivision k , segment s	[kW]
X_{bh}^{se}	State of charge of storage system b at the end of time step h	[kWh]
X_{uh}^{stg}	Exports from storage to the grid in demand tier u during time step h	[kW]
X_{th}^{tp}	Thermal production of technology t in time step h	[kW]
X_{th}^{tpb}	y -intercept of thermal production of CHP technology t in time step h	[kW]

Binary Variables

Z_{mn}^{dmt}	1 If tier n has allocated demand during month m ; 0 otherwise	[unitless]
Z_{de}^{dt}	1 if tier e has allocated demand during time-of-use period d ; 0 otherwise	[unitless]
Z_v^{nmil}	1 If generation is in net metering interconnect limit regime v ; 0 otherwise	[unitless]

Z_t^{pi}	1 If production incentive is available for technology t ; 0 otherwise	[unitless]
Z_{tks}^s	1 If technology t in subdivision k , segment s is chosen; 0 otherwise	[unitless]
Z_{th}^{to}	1 If technology t is operating in time step h ; 0 otherwise	[unitless]
Z_{mu}^{ut}	1 If demand tier u is active in month m ; 0 otherwise	[unitless]

1.3 Objective Function

$$\begin{aligned}
(\mathcal{R}) \text{ minimize } & \times c_{ts}^{cm} X_{tks}^s + c_{ts}^{cb} Z_{tks}^s + \\
& \left| \frac{t2T;k2K^c;s2S_{tk}}{\text{Generating Technology Capital Costs}} \{Z\} \right. \\
& \times c_b^{kW} X_b^{bKW} + (c_b^{kWh} + c_b^{omb}) X_b^{bKWh} + \\
& \left. \left| \frac{t2B}{\text{Storage Capital Costs}} \{Z\} \right. \right. \\
(1 \ f^{tow}) \ f^{om} & \times c_t^{om} X_t + \times c_t^{omp} X_{th}^{rp} + \\
& \left| \frac{t2T}{\text{Fixed O\&M Costs}} \{Z\} \right. \left| \frac{t2T^f;h2H}{\text{Variable O\&M Costs}} \{Z\} \right. \\
(1 \ f^{tot}) \ \Delta & \times c_f^u \times f_t^{pf} X_{th}^f + \\
& \left| \frac{f2F}{\text{Fuel Charges}} \frac{t2T^f;h2H}{\{Z\}} \right. \\
(1 \ f^{tot}) \ f^e & \Delta \times c_{uh}^g X_{uh}^g + \\
& \left| \frac{u2U^p;h2H^g}{\text{Grid Energy Charges}} \{Z\} \right. \\
& \times c_{de}^r X_{de}^{de} + \times c_{mn}^{rm} X_{mn}^{dn} + \\
& \left| \frac{d2D;e2E}{\text{Time-of-Use Demand Charges}} \{Z\} \right. \left| \frac{m2M;n2N}{\text{Monthly Demand Charges}} \{Z\} \right. \\
& \left. \left| \frac{afc}{\text{Fixed Charges}} \{Z\} \right. \right. \\
\Delta & \times \times c_{uh}^e X_{uh}^{stg} + \times c_{uh}^e X_{tuh}^{ptg} \\
& \left| \frac{h2H^g}{\text{Energy Export Payment}} \frac{u2U^{sb}}{\{Z\}} \frac{t2T;u2U_t^s}{\{Z\}} \right. \\
& (1 \ f^{tow}) \times X_t^{pi} \\
& \left| \frac{t2T}{\text{Production Incentives}} \{Z\} \right.
\end{aligned}$$

The objective function is the same as that in (\mathcal{R}) and minimizes energy life cycle cost, i.e., capital costs, O&M costs, and utility costs; it maximizes (by subtracting) payments for energy exports

and other incentives.

1.4 Constraints

1.4.1 Fuel Consumption

$$\Delta \sum_{t \in T} \sum_{h \in H} X_{th}^f \leq b_f^a \quad \forall f \in F \quad (1.1a)$$

$$X_{th}^f = m_t^{fm} f_{th}^p X_{th}^{rp} + m_t^{fb} Z_{th}^{to} \quad \forall t \in T, h \in H, f \in F \quad (1.1b)$$

$$X_{th}^f = m_t^{fm} X_{th}^{tp} \quad \forall t \in T, h \in H, f \in F \quad (1.1c)$$

$$X_{th}^f = f_{th}^{fa} X_{th}^{fb} + f_{th}^{fp} m_t^{fm} X_{th}^{rp} \quad \forall t \in T, h \in H, f \in F \quad (1.1d)$$

$$m_t^{fbm} X_t \leq M (1 - Z_{th}^{to}) \quad \forall t \in T, h \in H \quad (1.1e)$$

Constraint (1.1a) limits fuel consumption for each fuel type, which can be burned by different technologies. Constraint (1.1b) uses a linear function to relate a non-CHP, fuel-burning electricity-producing technology's output to the corresponding consumption. Constraint (1.1c) defines the fuel burn of each non-CHP heating technology as directly proportional to its thermal production in each hour. Constraint (1.1d) defines fuel consumption using a size-dependent y -intercept and fixed slope, for every CHP technology and hour. Constraint (1.1e) limits the y -intercept of fuel burned by a CHP technology in a given time step based on the power rating of the technology as long as the technology is operating, and is void otherwise.

1.4.2 Thermal Production

$$X_{th}^{tpb} \leq \min \{ k_t^{tp} X_t; M Z_{th}^{to} \} \quad \forall t \in T, h \in H \quad (1.2a)$$

$$X_{th}^{tpb} \leq k_t^{tp} X_t \quad \forall t \in T, h \in H \quad (1.2b)$$

$$f_{th}^{fa} f_{th}^{ht} k_t^{te} f_{th}^p X_{th}^{rp} + X_{th}^{tpb} = X_{th}^{tp} \quad \forall t \in T, h \in H \quad (1.2c)$$

Constraints (1.2a)-(1.2b) limit the fixed component of thermal production of CHP technology t in time step h to the product of the thermal power production per unit of power rating and the power rating itself if the technology is operating, and 0 if it is not. Constraint (1.2c) relates the thermal production of a CHP technology to its constituent components, where the relationship includes a term that is proportional to electrical power production in each time step.

1.4.3 Storage System

Boundary Conditions and Size Limits

$$X_{b,0}^{se} = w_b^0 X_b^{bkWh} \quad \forall b \in B \quad (1.3a)$$

$$\underline{w}_b^{bkWh} X_b^{bkWh} \leq \bar{w}_b^{bkWh} \quad \forall b \in B \quad (1.3b)$$

$$\underline{w}_b^{bkW} X_b^{bkW} \leq \bar{w}_b^{bkW} \quad \forall b \in B \quad (1.3c)$$

Constraint (1.3a) initializes a storage system's state of charge using a fraction of its energy rating; constraints (1.3b) - (1.3c) limit the storage system size under the implicit assumption that a storage system's power and energy ratings are independent. These constraints are identical to those given in (R), but work in conjunction with significantly modified storage constraints that directly follow.

Storage Operations

$$X_{bth}^{pts} + \sum_{t \in T^e} X_{tuh}^{ptg} f_{th}^p f_t^d X_{th}^{rp} \quad \forall b \in B^e; t \in T^e; h \in H^g \quad (1.3d)$$

$$X_{bth}^{pts} f_{th}^p f_t^d X_{th}^{rp} \quad \forall b \in B^e; t \in T^e; h \in H n H^g \quad (1.3e)$$

$$X_{bth}^{pts} f_{th}^p X_{th}^{tp} \quad \forall b \in B^{th}; t \in T_b n T^{CHP}; h \in H \quad (1.3f)$$

$$X_{bth}^{pts} + X_{th}^{ptw} X_{th}^{tp} \quad \forall b \in B^h; t \in T^{CHP}; h \in H \quad (1.3g)$$

$$X_{bh}^{se} = X_{b,h}^{se} + \Delta \sum_{t \in T^e} (X_{bth}^{pts}) + X_h^{gts} X_{bh}^{dfs} \quad \forall b \in B^e; h \in H^g \quad (1.3h)$$

$$X_{bh}^{se} = X_{b,h}^{se} + \Delta \sum_{t \in T^e} (X_{bth}^{pts}) X_{bh}^{dfs} \quad \forall b \in B^e; h \in H n H^g \quad (1.3i)$$

$$X_{bh}^{se} = X_{b,h}^{se} + \Delta \sum_{t \in T_b} (X_{bth}^{pts}) X_{bh}^{dfs} \leq w_b^d X_{bh}^{se} \quad \forall b \in B^{th}; h \in H \quad (1.3j)$$

$$X_{bh}^{se} \leq \underline{w}_b^{mcp} X_b^{bkWh} \quad \forall b \in B; h \in H \quad (1.3k)$$

Constraints (1.3d) and (1.3e) restrict the electrical power that charges storage and is exported to the grid (in the former case), or that charges storage only (in the latter case, when grid export is unavailable) from each technology in each time step relative to the amount of electricity produced. Constraint (1.3f) provides an analogous restriction to that of constraint (1.3e) for

thermal production, and constraint (1.3g) provides the same restriction for the thermal production of CHP systems. Constraints (1.3h), (1.3i), and (1.3j) balance state-of-charge for each storage system and time period for three specific cases, respectively: (i) available grid-purchased electricity, (ii) lack of grid-purchased electricity, and (iii) thermal storage, in which we account for decay. Constraint (1.3k) ensures that minimum state of charge requirements are not violated.

Charging Rates

$$X_b^{bkW} \leq X_{bth}^{pts} + X_h^{gts} + X_{bh}^{dfs} \quad \forall b \in B^e; h \in H^g \quad (1.3l)$$

$$X_b^{bkW} \leq X_{bth}^{pts} + X_{bh}^{dfs} \quad \forall b \in B^e; h \in H \cap H^g \quad (1.3m)$$

$$X_b^{bkW} \leq X_{bth}^{pts} + X_{bh}^{dfs} \quad \forall b \in B^{th}; h \in H \quad (1.3n)$$

$$X_{bh}^{se} \leq X_b^{bkWh} \quad \forall b \in B; h \in H \quad (1.3o)$$

Constraints (1.3l) and (1.3m) require that power available must meet or exceed that put into or discharged from storage; the latter constraint considers the case in which the grid is not available. Constraint (1.3n) reflects the power requirements for the thermal system. Constraint (1.3o) requires a storage system's energy level to be at or below the corresponding rating.

Cold and Hot Thermal Loads

$$f_{th}^p X_{th}^{tp} + X_{bh}^{dfs} = c_h^{ec} + X_{bth}^{pts} \quad \forall h \in H \quad (1.4a)$$

$$f_{th}^p X_{th}^{tp} + X_{bh}^{dfs} = h_b^{b2B^c; t2T^{cl}} + X_{bth}^{pts} + X_{th}^{tp} = ac \quad \forall h \in H \quad (1.4b)$$

Constraints (1.4a) and (1.4b) balance cold and hot thermal loads, respectively, by equating the power production and the power from storage with the sum of the demand, the power to storage, and, in the case of cold loads, from the absorption chillers as well. Here, for legacy reasons, we have scaled the power by the efficiency of the respective technology; based on our variable definitions, we could have equivalently adjusted these by a coefficient of performance.

1.4.4 Production

$$X_{th}^{rp} \leq \bar{b}_t Z_{th}^{to} \quad \forall t \in T; h \in H \quad (1.5a)$$

$$f_t^{td} \leq X_t - X_{th}^{rp} \leq \bar{b}_t (1 - Z_{th}^{to}) \quad \forall t \in T; h \in H \quad (1.5b)$$

$$X_{th}^{tp} \leq X_t \quad \forall t \in T; n \in T^e; h \in H \quad (1.5c)$$

Constraint set (1.5) ensures that the rated production lies between a minimum turn-down threshold and a maximum system size; constraints (1.5a)-(1.5b) are copied from Ogunmodede et al. [10], while constraint (1.5c) is new. Constraint (1.5a) restricts system power output to its rated capacity when the technology is operating, and to 0 otherwise. Constraint (1.5b) ensures a minimum power output while a technology is operating; otherwise, the constraint is dominated by simple bounds on production. Constraint (1.5c) ensures that the thermal production of non-CHP heating and cooling technologies does not exceed system size.

1.4.5 Production Incentives

$$X_t^{pi} = \min \left\{ \bar{f}_t Z_t^{pi}; \sum_{h \in H} \Delta f_t^r f_t^{pi} f_{th}^p f_t^{li} X_{th}^{rp} \right\} \quad \forall t \in T \quad (1.6a)$$

$$X_t \leq \bar{f}_t + M (1 - Z_t^{pi}) \quad \forall t \in T \quad (1.6b)$$

Constraint (1.6a) calculates total production incentives, if available, for each technology. Constraint (1.6b) sets an upper bound on the size of system that qualifies for production incentives, if production incentives are available.

1.4.6 Power Rating

$$X_t \leq \bar{b}_t \sum_{s \in S_{tk}} Z_{tks}^s \quad \forall t \in T; k \in K_t \quad (1.7a)$$

$$\sum_{s \in S_{tk}} Z_{tks}^s \leq 1 \quad \forall t \in T; k \in K_t \quad (1.7b)$$

$$\sum_{t \in T; s \in S_{tk}} X_t \leq \bar{b}_c \quad \forall c \in C \quad (1.7c)$$

$$X_{th}^{rp} = X_t \quad \forall t \in T; h \in H \quad (1.7d)$$

$$X_{th}^{rp} \leq f_{th}^{ed} X_t \quad \forall t \in T; n \in T^e; h \in H \quad (1.7e)$$

$$\bar{b}_{tks}^s \leq Z_{tks}^s \leq \bar{b}_{tks}^s \quad \forall t \in T; k \in K_t; s \in S_{tk} \quad (1.7f)$$

$$\sum_{s \in S_{tk}} X_{tks}^s = X_t \quad \forall t \in T; k \in K_t \quad (1.7g)$$

Constraint (1.7a) permits nonzero power ratings only for the selected technology and corresponding subdivision in each class. Constraint (1.7b) allows at most one technology to be chosen for each subdivision in each class. Constraint (1.7c) limits the power rating to the minimum allowed for a technology class. Constraint (1.7d) prevents renewable technologies from turning down; rather, they must provide output at their nameplate capacity. Constraint (1.7e) limits rated production from all non-renewable technologies to be less than or equal to the product of the power rating and the derate factor for each time period. Constraint (1.7f) imposes both lower and upper limits on power rating of a technology, allocated to a subdivision in a segment, and constraint (1.7g) sums the segment sizes to the total for a given technology and subdivision.

1.4.7 Load Balancing and Grid Sales

$$\sum_{t \in T^e} (f_{th}^p - f_t^l - X_{th}^{rp}) + \sum_{b \in B^e} X_{bh}^{dfs} + \sum_{u \in U^p} X_{uh}^g = \sum_{t \in T^e} \sum_{b \in B^e} X_{bth}^{pts} + \sum_{u \in U_i^s} X_{tuh}^{ptg} + \sum_{u \in U^{sb}} X_{uh}^{stg} + X_h^{gts} + \sum_{t \in T^{ec}} X_{th}^{tp=ec} + d_h \quad \forall h \in H^g \quad (1.8a)$$

$$\sum_{t \in T^e} (f_{th}^p - f_t^l - X_{th}^{rp}) + \sum_{b \in B^e} X_{bh}^{dfs} = \sum_{b \in B^e; t \in T^e} X_{bth}^{pts} + \sum_{u \in U^c} X_{tuh}^{ptg} + \sum_{t \in T^{ec}} X_{th}^{tp=ec} + d_h \quad \forall h \in H \setminus H^g \quad (1.8b)$$

$$\sum_{u \in U^p} X_{uh}^g - X_h^{gts} \geq 0 \quad \forall h \in H^g \quad (1.8c)$$

$$\sum_{b \in B^e} X_{bh}^{dfs} - \sum_{u \in U^{sb}} X_{uh}^{stg} \geq 0 \quad \forall h \in H^g \quad (1.8d)$$

$$\Delta \sum_{h \in H^g} X_{uh}^{stg} + \sum_{t \in T_u} X_{tuh}^{ptg} - \bar{g}_u^s \geq 0 \quad \forall u \in U^{sb} \setminus U^{nm} \quad (1.8e)$$

$$\Delta \sum_{h \in H^g; t \in T_u} X_{tuh}^{ptg} - \bar{g}_u^s \geq 0 \quad \forall u \in U^{nm} \setminus U^{sb} \quad (1.8f)$$

Constraint (1.8a) balances load by requiring that the sum of power (i) produced, (ii) discharged from storage, and (iii) purchased from the grid is equal to the sum of (i) the power charged to storage, (ii) the power sold to the grid from in-house production or storage, (iii) the power charged to storage directly from the grid, (iv) any additional power consumed by the

electric chiller (where this is an additional term relative to the original model (R)), and (v) the electrical load on site. Constraint (1.8b) provides an analogous load-balancing requirement for hours in which the site is disconnected from the grid due to an outage (and contains the same additional term relative to the original model (R)). Constraint (1.8c) restricts charging of storage from grid production to the grid power purchased for each hour. Similarly, constraint (1.8d) restricts the sales from the electrical storage system to its rate of discharge in each time period. Constraints (1.8e) and (1.8f) restrict the annual energy sold to the grid at net-metering rates; only one of these is implemented in each case according to user-specified options. While a collection of pre-specified technologies may contribute to net-metering rates in both cases, constraint (1.8e) allows storage to contribute to net-metering while constraint (1.8f) does not.

1.4.8 Rate Tariff Constraints

Net Metering

$$\sum_v z_v^{nmil} = 1 \quad (1.9a)$$

$$\sum_t f_t^d + \sum_v i_v^n z_v^{nmil} \leq V \quad (1.9b)$$

$$\sum_{u \in U^p} \sum_{h \in H^p} X_{uh}^g \leq \sum_{u \in U^{nm}} \sum_{t \in T_u} X_{tuh}^{ptg} + \sum_{u \in U^{sb}} X_{uh}^{stg} \quad (1.9c)$$

Constraint (1.9a) limits the net metering to a single regime at a time. Constraint (1.9b) restricts the sum of the power rating of all technologies to be less than or equal to the net metering regime. Constraint (1.9c) ensures that energy sales at net-metering rates do not exceed the energy purchased from the grid.

Monthly Total Demand Charges

$$\sum_{h \in H_m} X_{uh}^g \leq z_{mu}^{tu} \quad \forall u \in U^p; m \in M \quad (1.10a)$$

$$z_{mu}^{tu} \leq z_{m;u}^{tu} \quad \forall u \in U^p; m \in M \quad (1.10b)$$

$$z_{mu}^{tu} \leq \sum_{h \in H_m} X_{u,1,h}^g \quad \forall u \in U^p; m \in M \quad (1.10c)$$

Constraint (1.10a) limits the quantity of electrical energy purchased from the grid in a given month from a specified pricing tier to the maximum available. Constraint (1.10b) forces pricing

tiers to be charged in a specific order, and constraint (1.10c) forces one pricing tier's purchases to be at capacity if any charges are applied to the next tier.

Peak Power Demand Charges: Months

$$X_{mn}^{dn} \leq Z_{mn}^{dmt} \quad \forall n \in N; m \in M \quad (1.11a)$$

$$Z_{mn}^{dmt} \leq Z_{m;n-1}^{dmt} \quad \forall n \in N; n \geq 2; m \in M \quad (1.11b)$$

$$Z_{mn}^{dmt} \leq X_{m;n-1}^{dn} \quad \forall n \in N; n \geq 2; m \in M \quad (1.11c)$$

$$X_{mn}^{dn} \leq X_{uh}^g \quad \forall m \in M; h \in H_m \quad (1.11d)$$

Constraint (1.11a) limits the energy demand allocated to each tier to no more than the maximum demand allowed. Constraint (1.11b) forces monthly demand tiers to become active in a prespecified order. Constraint (1.11c) forces demand to be met in one tier before the next demand tier. Constraint (1.11d) defines the peak demand to be greater than or equal to all of the demands across the time horizon, where an equality is actually induced by the sense of the objective function. A user-defined option precludes CHP technology production from reducing peak demand; if selected, constraint (1.11d) becomes:

$$X_{mn}^{dn} \leq X_{uh}^g + \sum_{t \in T}^{CHP} \circ @ f_{th}^p f_t^l X_{th}^{rp} \quad \forall m \in M; h \in H_m: \quad (1.11d')$$

Peak Power Demand Charges: Time-of-Use Demand and Ratchet Charges

$$X_{de}^{de} \leq Z_{de}^{dt} \quad \forall e \in E; d \in D \quad (1.12a)$$

$$Z_{de}^{dt} \leq Z_{d;e-1}^{dt} \quad \forall e \in E; e \geq 2; d \in D \quad (1.12b)$$

$$Z_{de}^{dt} \leq X_{d;e-1}^{de} \quad \forall e \in E; e \geq 2; d \in D \quad (1.12c)$$

$$X_{de}^{de} \leq \max_{u \in U^p} f_{uh}^g \quad \forall d \in D; h \in H_d \quad (1.12d)$$

$$X_{de}^{de} \leq X_{mn}^{dn} \quad \forall m \in M \quad (1.12e)$$

Constraints (1.12a)-(1.12d) correspond to constraints (1.11a)-(1.11d), respectively, but pertain to a type of charge not related to monthly use, but rather to time of use within a month. These *ratchet charges* are implemented using constraints (1.12d). The charge applied for each time-of-use

period is a linearizable function of the greater of the peak electrical demand during that period (as given by the first term on the right-hand side of (1.12d)) and a fraction of the peak demand that occurs over a collection of months (known as *look-back months*) during the year (as given by the second term on the right-hand side of (1.12d)). Constraint (1.12d) ensures the peak demand over the set of look-back months is no lower than the peak demand for each look-back month. In this way, charges are based not only on use in a given month, but also on a fraction of use over the last several months, and becomes relevant when this latter use is high relative to current use. If CHP technologies are not allowed to reduce peak demand, constraint (1.12d) becomes:

$$X_{de}^{e2E} \times X_{uh}^g + \frac{\circ}{t2T_{CHP}} \times \frac{\circ}{f_{th}^p} \times \frac{\circ}{f_t^l} \times X_{th}^{rp} \times X_{bth}^{pts} \times X_{tuh}^{ptgA} \times \frac{1}{u2U_t^s} \quad 8d \ 2 \ D; \ h \ 2 \ H_d:$$

1.4.9 Minimum Utility Charge

$$X^{mc} \times c^{amc} \times \frac{\circ}{\Delta} \times \left[\frac{c_{uh}^g \times X_{uh}^g}{\underbrace{u2UP; h2H^g}_{\{Z\}}} + \frac{c_{de}^r \times X_{de}^{de}}{\underbrace{d2D; e2E}_{\{Z\}}} + \frac{c_{mn}^{rm} \times X_{mn}^{dn}}{\underbrace{m2M; n2N}_{\{Z\}}} \right] + \frac{\circ}{\Delta} \times \frac{\circ}{@} \times \frac{\circ}{@} \times \frac{c_{uh}^e \times X_{uh}^{stg} + c_{uh}^e \times X_{tuh}^{ptgA}}{\underbrace{h2H^g \ u2U^{sb} \ t2T; u2U_t^s}_{\{Z\}}} \quad (1.13)$$

Energy Export Payment

Constraint (1.13) enforces a minimum payment to the utility provider, which is a fixed constant less charges incurred from grid energy, time-of-use demand and monthly demand payments, plus sales from exports to the grid.

1.4.10 Non-negativity

$$X^{plb}; X^{mc} \geq 0 \quad (1.14a)$$

$$X_t; X_t^{pi} \geq 0 \quad 8t \ 2 \ T \quad (1.14b)$$

$$X_{tuh}^{ptg} \geq 0 \quad 8u \ 2 \ U; \ t \ 2 \ T_u; \ h \ 2 \ H \quad (1.14c)$$

$$X_{uh}^{stg}, X_{uh}^g \quad 0 \quad 8u \ 2 \ U; h \ 2 \ H \quad (1.14d)$$

$$X_{de}^{de} \quad 0 \quad 8d \ 2 \ D; e \ 2 \ E \quad (1.14e)$$

$$X_{mn}^{dn} \quad 0 \quad 8m \ 2 \ M; n \ 2 \ N \quad (1.14f)$$

$$X_h^{gts} \quad 0 \quad h \ 2 \ H \quad (1.14g)$$

$$X_b^{bkW}, X_b^{bkWh} \quad 0 \quad b \ 2 \ B \quad (1.14h)$$

$$X_{tks}^s \quad 0 \quad 8t \ 2 \ T; k \ 2 \ K; s \ 2 \ S_{tk} \quad (1.14i)$$

$$X_{bth}^{pts} \quad 0 \quad 8b \ 2 \ B; t \ 2 \ T; h \ 2 \ H \quad (1.14j)$$

$$X_{bh}^{se}, X_{bh}^{dfs} \quad 0 \quad 8b \ 2 \ B; h \ 2 \ H \quad (1.14k)$$

$$X_{th}^{rp}, X_{th}^f, X_{th}^{fb}, X_{th}^{tpb}, X_{th}^{tp}, X_{th}^{ptw} \quad 0 \quad 8t \ 2 \ T; h \ 2 \ H \quad (1.14l)$$

1.4.11 Integrality

$$Z_v^{nmil} \ 2 \ f0; 1g \ 8v \ 2 \ V \quad (1.15a)$$

$$Z_{tks}^s \ 2 \ f0; 1g \ 8t \ 2 \ T; k \ 2 \ K; s \ 2 \ S_{tk} \quad (1.15b)$$

$$Z_t^{pi} \ 2 \ f0; 1g \ 8t \ 2 \ T \quad (1.15c)$$

$$Z_{th}^{to} \ 2 \ f0; 1g \ 8t \ 2 \ T; h \ 2 \ H \quad (1.15d)$$

$$Z_{de}^{dt} \ 2 \ f0; 1g \ 8d \ 2 \ D; e \ 2 \ E \quad (1.15e)$$

$$Z_{mn}^{dmt} \ 2 \ f0; 1g \ 8m \ 2 \ M; n \ 2 \ N \quad (1.15f)$$

$$Z_{mu}^{ut} \ 2 \ f0; 1g \ 8m \ 2 \ M; u \ 2 \ U \quad (1.15g)$$

Finally, constraints (1.14) ensure all of the variables in our formulation assume non-negative values. In addition to non-negativity restrictions, constraints (1.15) establish the integrality of the appropriate variables.

CHAPTER 2
A MATHEURISTIC FOR DESIGN AND DISPATCH OF A UTILITY-CONNECTED
DISTRIBUTED ENERGY SYSTEM

Modified from a paper submitted to the *Journal of Heuristics* James Grymes^{1,2}, Alexandra Newman¹, Alexander Zolan³, Dinesh Mehta⁴

2.1 Abstract

Modeling distributed power generation systems often requires complicated mathematical expressions that present challenges for commercial optimization solvers. This paper presents a *Matheuristic* to solve a mixed-integer optimization model that informs decisions regarding the design and dispatch of a utility-connected microgrid. We deploy a Genetic Algorithm to search the system design space and a linear program to solve the economic dispatch problem. The model is a component of an open-source web tool that requires near-real-time solutions. Our method yields objective function values within 5% of an exogenously produced optimal in fewer than 30 seconds for 90% of our test cases compared to only 10% of our test cases by a traditional optimization solver in the same amount of time.

2.2 Introduction

The adoption of distributed energy resources (DER) that incorporate renewable and storage technologies is growing, in part due to significant reductions in the cost of electrical storage photovoltaic (PV) systems [11]. Replacing fossil-fueled power plants with renewable electricity generation offers both environmental benefits [12] and reduced costs [13]. Furthermore, private customers can employ a peak-shaving dispatch strategy using behind-the-meter DERs to diminish utility demand charges [14]. However, accurate energy-system models often require complex mathematical structures, precluding traditional optimization software from finding good solutions under practical run-time limits. Practitioners, therefore, seek alternate strategies, such as heuristics, to provide fast solutions of acceptable quality.

¹Operations Research with Engineering Graduate Program,

²Primary researcher and author

³National Renewable Energy Laboratory

⁴Computer Science, Colorado School of Mines

2.2.1 Motivation

Models help decision-makers assess the trade-offs of procuring and deploying on-site microgrids. In most cases, clients must rely on consultant work to formulate the model, conduct analysis, and make recommendations. While appropriate for large corporations or municipalities, this approach is not tenable for smaller-scale projects or companies devoid of large operating budgets. Commercial software includes both paid tools such as HOMER [15] and publicly available tools such as DER-CAM [16]. Krah [17] and Theo et al. [18] compare behind-the-meter microgrid planning and distributed generation optimization techniques, including 51 distinct models.

The National Renewable Energy Laboratory hosts Renewable Energy Integration and Optimization (REopt[®]), an open-source web tool for microgrid planning that integrates conventional energy generation. The tool enables users to conduct an *analysis of alternatives* using their facilities' parameters while relying on proven defaults for cost and performance of candidate DER technologies. Figure 2.1 depicts a notional system consisting of a utility-connected microgrid, a distribution network, a series of electrical and thermal load profiles, and energy markets. In both DER-CAM and REopt, a mixed-integer program determines an optimal microgrid configuration (design) and the associated system controls (dispatch), often by minimizing life-cycle costs.

While there have been considerable advancements in commercial solvers over the last 20 years, many types of large-scale, mixed-integer programs present challenges, especially for large instances. Classical models, such as the *Vehicle Routing Problem* and the *Winner Determination Problem*, present computational challenges for even the most sophisticated software [19, 20]. Similarly, distributed generation models solved with commercial optimizers can require an unacceptable amount of time to reach a feasible solution [9, 21, 22]. Therefore, we suggest heuristics to aid or supplant solvers in determining an appropriate design and dispatch of a grid-connected distributed generation system.

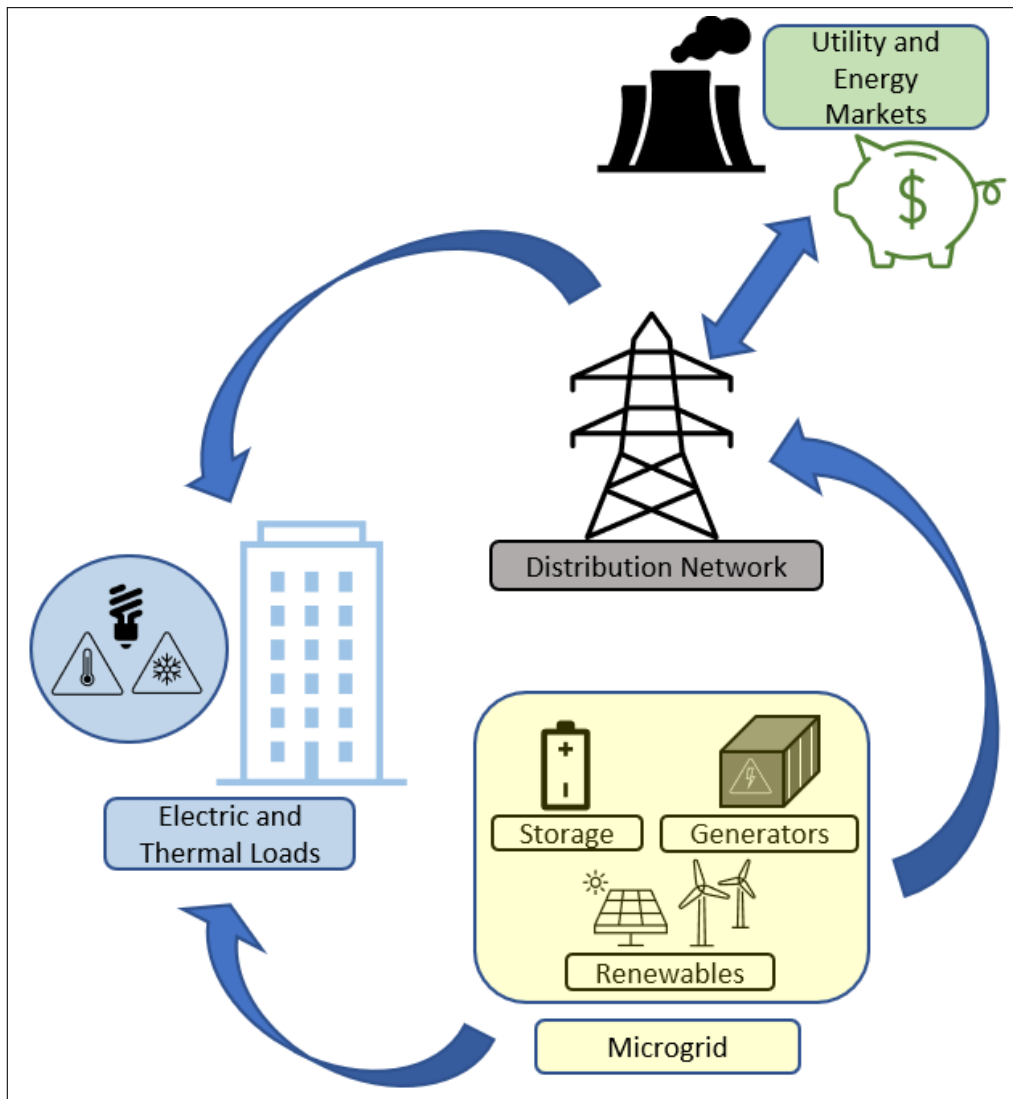


Figure 2.1 An example of a utility-connected microgrid showing design (yellow) and dispatch (blue arrows) components.

2.2.2 Literature Review

Mixed-integer linear models and, more generally, combinatorial optimization problems, relate to many applications, but can become intractable for realistically sized instances. Practitioners may prefer to rely on near-optimal solutions generated by heuristics such as naturally inspired algorithms (e.g., *Simulated Annealing*), evolutionary searches (e.g., *Genetic Algorithm*), and trajectory methods (e.g., *Tabu Search*) [23]. These techniques afford the advantages of being problem-agnostic and easy to implement. However, fast convergence is not guaranteed for large

problem instances.

Various literature explores mixed-integer linear optimization models, such as DER-CAM and REopt[®] discussed above, for determining optimal microgrid design and dispatch. Often, distributed generation models that incorporate system design variables mandate the commitment of significant capital investments that dominate the objective function. This, coupled with discrete control variables that govern dispatch, requires solution techniques other than direct execution of the monolith using off-the-shelf software. Jeddi et al. [24] and Xu et al. [25] present exact approaches, specifically, *Dynamic Programming*, by discretizing the electrical storage system’s state of charge and determining the optimal dispatch strategy. While theoretically able to yield optimal solutions, distributed energy control problem instances can contain long time horizons and many technologies, precluding exact methods in a practical amount of time due to the “curse of dimensionality” [26]. Niu et al. [27] provide a detailed review of competing heuristics for power-flow models. Conversely, Foster et al. [28] show how simple knapsack formulations are capable of yielding solutions to distributed generation planning models but comment on computational challenges relative to solution quality generated by heuristics such as genetic algorithms.

Scheduling large-scale systems for economic dispatch of electrical and thermal power, referred to as *unit commitment*, has been an active area of research for over 50 years [29]. Our formulation contains many similarities to this classical *NP-Hard* problem for which researchers leverage heuristics [30]. Valenzuela and Smith [31] propose a memetic algorithm, in concert with a local-search genetic algorithm, for large-scale unit commitment in electrical power systems. However, this work omits decisions concerning system configuration. Additionally, Ting et al. [32] utilize hybrid particle swarm optimization to solve the unit commitment problem involving only electrical generators and the utility.

Nazari-Heris et al. [33] and Alsagri and Alrobaian [34] present a detailed review of meta-heuristic techniques for optimal dispatch of co-generational technology; however, neither consider procurement decisions or energy storage, which necessitate our heuristic approach. Ren et al. [35] solve a model that includes combined heat and power and present a methodology that decouples design and dispatch using a meta-heuristic for the design and a rules-based myopic approach for dispatch. The authors omit discussions of the efficacy of their solutions or the speed

with which they are attained, and their model does not include peak-demand charges.

While many works utilize heuristics to handle these challenges, they differ from ours in that they are absent the ability to source power from the grid [36–38]. Without the utility, dispatch becomes a function of the rated capacity of the microgrid; correspondingly, the domain for the design variables is drastically reduced. Other models consider a subset of technologies that we incorporate and therefore do not present the complexities found in our model, such as energy storage or the interactions between thermal and electric-producing technologies [39, 40]. Objective function criteria differ from ours, such as reducing emissions or minimizing energy demand through co-generational DERs [41, 42]. Some models are similar in structure; Letchford et al. [43] use the *dynamic local search* heuristic for resource allocation with overloaded demand but address wireless communication instead of power systems. Freitas et al. [44] propose a *Fix-and-Optimize* heuristic to minimize power losses through grid configurations and corresponding power flows.

Moretti et al. [45] consider the electrification of rural communities and compare solving a design and dispatch microgrid model using two different approaches. One considers a configuration search coupled with a myopic dispatch policy; the other uses a predictive optimization algorithm for a mixed-integer linear program. The heuristic treats hourly decisions independently, leading to sub-optimal solutions. The predictive optimization method produces better results, but solve times are not practical. Nikmehr and Najafi-Ravadanegh [46] show how heuristics can handle probabilistic inputs using Monte Carlo simulation; however, design decisions are absent in their application. Maniezzo et al. [47] explore a variety of techniques, referred to as *Matheuristic*, for solving mixed-integer linear programs. This type of strategy combines meta-heuristics with mathematical optimization. Dupin and Talbi [48] propose several constructive Matheuristics for planning nuclear power plant maintenance and refueling operations; these heuristics invoke pre-processing, partial solutions, a simplified model, and the restoration of feasibility.

Our contribution is the development of a Matheuristic that includes (i) a genetic algorithm for candidate design selection, (ii) a scheduling policy for CHP operations, and (iii) a linear program to obtain a solution to a design and dispatch techno-economic model. We also explore multiple microgrid configurations using parallel processing to expedite the design search. Our approach simultaneously addresses design and dispatch decisions to obtain objective function values

comparable to or better than those produced by commercial solvers, and in less time.

The remainder of the paper is organized as follows: Section 2.3 describes our mathematical formulation and the components that present challenges. Section 2.4 details our methodology to quickly generate solutions that minimize lifecycle costs. Section 2.5 presents inputs of our model, an analysis of each sub-process of the methodology, and a comparative performance evaluation of our method and the optimization software. Finally, Section 2.6 concludes.

2.3 Modeling the System

REopt[®] is a techno-economic, mixed-integer linear program hooked to a commercial solver. This model, (\mathcal{P}), presented by Hirwa et al. [9] and detailed in Chapter 1, minimizes the total lifecycle cost associated with meeting electric, heating, and cooling loads at hourly fidelity. The web-based tool consists of deterministic inputs and requires assumptions about future-technology capital costs, utility tariffs, solar irradiance, and electrical and thermal loads. Its distinguishing feature relative to other microgrid planning tools is its intended use to quickly assess various scenarios. Hirwa et al. [9] show that only five of the 12 test instances achieve better than a 1% optimality gap after 10 minutes. Furthermore, a more realistic time limit (e.g., two minutes) for a web-tool, often used repeatedly for parametric analysis, results in two instances without a feasible solution and more than 40% of instances failing to achieve a 5% optimality gap. This work aims to improve the tool’s ability to return good solutions quickly by implementing a Matheuristic.

2.3.1 Model Overview

Figure 2.2 illustrates REopt’s[®] variables, objective, and constraints. We group distributed energy technologies into renewable, traditional, and CHP. Additionally, the model includes electrical (lithium-ion), hot-thermal, and cold-thermal storage for the energy produced by distributed technologies or purchased from the utility, which can then be dispatched to meet electrical, heating, and cooling loads, respectively.

REopt[®] seeks to minimize total lifecycle costs while adhering to realistic system constraints and meeting 100% of demanded electrical and thermal load. The objective function is composed of (i) capital and installation costs, (ii) fixed and variable operations and maintenance costs, (iii) production costs, (iv) utility charges, and (v) variable production incentives.

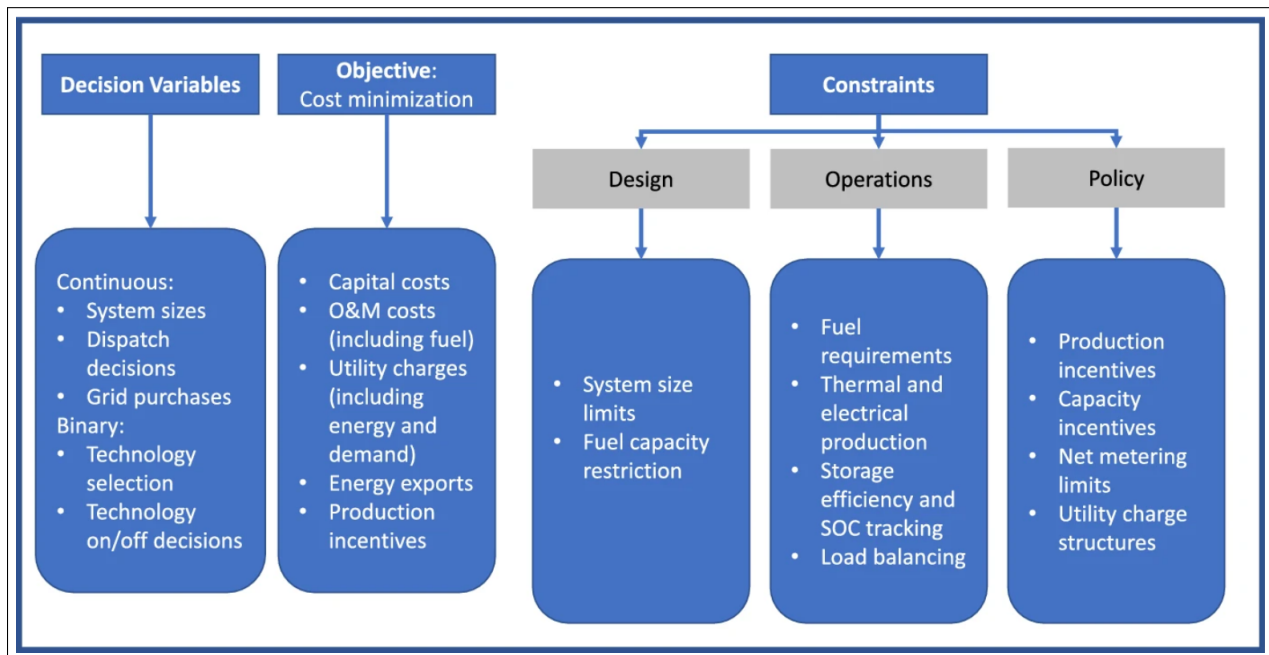


Figure 2.2 A categorical overview of the decision variables, objective function, and constraints that comprise the REopt[®] optimization model, (P), where SOC denotes state of charge [9].

The constraint set is categorized into nine distinct subgroups in addition to simple variable bounds:

- *Fuel Consumption* (given in 1.4.1)
- *Thermal Production* (given in 1.4.2)
- *Storage System* (given in 1.4.3)
- *Production* (given in 1.4.4)
- *Production Incentives* (given in 1.4.5)
- *Power Rating* (given in 1.4.6)
- *Load Balancing and Grid Sales* (given in 1.4.7)
- *Rate Tariff* (given in 1.4.8)
- *Minimum Utility Charge* (given in 1.4.9)

The main components of this work address difficulties presented through the enforcement of the italicized constraints. Table 2.1 contains relevant notation from model (P). For notational consistency, we use math calligraphic font to denote sets, subsets, and indexed sets and lower and uppercase math script for parameters and variables, respectively.

Table 2.1 A selection of notation from model (P)

Sets		
H		Time steps
T		Technologies
Subsets and Indexed Sets		
T^{CHP}	T	CHP technologies
Parameters		
f_{th}^a		Fuel burn ambient correction factor of technology t at time step h [unitless]
f_{th}^p		Production factor of technology t during time step h [unitless]
m_t^m		Slope of the fuel rate curve for technology t [MMBTU/kWh]
Variables		
X_{th}^f		Fuel burned by technology t in time step h [MMBTU/h]
X_{th}^{rp}		Rated production of technology t during time step h [kW]
X_t		Power rating of technology t [kW]
Z_{th}^o		1 If technology t is operating in time step h ; 0 otherwise [unitless]

2.3.2 Model Contribution to Solution Latency

REopt[®] contains hundreds of thousands of variables and constraints for realistically sized instances. Our threshold for success is defined as a solution yielding an optimality gap of less than 5% in fewer than two minutes. Three attributes thwart our efforts when we deploy an optimization model: (i) the simultaneous presence of design and dispatch variables, (ii) the binary representation of scheduling decisions of the CHP system, and (iii) the incorporation of utility peak-demand charges coupled with electrical storage systems.

2.3.2.1 Design and Dispatch

Distributed generation models that determine design and dispatch consist of continuous and integer variables that govern procurement and deployment of distributed generation, respectively. Techno-economic models attempt to balance the cost of procuring, maintaining, and deploying the system with the economic tradeoff of purchasing electricity from the utility. We attempt a naïve approach to (P) by solving the linear relaxation, fixing the design variables, and solving (P) with the fixed design. Empirical testing yields optimal solutions to the fixed-design model (P^{FD}) in fewer than 16 seconds for over 75% of test cases. However, some instances of (P^{FD}) fail to return an optimal solution in under 10 minutes, indicating that fixing a subset of the variables can lead to slow solve times.

2.3.2.2 Binary Variables for CHP Scheduling

Constraints (1.1d)-(1.2c), found in Chapter 1, control how the CHP system operates, including the amount of fuel consumed and the amount of thermal power produced as a function of electric production. CHP fuel consumption is calculated as an affine function of electrical production (X_{th}^{rp}) in hour h and the system size (X_t) . However, to enforce a fuel burn commensurate with system size when the system is deployed, and to preclude fuel burn when the system is off, we include the bilinear term $X_t Z_{th}^{\text{to}}$. Hirwa et al. [9] use standard linearization techniques that result in Constraints (1.1d) and (1.1e). We create a new model variant (P^{LF}) by performing a simple relaxation in which we approximate the CHP fuel burn using a linear constraint by removing the binary variable Z_{th}^{to} and replacing Constraints (1.1d) and (1.1e) with Constraint (2.1), in which \hat{m}_t^{fm} represents a modified variable fuel burn rate m_t^{fm} .

$$X_{th}^f = f_{th}^{\text{fa}} f_{th}^{\text{p}} \hat{m}_t^{\text{fm}} X_{th}^{\text{rp}} \quad \forall t \in T^{\text{CHP}}; h \in H \quad (2.1)$$

This approximation yields better performance; the solver returns optimal solutions to all test cases in fewer than 35 seconds, on average, and no case requires more than 93 seconds. While there is a significant improvement in run time, the approximation used incentivizes part-load CHP operations when it is not economical to do so under the original model, leading solutions with significantly greater objective function values. Therefore, we conclude that using the linear

approximation is not suitable for the heuristic.

2.3.2.3 Peak Demand Charges and Battery Energy Storage Systems

Utility tariffs further exacerbate the run-time latency by including monthly and time-of-use peak demand charges. According to a National Renewable Energy Laboratory report, peak-demand charges can constitute up to 70% of a customer’s utility bill [49]. Figure 2.3 shows an example of a 24-hour load profile, resulting in large peak-demand charges and associated “managed demand thresholds.” Simple marginal cost computations cannot determine optimal controls for a battery energy storage system. Including peak-demand charges and electrical storage precludes a strictly myopic approach to determining the optimal economic dispatch. Therefore, our methodology separates the problem into decisions related to the design, the CHP scheduling operations, and the economic dispatch of the committed system.

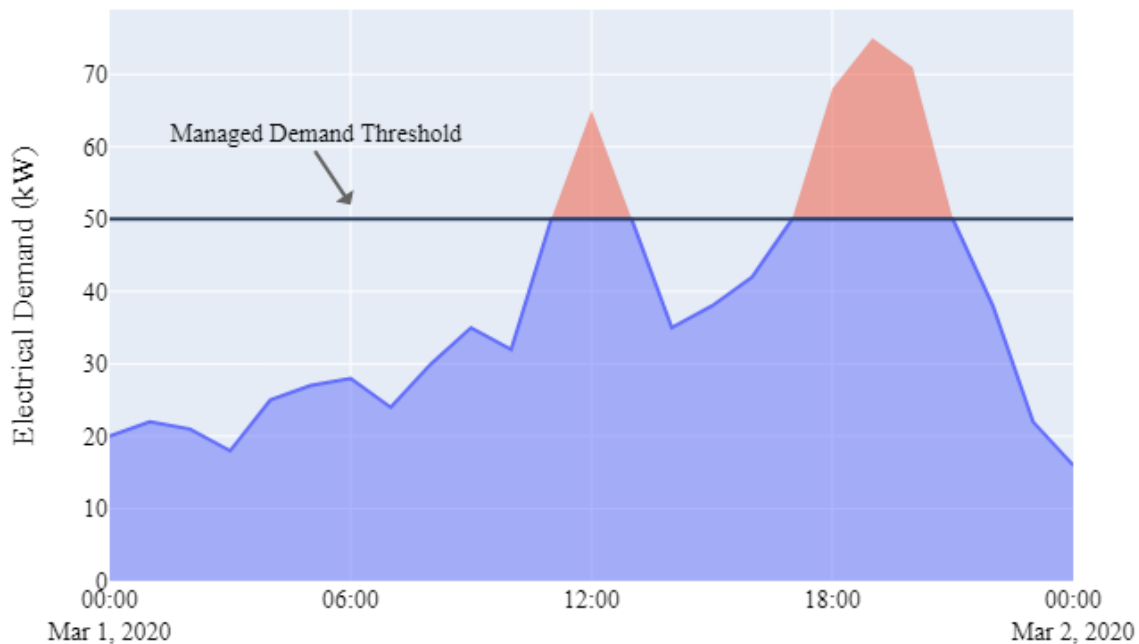


Figure 2.3 An example of a 24-hour load profile with unmanaged demand peaks.

2.4 Method

We generate solutions to a complex, techno-economic design and dispatch mixed-integer linear program by devising a Matheuristic (\mathbf{M}^H). Our method addresses the three main contributing factors to solution latency: the coupling of design and dispatch decisions, the operational scheduling of the CHP system, and the simultaneous presence of peak-demand charges with battery energy storage.

Our methodology consists of three phases: (i) employing a meta-heuristic (genetic algorithm) to search the state-space for a suitable microgrid design (Section 2.4.1), (ii) determining the CHP system’s operational schedule (Section 2.4.2.1), and (iii) solving a linear program that models economic dispatch (Section 2.4.2.2). Components (ii) and (iii) form the dispatch routine and return the fitness value for a fixed microgrid design for the genetic algorithm. Figure 2.4 presents a graphical representation of (\mathbf{M}^H). The blocks outlined by the dashed box reflect the dispatch decisions for each design k executed as a parallel process.

2.4.1 A Genetic Algorithm for Candidate Design Selection

We employ a genetic algorithm designed to work in continuous space [50] to search for suitable microgrid configurations. While numerous suitable meta-heuristics exist, a genetic algorithm presents the ability to utilize parallel processing to evaluate the design’s fitness. Each design and the associated dispatch decisions are independent; therefore, assuming that the necessary computing resources are available, the algorithm’s theoretical complexity is dominated by the maximum time to solve the corresponding dispatch model over the k designs in the population for each generation. The class of evolutionary algorithms, of which the genetic algorithm is a member, consists of three main steps: (1) initialization, (2) iteration, and (3) termination. Algorithm 1 documents the genetic algorithm’s process of creating new generations of candidate designs (populations), and we present the associated notation in Table 2.2.

$$i = a - 1 \frac{(1 - a)^i}{1 - (1 - a)^i} \quad (2.2a)$$

$$\Delta_{ti} = U(R_{ti}; R_{ti}^+) \quad (2.2b)$$

$$R_{ti} = \max_{r_t} f(r_t; r_t, (C_{ti}, b_t))g \quad (2.2c)$$

$$R_{ti}^+ = \min_{r_t} f(r_t; r_t, (b_t, C_{ti}))g \quad (2.2d)$$

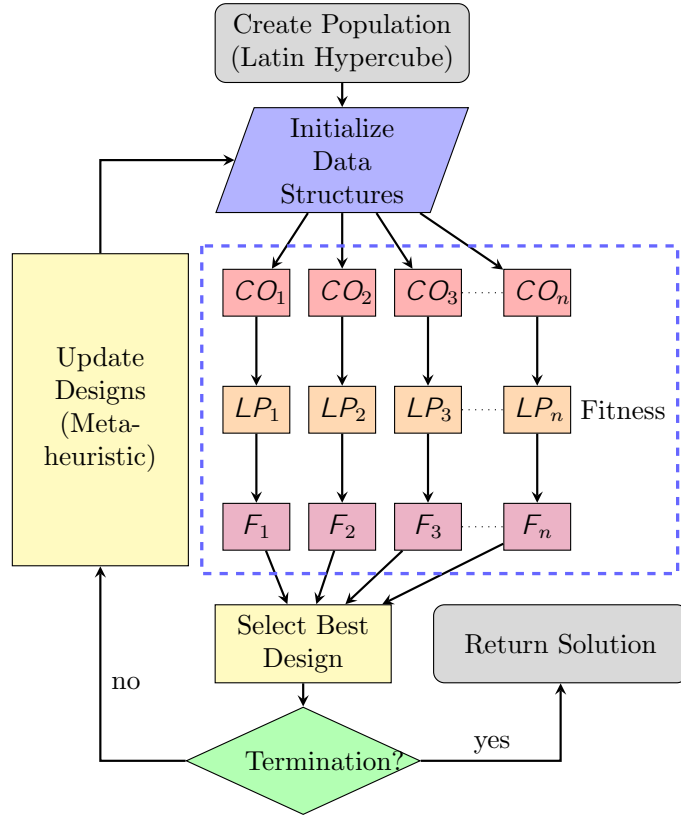


Figure 2.4 Heuristic methodology (\mathbf{M}^H), including parallelization of dispatch subroutine.
 n : Number of parallel processes; CO_k : CHP operations for process k ; LP_k : Linear program for remaining dispatch for process k ; F_k : Feasibility step for process k .

$$C_{t,i+1} = \min f \bar{b}_t ; \max f \underline{b}_t ; (C_{ti} + i \Delta_{ti}) gg \quad (2.2e)$$

1. **Population:** Each population contains a set of individuals which are unique candidate microgrid configurations represented by the two-dimensional array $C_{ti} \in [\underline{b}_t ; \bar{b}_t] \quad \forall t$, where t is a technology and i is an iteration of the algorithm.
2. **Initialization:** Through experimentation, we determine that convergence speed is strongly influenced by the quality of the initial population, which we generate by utilizing orthogonal, array-based Latin hypercube sampling [51]. To effect low memory requirements, we create a conservative population size of $n = c - 2$, in which n is the size of the population and c is the number of available computer cores.
3. **Iteration:** The iteration step creates the next generation and consists of determining a population's fitness, followed by selection, and ending with crossover and mutation.

Table 2.2 Notation used for the Genetic Algorithm.

Sets		
$i \in I$	Iteration count	
Parameters		
μ	Mutation scalar at iteration i	[-]
a	Scalar value at iteration 1	[-]
\underline{b}_t	Minimum power rating for technology t	[kW]
\bar{b}_t	Maximum power rating for technology t	[kW]
α	Fraction of scalar a value as $i \rightarrow j$	[-]
\hat{i}	Iteration of inflection for sigmoid function	[-]
ρ	probability of crossover and mutation, respectively	[-]
n	Population size	[-]
r_t	Magnitude of the range of technology t , $\bar{b}_t - \underline{b}_t$	[kW]
Variables		
p_t^a, p_t^b	Individual parents selected for crossover	[kW]
R_{ti}	Maximum of r_t and $r_t C_{ti}$ for technology t at iteration i	[kW]
R_{ti}^+	Minimum of r_t and $r_t (\bar{b}_t - X_{ti})$ for technology t at iteration i	[kW]
Δ_{ti}	Change of technology t in iteration i , sampled from $U(R_{ti}, R_{ti}^+)$	[kW]
C_{ti}	Intermediate size of candidate technology t at iteration i	[kW]
X_{ti}	Size of candidate technology t at iteration i	[kW]

3.1 **Fitness:** The fitness function determines the cost of meeting the electric, heating, and cooling loads under the heuristic dispatch policy described in Section 2.4.2, using the microgrid configuration as input. The dispatch cost is then paired with the system design cost, providing the full lifecycle cost, or design fitness.

3.2 **Selection:** The population is then ordered, decreasing by the individual's fitness, and we select the $dn=2e$ lowest-cost designs as parents for propagation in the next generation.

3.3 **Crossover:** We then pair parents and execute a crossover step, also referred to as recombination, whereby a new microgrid candidate is created using information from well-performing designs with respect to lifecycle costs. We implement the discrete recombination procedure described by Nissen [52], which resembles the classical Uniform Crossover [53], in which, with equal probability, we swap sizes for technology t between two selected parents.

3.4 **Mutation:** The newly created system designs (children) undergo a mutation, which is critical to the theoretical possibility of exploring the full state-space by generating any

feasible microgrid configuration. Each technology (allele) in the newly created child (chromosome) is considered for mutation with probability $p_m = 0.2$. If an allele is selected for mutation, the technology size is modified by a scaled, (2.2a), uniformly distributed value Δ_{ti} between R_{ti} and R_{ti}^+ , defined by Equations (2.2b), (2.2c), and (2.2d), respectively. We use a sigmoid function for the decay scalar α_i to generate a wide search area which we narrow over the execution of the algorithm. Finally, Equation (2.2e) updates the technology size t in iteration i and ensures that the new child does not fall outside the feasible region. The mutated child is then added to the population for the next generation if it does not already exist.

4. **Termination:** The genetic algorithm terminates if one of two criteria is satisfied: either an iteration limit of \hat{n} is reached or the best-found fitness fails to improve by more than ϵ after five iterations.

Figure 2.5 shows an example of the implementation of the mutation step. The blue and red line segments represent the feasible and infeasible regions of the variable C_{ti} for technology t at iteration i , respectively.

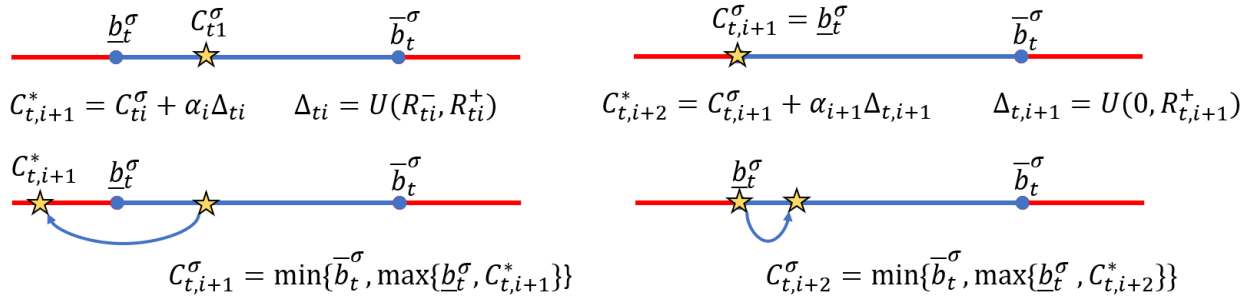


Figure 2.5 Genetic algorithm mutation example Example of two iterations of the child mutation routine of the genetic algorithm, respectively. Blue and red line segments represent the feasible and infeasible regions for technology t , respectively. Note: In iteration 1, the infeasible intermediate value of X_{t2} is moved to the lower bound \underline{b}_t , and in iteration 2, the random change (Δ_{t2}) is restricted to the positive direction.

Algorithm 1 documents the iterative process, beginning on Line 6, of generating a new population. Lines 8-10 compute each individual's fitness (e.g. lifecycle cost) in the population and then select half of the individuals with the lowest lifecycle cost. Lines 12-16 iterate over each parent and technology, performing crossover with probability p_c to create the children. Lines

17-23 form the next generation's population (candidate designs) through mutation with probability μ . The algorithm includes two possible termination criteria: (i) iteration limit or (ii) insufficient objective value improvement after a specified number of iterations. Table 2.1 and Table 2.2 provide the notation for Algorithm 1.

Algorithm 1 Genetic Algorithm for determining the microgrid configuration.

```

1: Inputs:  $b$  ; ; ;  $n$ ;  $term\_limit$ ;  $l$ 
2: Output:  $X$ 
3:  $count = 0$ 
4:  $best = 1$ 
5:  $X = b$ 
6:  $pop_0 = init\_latin(n)$  . Initialization
7: for  $i \geq 1$  do . Iteration
8:    $fit_i = dispatch(pop_i)$  . Fitness
9:    $pop_i = sort(pop_i; fit_i)$ 
10:   $parents_i = pop_i[1 : d_{2}^n e] [ fX g$  . Selection
11:   $children_i = ;$ 
12:  for  $p; q \geq 2$   $parents_i : p \neq q$  do
13:    for  $t \geq T$  do
14:      if  $U(0;1) < \theta$  then . Crossover
15:         $swap(p_t; q_t)$ 
16:         $children_i = children_i [ fp; qg$  if  $fp; qg \geq \sum_{k=1}^{S_i-1} children_k$ 
17:      for  $c \geq 2$   $children_i$  do
18:        for  $t \geq T$  do
19:          if  $U(0;1) < \theta$  then . Mutation
20:             $d_{ti} = C_{ti} + i \Delta_{ti}$ 
21:          else
22:             $d_{ti} = C_{ti}$ 
23:           $pop_{i+1} = pop_{i+1} [ fdg$ 
24:           $change = best - minffit_i g$ 
25:          if  $change > 0$  then
26:             $best = minffit_i g$ 
27:             $X = pop_i[1]$ 
28:          if  $change < \epsilon$  then . Termination
29:             $count = count + 1$ 
30:            if  $count > term\_limit$  then
31:              return  $X$ 
32:          else
33:             $count = 0$ 
34: return  $X$ 

```

2.4.2 Energy Dispatch

The dependencies between technologies, the presence of peak demand charges, and the inclusion of energy storage systems preclude the deployment of a strictly myopic procedure. For example, Figure 2.6 depicts a notional system with various technologies and the corresponding energy flows. The dispatch subroutine is separated into two processes: (i) CHP system scheduling and (ii) a linear program that minimizes the cost of meeting electrical and thermal loads.

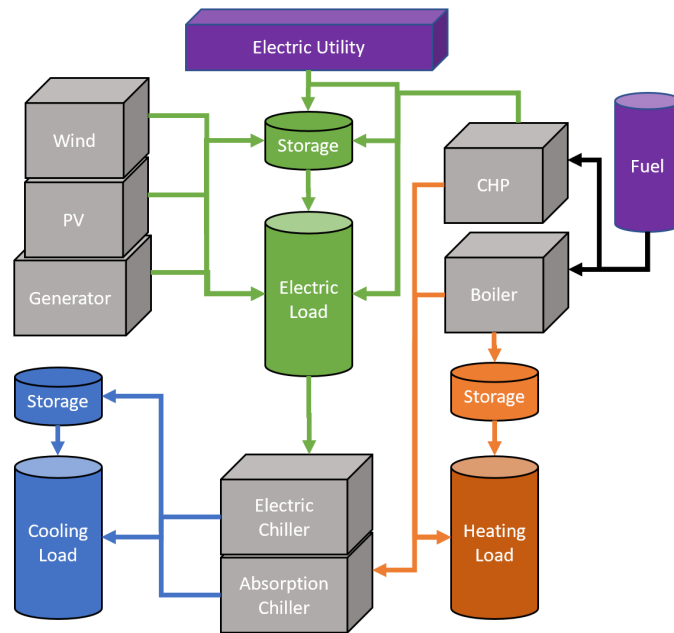


Figure 2.6 REopt[®] System and Dependencies. Green, orange, and blue arrows represent electrical, hot-thermal, and cold-thermal flows, respectively.

The CHP system scheduling routine is accomplished through a set of myopic, policy-based decisions that choose the least expensive strategy to meet the load in a particular hour and are made without considering electric and thermal storage impacts. Once the operational schedule is determined, we solve the economic dispatch problem. Due to the complex nature of the charging and discharging decisions associated with energy storage, we explore three diverse approaches with advantages and limitations: policy-based, dynamic programming, and linear optimization. The policy-based method is very fast, but the quality of the solution, defined by the corresponding objective function value, is poor for inputs in which a large energy storage system is a component of a cost-minimizing design.

Second, we implement the dynamic program using the procedure and notation defined in Appendix A.1, where we discretize the state of charge of our energy storage systems. Testing yields favorable results with respect to solution time and quality when only electrical energy storage systems are included, and we restrict the number of discretized states of charge to at most five. However, by introducing thermal storage systems and doubling the number of discrete states for the battery’s charge, the solve time grows by a factor of 30.

Lastly, we solve a linear optimization model (D) with a state-of-the-art optimizer [54] to obtain solutions for the economic dispatch problem. The solve-time of the linear program compares favorably with that of the dynamic program. Through empirical testing, we determine that the linear program yields the best results with respect to solution time and quality and therefore, we choose to employ it for solving the economic dispatch for the fixed design and pre-established CHP operational schedule. While we use a commercial solver to obtain optimal solutions to the economic dispatch, several open-source tools perform similarly.

2.4.2.1 CHP Scheduling

Model (P) incorporates the ability to purchase electricity from the grid and therefore includes a common representation of an electric utility tariff. The optimal solution to (P) yields an operational schedule for the CHP system that reduces the two costs that constitute the majority of a utility bill: energy and peak demand.

The CHP scheduling procedure is separated into two components. First, we determine the “managed demand threshold,” or peak-shaving target (as depicted in Figure 2.3), for each demand period, where a demand period consists of a collection of hours in which a customer is charged according to the maximum power demanded from the utility. (Standard utility tariffs consist of two types of demand periods, month and time-of-use.) We assume that by minimizing the monthly demand charges, we also minimize time-of-use demand charges. However, \mathcal{J} can be constructed as any set of demand periods such that $\sum_{j \in \mathcal{J}} H_j = H$. We schedule the CHP system for operation at any hour when the electrical demand exceeds the threshold, which, if set too high, precludes the desired realization of peak-demand cost-savings. Conversely, if we set the threshold too low, the cost to dispatch energy from the CHP system would dominate the utility bill savings. Therefore, we employ Algorithm 2 to determine an appropriate peak-shaving target

for each demand period.

Second, we execute Algorithm 3 to schedule the CHP system (e.g., $Z_{th}^{to} = 1$ for $t = \text{CHP}$ and hour h). We iterate over each demand period j and each hour h in demand period j and assess whether: (i) the electrical demand is greater than the target; or, (ii) the marginal cost of meeting electrical and thermal loads through traditional means (i.e., utility and boiler) exceeds that of dispatching energy from the CHP system. We do not consider the cost-benefit tradeoff of dispatch to charge electrical storage. We use these values for Z_{th}^{to} to set the upper and lower bounds for CHP dispatch in phase (iii). The notation presented in Table 2.3 supports Algorithms 2 and 3.

Table 2.3 Additional notation for CHP scheduling.

Sets		
\mathcal{P}	Set of CHP sizes $\mathcal{Z}[b_t; X_t]$ for $t = \text{CHP}$	
\mathcal{J}	Demand periods	
H_j	Time steps within a given demand period j	
Parameters		
d_h^d	Electrical load in time step h	[kW]
h_h^h	Heating load in time step h	[kW]
f_{th}^{ha}	Hot water ambient correction factor of technology t at time step h	[-]
f_{th}^{ht}	Hot water thermal grade correction factor of technology t at time step h	[-]
k_t^{te}	Thermal energy production of CHP technology t per unit electrical output	[-]
k_t^{tp}	Thermal power production of CHP technology t per unit power rating	[-]
f_t^{td}	Minimum turn down for technology t	[-]
Variables		
X_j^t	Peak-shaving target for demand period j	[kW]

Algorithm 2 Determine peak-shaving targets, (i.e., the value to which the CHP system ought to be deployed to reduce peak-demand charges).

```

1: Inputs:  $P; J; H_j; \frac{d}{h}$ 
2: Output:  $X_j^t$ 
3:  $best \leftarrow 1$ 
4: for  $size \in P$  do
5:    $total \leftarrow 0$ 
6:   for  $j \in J$  do:
7:      $peak \leftarrow \max_{h \in H_j} \frac{d}{h}$ 
8:      $targ_j \leftarrow \max\{0, peak - size\}$ 
9:     for  $h \in H_j$  do
10:       $chp_h \leftarrow \max\{0, \frac{d}{h} - targ_j\}$ 
11:       $grid_h \leftarrow P_h^d - chp_h$ 
12:       $chp\_cost \leftarrow \sum_{h \in H_j} (cost^{chp}(chp_h))$ 
13:       $util\_cost \leftarrow cost^{demand}(targ_j) + \sum_{h \in H_j} cost^{energy}(grid_h)$ 
14:       $total \leftarrow total + chp\_cost + util\_cost$ 
15:      if  $total < best$  then
16:         $X_j^t \leftarrow targ_j$   $\quad .$  Update peak-shaving target for each tier  $j$ 
17:         $best \leftarrow total$ 
18: return  $X_j^t$ 

```

Algorithm 3 Determines hours during which to operate the CHP system using demand targets and marginal costs.

```

1: Inputs:  $J; H_j; X_t; X_j^t; \frac{d}{h}; \frac{h}{h}; f_{th}^{ha}; f_{th}^{ht}; f_{th}^p; f_{th}^{td}; k_t^{te}; k_t^{tp}$ 
2: Output:  $Z_{th}^{to}$ 
3:  $t \leftarrow \text{CHP}$ 
4:  $chp \leftarrow \frac{f_{th}^{td}}{k_t^{tp}} X_t$   $\quad .$  set CHP dispatch to minimum turn-down
5:  $chp\_cost \leftarrow cost^{chp}(chp)$ 
6: for  $j \in J$  do
7:   for  $h \in H_j$  do
8:      $Z_{th}^{to} \leftarrow 0$ 
9:     if  $\frac{d}{h} > X_j^t$  then
10:       $Z_{th}^{to} \leftarrow 1$   $\quad .$  schedule CHP if electric demand exceeds target
11:     else
12:       if  $(\frac{d}{h} > 0)$  then
13:          $elec \leftarrow \min\{f_{th}^{ha}; \frac{d}{h}\}$ 
14:          $thermal \leftarrow 0$ 
15:         if  $\frac{h}{h} > 0$  then
16:            $thermal \leftarrow \min\{f_{th}^{ha}; f_{th}^{ht} (k_t^{te} f_{th}^p chp + k_t^{tp} X_t)\}; \frac{h}{h}$ 
17:            $util\_boil \leftarrow cost^{util}(elec) + cost^{boil}(thermal)$ 
18:           if  $chp\_cost < util\_boil$  then
19:              $Z_{th}^{to} \leftarrow 1$   $\quad .$  schedule CHP if its cost is lower than that associated with tradi-
            tional means
20: return  $Z_{th}^{to}$ 

```

2.4.2.2 Economic Dispatch

Instead of a myopic policy that produces low-quality solutions to model (P) or a dynamic program that results in slow solve times, we incorporate an optimization model (D) to perform the economic dispatch. Model (P) contains seven types of discrete (binary) variables, three of which relate to the microgrid's configuration which are fixed according to the method given in Section 2.4.1. The CHP scheduling routine presented in Section 2.4.2.1 obtains the value of the binary variable Z_{th}^{to} , which constitutes more than 95% of the discrete variables, and, with that, we calculate the fixed y -intercept b_h^{chp} found in Constraint (2.6c). We remove the remaining three discrete variables which force utility pricing tiers to be charged in a specific order by aggregating the utility demand tiers and eliminating the need for constraint groups (1.10)-(1.12). The removal of the binary variables and associated constraints yields the linear model (D) for which we present the notation and the mathematical formulation. The output of the model is the economic dispatch associated with a fixed system design. We repair the solution returned by (D) to restore feasibility to (P) by computing, ex post, the binary variable values for each of the utility demand tiers.

Sets

B		Storage systems
H		Hours
\mathcal{M}		Months
R		Time-of-use demand periods
T		Technologies
B^e	B	Electrical storage system
B^c	B	Cold thermal storage system
B^h	B	Hot thermal storage system
H_m^m	H	Hours in month m
H_r^f	H	Hours in tier r
T^e	T	Electric producing technologies
T^{CHP}		CHP producing technologies
T		
T^{th}	T	Thermal energy producing technologies
T^c	T^{th}	Cold producing technologies
T^{ec}	T^{th}	Electric chiller technologies
T^{ac}	T^{th}	Absorption chiller technologies
T^s	T^e	Technologies that can sell to the utility
T_b^b	T	Technologies that can charge storage system
	b	

Load Parameters

Units

d_h	Electric load in hour h	[kW]
h_h	Heating load in hour h	[kW]
c_h	Cooling load in hour h	[kW]
Cost Parameters		Units
ac	Capital cost of absorption chiller	[\$/kW]
c_{th}	Fuel cost for technology t in hour h	[\$/kWh]
d_m	Peak demand charge in month m	[\$/kW]
e_h	Energy price in hour h	[\$/kWh]
r_r	Peak demand charge in time-of-use period r	[\$/kW]
s_h	Energy sales price in hour h	[\$/kWh]

Power Rating and Fuel Limit Parameters

\bar{b}_{th}^e	Maximum electric production available for technology t in hour h	[kW]
\bar{b}_{th}^{th}	Maximum thermal production available for technology t in hour h	[kW]
\bar{g}_s	Maximum allowable grid sales	[kWh]

Storage Parameters

\bar{w}_b^{kW}	Maximum power output of storage system b	[kW]
\bar{w}_b^{kWh}	Maximum state of charge of storage system b	[kWh]
\bar{w}_b^{mcp}	Minimum percent state of charge of storage system b	[fraction]
w_b^d	Decay rate of storage system b	[1/h]
w_b^0	Initial percent state of charge of storage system b	[fraction]

E fficiency Parameters

\bar{b}_{bt}^+	Efficiency of charging storage system b using technology t	[fraction]
\bar{b}_b^-	Efficiency of discharging storage system b	[fraction]
ac	Absorption chiller efficiency	[fraction]
ec	Electric chiller efficiency	[fraction]
g^+	Efficiency of charging electrical storage using grid power	[fraction]
$mchp$	Thermal efficiency slope for CHP	[fraction]
$bchp_h$	Thermal efficiency intercept for CHP in hour h	[kW]

Scaling Parameters

Γ	Time step scaling	[h]
----------	-------------------	-----

Decision Variables

X^{ac}	Size of absorption chiller	[kW]
X_m^d	Peak energy purchased in month m	[kW]

X_{bh}^{dfs}	Energy discharged from storage system b in hour h	[kW]
X_h^g	Energy from the grid in hour h	[kW]
X_h^{gts}	Energy from the grid used to charge the battery in hour h	[kW]
X_{th}^{ptg}	Energy produced by technology t in hour h and sold to the grid	[kW]
X_{th}^{pts}	Energy energy from technology t used to charge the battery in hour h	[kW]
X_r^r	Peak energy purchased in time-of-use period r	[kW]
X_{th}^{rp}	Energy produced by technology t during hour h	[kW]
X_{bh}^{sc}	State of charge of storage system b in hour h	[kWh]
X_h^{stg}	Energy from the battery sold to the utility in hour h	[kW]
X_{th}^{tp}	Thermal energy produced by technology t during hour h	[kW]

(D) **Objective:** Minimize Cost:

$$\begin{aligned}
\text{minimize} \quad & \sum_{h \in \mathcal{H}} e_h \Gamma X_h^g + \sum_{m \in \mathcal{M}} d_m X_m^d + \sum_{r \in \mathcal{R}} r_r X_r^r + \sum_{h \in \mathcal{H}} s_h \Gamma (X_{th}^{ptg} + X_h^{stg}) \\
& + \sum_{t \in \mathcal{T}^{CHP}; h \in \mathcal{H}} c_{th} \Gamma X_{th}^{rp} + \sum_{t \in \mathcal{T}^{th}; h \in \mathcal{H}} r_{2B} X_{th}^{tp} + \sum_{t \in \mathcal{T}^e} c_{th} \Gamma X_{th}^{tp} + \sum_{t \in \mathcal{T}^{ac}} ac X^{ac}
\end{aligned}$$

The objective function minimizes the cost of energy purchased from the utility, including peak demand costs, less energy sales, plus the cost to dispatch available technologies and the cost to procure the absorption chiller.

Model (D) minimizes lifecycle costs subject to the following constraints:

Load Balance

$$\begin{aligned}
& \sum_{h \in \mathcal{H}} d_h + \sum_{t \in \mathcal{T}^e} X_{th}^{pts} + \sum_{t \in \mathcal{T}^s} X_{th}^{ptg} + X_h^{gts} + X_h^{stg} + \sum_{t \in \mathcal{T}^{ec}} \frac{X_{th}^{tp}}{ec} - \sum_{b \in \mathcal{B}^e} X_{bh}^{dfs} - \sum_{t \in \mathcal{T}^{ac}} X_{th}^{tp} = 0 \quad \forall h \in \mathcal{H} \quad (2.3a)
\end{aligned}$$

$$\begin{aligned}
& \sum_{t \in \mathcal{T}^{th}} X_{th}^{tp} + \sum_{b \in \mathcal{B}^h} X_{bh}^{dfs} - \sum_{b \in \mathcal{B}^h; t \in \mathcal{T}_b^b} X_{th}^{pts} + \sum_{t \in \mathcal{T}^{ac}} \frac{X_{th}^{tp}}{ac} = 0 \quad \forall h \in \mathcal{H} \quad (2.3b)
\end{aligned}$$

$$\sum_{t \in T^c} X_{th}^{tp} + \sum_{b \in B^c} X_{bh}^{dfs} + \sum_{h \in H} c_h + \sum_{b \in B^c; t \in T_b^b} X_{th}^{pts} \quad (2.3c)$$

Constraints (2.3a)-(2.3c) ensure that the energy dispatched from the installed technologies plus the energy purchased from the utility (if applicable) meets or exceeds the demanded electric, heating, and cooling load, respectively.

Storage Operations

$$X_{bh}^{sc} - X_{b,h-1}^{sc} = \sum_{t \in T_b^b} \left(\Gamma X_{th}^{pts} + \Gamma X_h^{gts} - \frac{\Gamma X_{bh}^{dfs}}{b} \right) \quad \forall b \in B^e; h \in H \quad (2.4a)$$

$$X_{bh}^{sc} - X_{b,h-1}^{sc} = \sum_{t \in T_b^b} \left(\Gamma X_{th}^{pts} + \Gamma X_h^{gts} - \frac{\Gamma X_{bh}^{dfs}}{b} \right) - w_b^d X_{bh}^{sc} \quad \forall b \in B \cap B^e; h \in H \quad (2.4b)$$

$$X_{b,0}^{sc} = w_b^0 \bar{w}_b^{bkWh} \quad \forall b \in B \quad (2.4c)$$

$$\sum_{h \in H} \left(\frac{w_b^{mcp} \bar{w}_b^{bkWh}}{w_b^{bkWh}} X_{bh}^{sc} - \bar{w}_b^{bkWh} \right) \leq B \quad \forall b \in B; h \in H \quad (2.4d)$$

$$\sum_{h \in H} \left(X_{th}^{pts} + X_h^{gts} + X_{bh}^{dfs} \right) \leq \bar{w}_b^{bkW} \quad \forall b \in B^e; h \in H \quad (2.4e)$$

$$\sum_{t \in T_b^b} \left(X_{th}^{pts} + X_{bh}^{dfs} \right) \leq \bar{w}_b^{bkW} \quad \forall b \in B \cap B^e; h \in H \quad (2.4f)$$

Energy inventory in electrical and thermal storage is governed by constraints (2.4a) and (2.4b). The net difference in the storage system equals the amount of energy sent to storage less the amount dispatched from storage. We incorporate thermal loss through the parameter w_b^d for the storage system b . Constraint (2.4c) dictates an initial state of charge equal to a specified percentage of storage capacity. Constraint (2.4d) limits the state of charge of storage system b to be between the installed capacity and a minimum percent of the capacity. Constraints (2.4e) and (2.4f) ensure that the amount of energy sent to storage or dispatched from storage in hour h does not exceed the specified power rating.

Utility Operations

$$X_m^d - X_h^g \leq M \quad \forall m \in M; h \in H_m^m \quad (2.5a)$$

$$X_r^r - X_h^g \leq R \quad \forall r \in R; h \in H_r^r \quad (2.5b)$$

$$\sum_{h \in H} \left(X_h^g - X_h^{gts} \right) \leq H \quad (2.5c)$$

$$\sum_{b \in B^e} \left(X_{bh}^{dfs} - X_h^{stg} \right) \leq H \quad (2.5d)$$

$$\sum_{h \in H} \left(\sum_{t \in T^s} \Gamma X_{th}^{ptg} + \Gamma X_h^{stg} \right) \leq \bar{x}_{gs} \quad (2.5e)$$

$$\sum_{h \in H} \left(\sum_{t \in T^s} X_{th}^{ptg} + X_h^{stg} \right) \leq \sum_{h \in H} X_h^g \quad (2.5f)$$

Constraints (2.5a) and (2.5b) ensure that the peak grid purchase for month m and time-of-use period r exceed the amount of energy purchased in all hours of the associated time frame.

Constraint (2.5c) limits the energy from the utility used to charge the storage system to be less than what is purchased from the grid. Likewise, Constraint (2.5d) ensures that energy sold to the grid is less than what is dispatched from the electrical storage system. Constraints (2.5e) and (2.5f) prohibits grid sales from exceeding the net-metering limit and the total amount of energy purchased.

Production

$$X_{th}^{rp} \leq \bar{b}_{th}^e \quad \forall t \in T^e; h \in H \quad (2.6a)$$

$$X_{th}^{tp} \leq \bar{b}_{th}^{th} \quad \forall t \in T^{th}, n \in T^{CHP}; h \in H \quad (2.6b)$$

$$X_{th}^{tp} = X_h^{bchp} + X_{th}^{mchp} \quad \forall t \in T^{CHP}; h \in H \quad (2.6c)$$

$$X_{th}^{tp} \leq X_{th}^{ac} \quad \forall t \in T^{ac}; h \in H \quad (2.6d)$$

$$X_{th}^{pts} \leq X_{th}^{rp} \quad \forall t \in T_b^e; h \in H \quad (2.6e)$$

$$X_{th}^{pts} + X_{th}^{ptg} \leq X_{th}^{rp} \quad \forall t \in T_b^e \setminus T^s; h \in H \quad (2.6f)$$

$$X_{th}^{pts} \leq X_{th}^{tp} \quad \forall t \in T_b^b; h \in H \quad (2.6g)$$

Constraints (2.6a)-(2.6d) govern the production of electric and thermal technologies.

Specifically, the CHP scheduling routine determines the values of \bar{b}_{th}^e , X_h^{bchp} and X_{th}^{mchp} which yield both the upper limit of electrical production for the CHP system and also the thermal contribution. Constraint (2.6d) limits the amount of production from the absorption chiller to be less than its rated capacity. The absorption chiller is the only technology with a sizing variable in the economic dispatch linear program. Constraints (2.6e)-(2.6g) limit the energy (electrical and thermal) from the microgrid that is either sold to the utility or sent to storage to what is produced by technology t in hour h .

Non-negativity

$$X_{th}^{ac} \geq 0 \quad (2.7a)$$

$$X_h^{gts}, X_h^{stg}, X_h^g \geq 0 \quad \forall h \in H \quad (2.7b)$$

$$X_m^d \quad 0 \quad 8m \quad 2 \quad M \quad (2.7c)$$

$$X_r^r \quad 0 \quad 8r \quad 2 \quad R \quad (2.7d)$$

$$X_{bh}^{dfs}, X_{bh}^{sc} \quad 0 \quad 8b \quad 2 \quad B; h \quad 2 \quad H \quad (2.7e)$$

$$X_{th}^{rp}, X_{th}^{tp}, X_{th}^{pts}, X_{th}^{ptg} \quad 0 \quad 8t \quad 2 \quad T; h \quad 2 \quad H \quad (2.7f)$$

2.5 Results

This section summarizes a collection of instances of model (P), then presents the performance of (M^H) relative to directly solving each instance using a commercial, off-the-shelf mixed-integer programming optimizer. We refer to the latter method as (M^O).

2.5.1 Inputs

We use the same inputs given in Hirwa et al. [9], which include differing building types, utility pricing schedules, monthly and time-of-use demand periods, and electrical and thermal loads. Table 2.5 reflects distinguishing features for the 12 test cases, providing only those inputs necessary to reveal the differences. All but one of the cases (6) include electrical and heating loads. The most complex test case (9) consists of the greatest number of technologies and incorporates a cooling thermal load.

Table 2.5 Salient features of the 12 cases.

Case	Technologies [†]	\bar{c}_m^d (\$/kW)	\bar{c}_r^r	\bar{c}_h^g (\$/kWh)	\bar{d}_h^d (kW)
1	CHP, Boiler	20	5	0.1	7,752
2	CHP, Boiler	19	5	0.11	7,752
3	CHP, Boiler, TES	19	5	0.11	7,752
4	CHP, Boiler, PV, BES	19	5	0.11	7,752
5	CHP, Boiler, PV, BES	16	0	0.04	7,752
6 ¹	PV, Wind, BES	19	0	0.06	30,015
7	CHP, Boiler, PV, BES	0	0	0.04	7,752
8	CHP, Boiler, PV, BES	20	5	0.1	7,752
9 ²	CHP, Boiler, PV, EC, BES, TES, AC	20	5	0.1	6,325
10	CHP, Boiler	20	5	0.1	6,085
11	CHP, Boiler	20	5	0.1	2,206
12	CHP, Boiler	20	5	0.1	229

Note: The right four columns are the average values for each parameter. We only include a subset of inputs to show distinguishing features between cases. The parameters \bar{c}_m^d , \bar{c}_r^r , \bar{c}_h^g , and \bar{d}_h^d designate the average values for monthly and time-of-use demand charges, hourly energy price, and hourly electric load, respectively.

[†]TES: Thermal Energy Storage, BES: Battery Electrical Storage, PV: Photovoltaic, EC: Electric Chiller, AC: Absorption Chiller.

¹ Electric only.

² Electric, heating, and cooling loads.

2.5.2 Genetic Algorithm

To measure the performance of our genetic algorithm, we compare the objective function value of the lowest-cost solution from each iteration to that of the solution at termination. Figure 2.7 depicts all 12 cases, of which some overlap, and shows how quickly our implementation converges. For all but two of the 12 cases, the genetic algorithm finds the best microgrid configuration in fewer than 90 seconds. Case 4 struggles with convergence due, in part, to the target size of the photovoltaic system. Case 9 is the only case that includes electric, heating, and cooling loads and all available technologies; although it requires more time to terminate, it finds a solution with an objective function value within 1% of the lowest-found objective function value almost immediately.

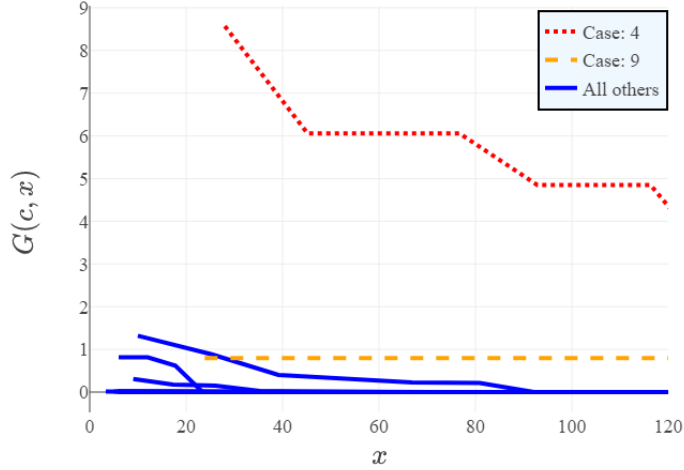


Figure 2.7 Genetic algorithm progress for which x is the wall-clock elapsed time, $G(c; x) = \frac{L_{cx} - L_c}{L_{cx}}$, L_x is the objective function value associated with the best-found design for case c at time x , and L_c is the lowest overall objective function value found by (\mathbf{M}^H) for case c .

2.5.3 Solution Quality

Heuristics are unable to return optimality gaps; therefore, we use optimization software, executed under a two-hour time limit, to obtain a lower bound (LB_c) for each case $c \in \mathcal{C}$ against which to compare with the objective function value of the best feasible solution from (\mathbf{M}^H) and (\mathbf{M}^O) . We utilize standard performance profiles [55] to show how the objective function values produced by (\mathbf{M}^H) compare to (\mathbf{M}^O) relative to our threshold for success. We define x as the percent difference between the objective function value of the best feasible solution after a two-minute time limit and LB_c for each case c . We define \hat{g}_{cm} as the percent difference from LB_c for case c obtained by method m . Figure 2.8 reflects $p_m^g(x)$ (Equation (2.8)), the proportion of the 12 cases that achieve the percent difference (x) after a two-minute time limit for each method m .

$$p_m^g(x) = \frac{\mathbb{P} \{ \hat{g}_{cm} < x \}}{jCj} \quad (2.8)$$

We show that using (\mathbf{M}^H) , just under 80% of the tested cases result in objective function values that achieve less than a 1% difference from LB_c after two minutes, whereas one-third of the cases solved by (\mathbf{M}^O) achieve the same performance. Furthermore, only one case yields a

solution with an objective function value that is greater than 5% or more relative to LB_c when solved using (\mathbf{M}^H) ; conversely, fewer than 60% of the cases solved by (\mathbf{M}^O) achieve less than a 5% optimality gap in the two-minute time limit.

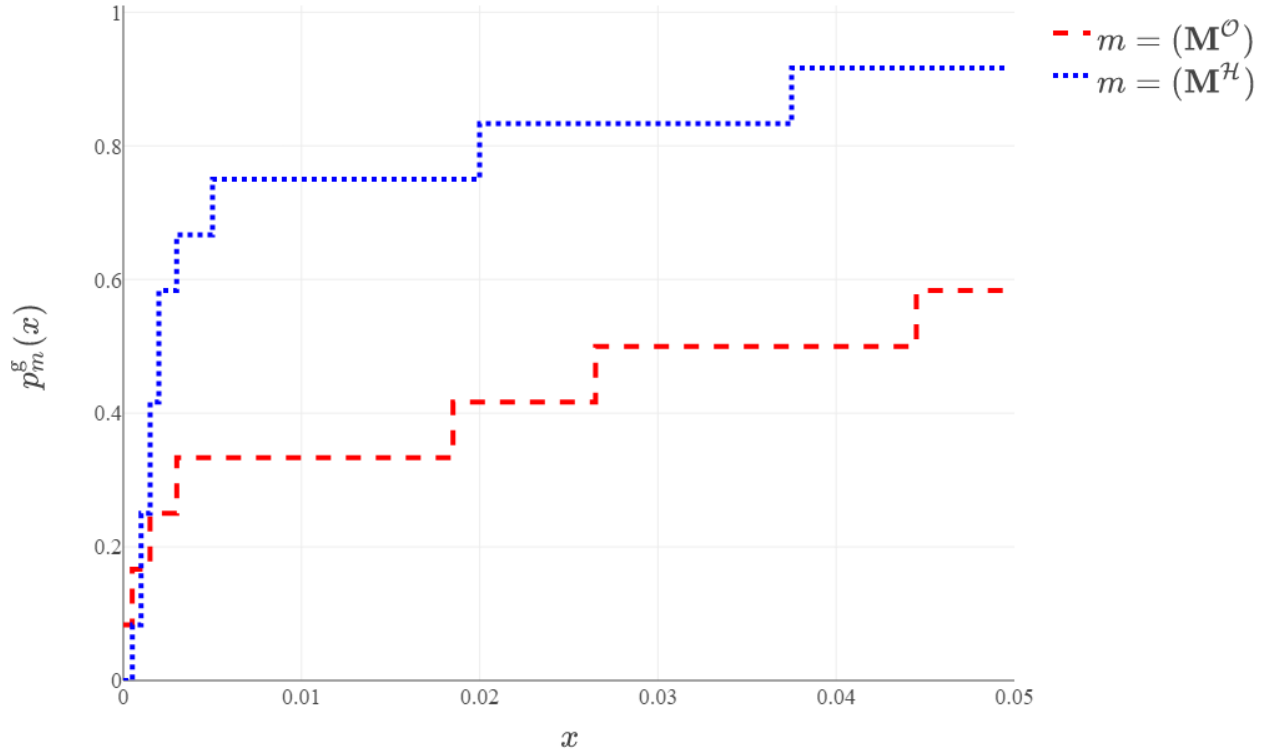


Figure 2.8 Performance plot comparison of objective function values returned by (\mathbf{M}^H) and (\mathbf{M}^O) , measuring the proportion of cases ($p_m^g(x)$) using method m that are below the optimality threshold x after two minutes using method m .

Figure 2.9 reflects a time-dependent (versus solution-dependent) performance measure, ideal for users interested in obtaining good solutions without lengthy wait times. We define \tilde{g}_{cxm} as the percent difference from LB_c for case c at wall-clock time x obtained by method m . Equation (2.9) defines the proportion of cases that achieve an objective function value of at most 5% gap relative to LB_c at wall-clock time x . Method (\mathbf{M}^H) outperforms (\mathbf{M}^O) with respect to time. Over 90% of the tested cases achieve the desired gap in under half a minute. Conversely, method (\mathbf{M}^O) yields only one objective function value, of the 12 tested, below a 5% gap in the same amount of time.

$$p_m^s(x) = \frac{c2c \mathbb{P}[\tilde{g}_{cxm} < 0.05]}{jCj} \quad (2.9)$$

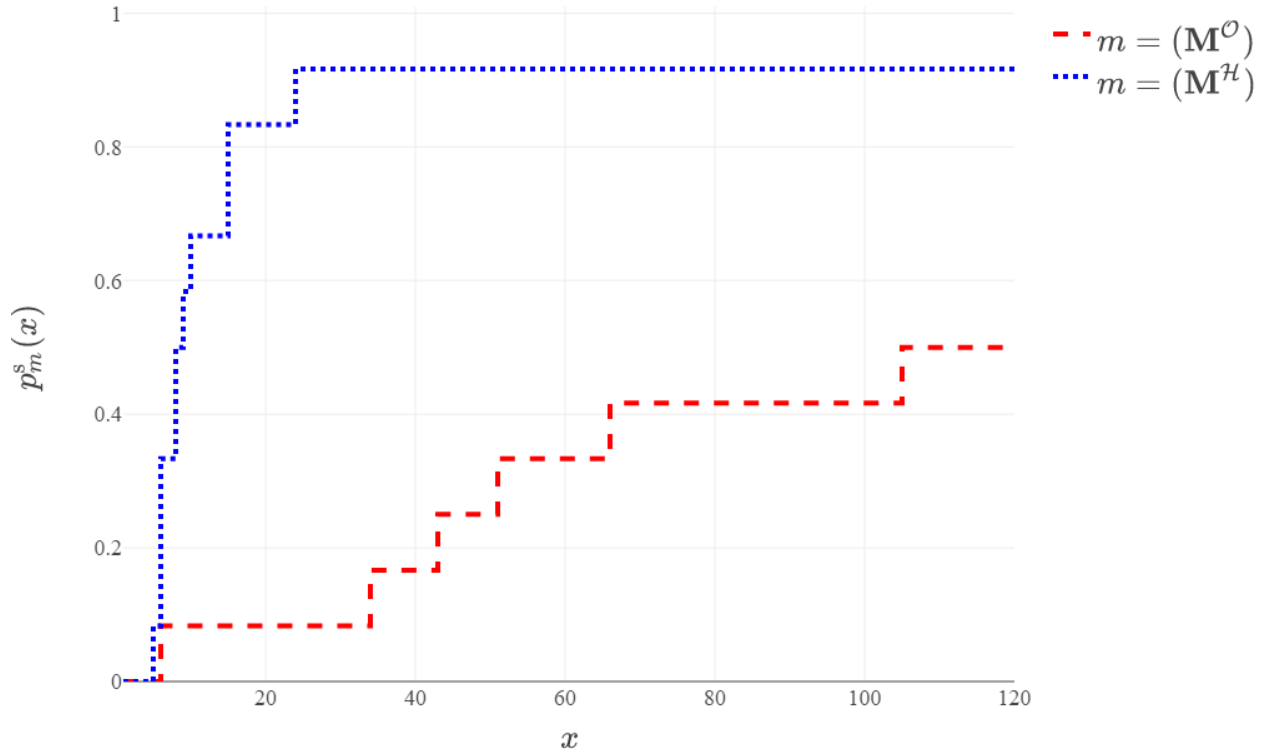


Figure 2.9 Performance plot comparison of solutions returned by (\mathbf{M}^H) and (\mathbf{M}^O) , measuring the proportion of cases $(p_m^s(x))$ using method m that are below 5% optimality gap after x seconds using method m .

Table 2.6 compares solutions returned by (\mathbf{M}^H) and (\mathbf{M}^O) for each of the 12 cases after a two-minute time limit. (\mathbf{M}^H) outperforms (\mathbf{M}^O) with respect to objective function value in eight of the 12 cases (shown in green). Method (\mathbf{M}^O) obtains a better objective function value for cases 2, 6, 7, and 8; however, the difference between solutions is less than one-third of a percent. (\mathbf{M}^O) is unable to return a solution for Case 4 in the allotted time.

Table 2.6 Solving (P) using (\mathbf{M}^O) and (\mathbf{M}^H) after a two-minute time limit. Microgrid capacity is the sum of that generated by all technologies, including the power rating of the electrical storage system.

Case	Microgrid Capacity (kW)		Objective Function (\$)		Cost Difference	
	(\mathbf{M}^O)	(\mathbf{M}^H)	(\mathbf{M}^O)	(\mathbf{M}^H)	(\$)	(%)
1	1,018	1,066	13,463,711	13,431,907	-31,804	-0.24
2	1,014	1,013	17,557,957	17,570,920	12,963	0.07
3	25,640	24,712	18,381,833	17,423,310	-958,523	-5.21
4 [†]	-	6,009	-	14,022,107	-	-
5	1,894	1,330	7,228,259	7,015,378	-212,881	-2.95
6	2,421	2,046	34,241,073	34,284,021	42,948	0.13
7	1,185	1,185	3,851,749	3,853,632	1,883	0.05
8	3,742	3,782	11,810,342	11,849,333	38,991	0.33
9	43,286	42,996	13,889,468	11,575,754	-2,313,714	-16.66
10	2,751	3,009	12,193,062	12,005,279	-187,783	-1.54
11	597	597	4,139,826	4,138,999	-827	-0.02
12	169	169	868,367	865,945	-2,422	-0.28

Note:

Time limit for optimizer is 120 seconds, Delta: Difference in objective function values obtained from the (\mathbf{M}^H) and (\mathbf{M}^O).

A negative value reflects that (\mathbf{M}^H) outperforms the solver in the allotted time.

†Solver did not return a feasible solution within the two-minute time limit.

A user of the REopt[®] tool is most interested in the microgrid configuration. Although dispatch informs the configuration, an operational strategy would be determined under a fixed design on a shorter (i.e., less-than-a-year) time horizon at a finer (i.e., less-than-an-hour) fidelity. To this end, we examine microgrid configurations that the heuristic produces relative to those determined by the optimizer. Figure 2.10 shows that, in each case, the configurations are almost identical, with slight differences for cases 3, 6, 8, and 9. The biggest discrepancy occurs in case 3, resulting from the added benefit of a large hot-thermal storage system which reduces the co-generational economic impact and thus contributes to a larger amount of energy dispatched from the CHP system associated with the solution returned by (\mathbf{M}^H). Despite these differences in design, there is less than a 2% difference in objective function values across all cases. In addition, the collection of top-performing configurations, examined by (\mathbf{M}^H), provides users key insights about the types of technologies whose installation would yield cost savings. Furthermore, the Matheuristic-produced solutions could be used to warm-start the solver.

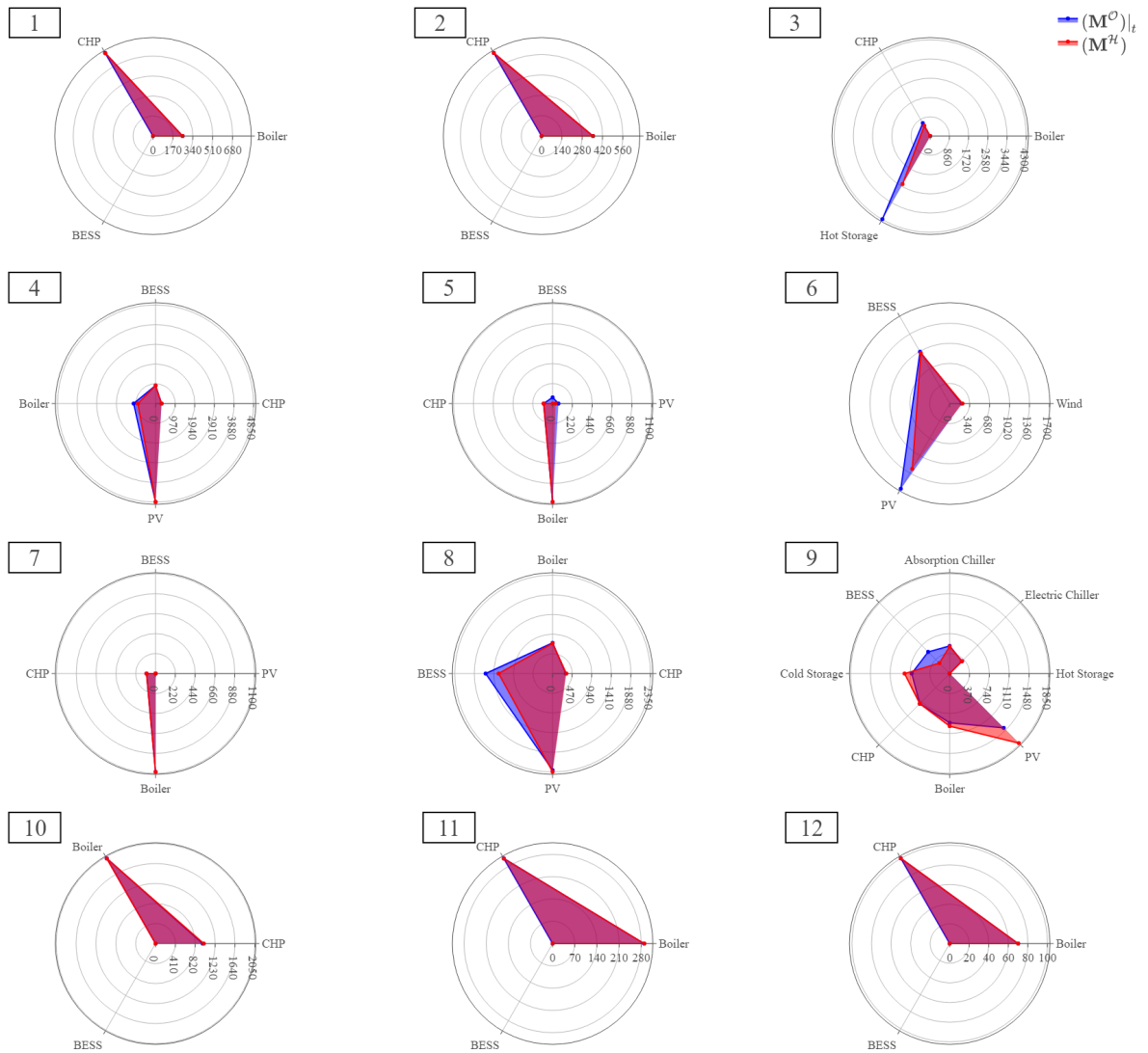


Figure 2.10 Microgrid configuration comparison of all 12 cases. Radial length reflects the installed capacity of the technology.

2.6 Conclusion

This paper proposes a custom Matheuristic for designing and dispatching a utility-connected microgrid to combat the long solve times associated with some instances of the optimization model. Because REopt[®] is leveraged by users as a web-based tool to test a variety of inputs, timely solutions are necessary. Our method, (\mathbf{M}^H), contains three phases: (i) a genetic algorithm to obtain a design; (ii) a policy-based procedure to determine the operational schedule for the CHP system; and, (iii) an optimization model to generate economic dispatch. We compare the performance of our heuristic, (\mathbf{M}^H), to a direct solve of the optimization model, (\mathbf{M}^O), using run time and the objective function value corresponding to best solution found as metrics. (\mathbf{M}^H) outperforms (\mathbf{M}^O) in eight of the 12 cases under a two-minute time limit. Furthermore, there are instances in which no solution is obtained using (\mathbf{M}^O), whereas (\mathbf{M}^H) is successful. Additionally, we show that using a more aggressive time limit of 30 seconds, (\mathbf{M}^O) yields only one case with an objective function value within 5% of LB_c (the exogenously produced lower-bound), whereas (\mathbf{M}^H) produces 11 of 12 within 5%.

In addition to obtaining good solutions quickly, (\mathbf{M}^H) can evaluate many potential, feasible designs that could be used in a sensitivity study or as a Pareto frontier for multi-objective optimization. The energy dispatch subroutine could be used as a stand-alone tool to inform operational control decisions of an existing microgrid with CHP. Absent a time limit, (\mathbf{M}^O) yields better solutions, but the required duration may be prohibitive for real-world applications.

Energy system models are becoming increasingly complicated, requiring the implementation of alternative solution methodologies to obtain optimal or near-optimal solutions. Our heuristic framework is extendable to mathematical programming formulations of other energy systems and allows modelers to incorporate complexities that might prove intractable if invoked as a direct solve of a monolithic optimization model. Additionally, while our approach is energy-focused, the concepts of our Matheuristic are generalizable to any problem that comprises strategic decisions utilizing operational controls, and helps to overcome the computational complexity of optimization problems while providing practical and efficient solutions, especially when addressing elaborate and large-scale systems.

Future work entails: (i) improving the Matheuristic performance and (ii) incorporating features to enhance the performance of microgrids. For example, including thermal storage impacts and electrical energy sales into CHP scheduling decisions can help address inconsistencies with system sizes, and can align solutions with optimal configurations. Users could also explore the tradeoff between emissions reduction and lifecycle cost in a multi-objective setting.

2.7 Acknowledgements

This work was authored by the National Renewable Energy Laboratory, operated by Alliance for Sustainable Energy, LLC, for the U.S. Department of Energy (DOE) under Contract No. DE-AC36-08GO28308. Funding was provided by the U.S. Department of Energy Advanced Manufacturing Office.

CHAPTER 3

NORTH CAROLINA WATER UTILITY BUILDS RESILIENCE WITH DISTRIBUTED ENERGY RESOURCES

Modified from a paper published in the *Journal of Applied Analytics*

Kate Anderson^{5,6}, James C. Grymes⁷, Alexandra Newman³, Adam Warren⁵

3.1 Abstract

As the frequency and duration of grid outages increase, backup power systems are becoming more important for ensuring critical infrastructure can continue to provide essential services. Most facilities rely on diesel generators, which may be ineffective during long outages due to limited fuel supplies and high generator failure rates. Distributed energy resources such as solar, storage, and combined-heat-and-power systems offer an alternative source of on-site generation that can provide both cost savings and resilience (i.e., the ability to respond to catastrophic events with longer-term consequences). A mixed-integer linear program minimizes costs and maximizes resilience at a wastewater treatment plant in Wilmington, North Carolina. We find that the plant can reduce life cycle energy costs by 3.1% through the installation of a hybrid combined-heat-and-power, photovoltaic, and storage system. When paired with existing diesel generators, this system can sustain full load for seven days while saving \$664,000 over 25 years and reducing diesel fuel use by 48% compared to the diesel-only solution. This analysis was used to inform a decision by Cape Fear Public Utility Authority to allocate funds for implementation of a combined heat and power system at the wastewater treatment plant in fiscal year 2023.

3.2 Introduction

Climate change is increasingly exposing weaknesses in the United States power system, evident in the widespread outages resulting from recent hurricanes, winter storms, and wildfires Fant et al. [4]. As the frequency and duration of grid interruptions increase NOAA [56], backup

⁵National Renewable Energy Laboratory

⁶Primary researcher and author

⁷Operations Research with Engineering Graduate Program, Colorado School of Mines

power systems are becoming more important for ensuring that critical infrastructure such as hospitals, water treatment facilities, and fire stations can continue to provide essential services during natural disasters. Most critical facilities rely on diesel generators Hotchkiss [57], with fuel storage typically sized to sustain power for periods of a few hours up to two days. For extended outages, facilities rely on periodic re-supplies of fuel. However, failures in supply chains are common during natural disaster-induced outages when roads become impassable due to fires or flooding, and limited fuel supplies may be diverted to higher priority needs Anderson et al. [58]. Furthermore, generators themselves are likely to fail during longer outages Marqusee et al. [59]. For these reasons, facility managers are seeking alternative backup power options.

Distributed energy resources such as solar, storage, and combined-heat-and-power systems are increasingly common sources of on-site power generation, and can reduce emissions and provide some or all of the energy needed at a lower cost than purchasing energy from a utility company. They can also be configured to yield backup power in the event of an outage Anderson et al. [60]. However, generation sized to maximize economic savings may be insufficient to sustain critical load for an extended outage. An important concept for strategic planning in uncertain environments is *energy resilience*, broadly defined as “the ability to anticipate, prepare for, and adapt to changing conditions and withstand, respond to, and recover rapidly from disruptions” Hotchkiss et al. [61], Bhusal et al. [62]. To increase resilience, operators may install a larger system whose operational cost savings may not be sufficient to cover the higher capital cost; site owners must therefore balance capital costs, operating expenses, and resilience.

We consider a wastewater treatment plant in North Carolina, a critical facility that is susceptible to hurricane-induced outages Chinoy [63]. This area was significantly impacted by Hurricane Matthew in 2016 Jisan et al. [64], which caused over \$5 billion of damage, and again by Hurricane Florence in 2018 Paul et al. [65] that caused approximately \$17 billion of damage. Driven by climate change, these high-magnitude storms are expected to become more frequent Mann and Emanuel [66].

As critical infrastructure, it is essential to ensure that wastewater treatment plants remain powered during grid outages. Pump failure may lead to direct discharge of untreated sewage to rivers and streams or sewage backup into homes and businesses. At the same time, water and wastewater facilities operate 24 hours a day, seven days a week, and can be among the largest

consumers of energy in a community. Drinking water and wastewater systems account for 3-4% of energy use in the United States, and about 35% of typical U.S. municipal energy budgets EPA [67]. Therefore, energy efficiency measures, distributed energy resources, and operational adjustments can provide significant savings.

For wastewater treatment plants with anaerobic digesters, combined-heat-and-power systems can effectively reduce utility-purchased electricity and heat while providing resilience on-site. Combined-heat-and-power systems concurrently produce electricity and thermal energy from a single source of energy. Because they are distributed generation sources, located at the point of use rather than at a central utility plant, the heat that is normally lost in the power generation process can be recovered to provide needed heating and/or cooling. Combined-heat-and-power systems can use a variety of fuels, and are particularly effective at wastewater treatment plants which require both electricity and heat, and generate free on-site methane gas in their anaerobic digesters. As an approximation, each million gallons per day of wastewater flow can generate enough biogas in an anaerobic digester to produce 26 kilowatts (kW) of electric capacity and 2.4 million British thermal units (BTU) per day of thermal energy in a combined-heat-and-power system EPA [67].

Operational adjustments, such as load shifting, can also provide cost savings and increase resilience at wastewater treatment plants by moving power demand from peak times when electricity is more expensive to off-peak times when electricity costs are lower, and by reducing loads during grid outage periods. Wastewater treatment plants are well suited to shed or shift electric loads in response to financial incentives, bill savings, or opportunities to enhance reliability of service. Variable frequency drives can be used to control the speed of aerator blower motors and pumps in order to reduce demand. If there is advance warning of a need to induce demand response or of an outage event, loads can also be shifted by over-oxygenating stored wastewater prior to the event, and then turning off aerators during the event. Shifting can also be accomplished by storing wastewater or treated effluent and then processing it later Aghajanzadeh et al. [68]. The ability to shift loads allows the plant to continue operating with reduced energy consumption during a grid outage.

This real-world application focuses on reducing energy costs and increasing resilience at the Northside wastewater treatment plant run by Cape Fear Public Utility Authority, the water

utility in Wilmington, North Carolina, which currently purchases all of its energy from the local electric utility, and uses two emergency backup diesel generators to provide power during grid outages. The utility identified two potential opportunities to improve current operations. First, approximately half of the methane gas produced on-site in the anaerobic digesters is flared, representing a free, underutilized energy source that could be converted to electricity, and used to power the facility at lower cost. Second, the plant is reliant on diesel fuel for backup power during grid outages, which are common due to frequent hurricanes. During emergencies, diesel fuel for county critical infrastructure is in high demand, and re-supply can be difficult. Therefore, reducing reliance on diesel fuel at the wastewater treatment plant would help ensure that not only the plant, but also over 150 other pump stations and wells in the county, have sufficient diesel to operate during grid outages. We investigate distributed energy technologies including combined heat and power, solar photovoltaics, and battery storage using an optimization model that balances the competing objectives of reducing cost and increasing resilience.

3.3 Literature Review

Many models minimize only the cost of designing a distributed energy system. Bollapragada et al. [69] offer a decision support tool used to guide renewable energy investment decisions to minimize the cost of meeting state renewable energy portfolio requirements. Udell and Toole [70] optimize the design of solar photovoltaic systems to minimize cost while meeting desired energy output, physical, and legal constraints, while Fischetti et al. [71] optimize offshore wind farm design to minimize installation and interconnection costs. For additional examples, Theo et al. [18] provide a review of 51 optimization models used in the design of distributed energy systems, many formulated to minimize cost.

Fewer models extend the consideration of cost to incorporate multiple objectives, such as minimizing emissions for combined-heat-and-power and district heating systems. For example, Fazlollahi and Maréchal [72] use a multi-objective mixed integer linear program to minimize cost and emissions of integrating biomass energy in a city district heating system via an evolutionary algorithm. Zhang et al. [73] employ a sigma-constraint method to optimize design of combined-heat-and-power-based microgrids for economic and environmental sustainability. Kang and Liu [74] optimize the design of a heat pump [74] to minimize annual cost and maximize annual

carbon dioxide emissions reduction, while Falke et al. [75] optimize efficiency measures and generation in a district energy system to develop a Pareto frontier of solutions that balance cost and emissions. Wu et al. [76] minimize the weighted sum of cost and emissions for a distributed energy network integrated with heating pipelines by considering technologies such as combined heat and power, solar, storage, and the utility grid. Di Somma et al. [77] apply a similar weighted sum approach to minimize cost and emissions in distributed energy systems including combined heat and power, but focus only on operational, to the exclusion of investment, decisions.

Some literature optimizes both economic and reliability objectives, where reliability is defined as the ability to “maintain power delivery to customers in the face of routine uncertainty in operating conditions” Kintner-Meyer et al. [78], reflecting typical uncertainty in load, generation, and fuel availability Murphy et al. [79]. For example, Moradi and Khandani [80] minimize energy costs while maximizing reliability for a microgrid composed of a fuel cell, storage, and boiler. Zhou et al. [81] present an optimal load distribution model of microgrids, in which they optimize cost, emissions, reliability, power line loss, and power generation efficiency. Borhanazad et al. [82] optimize a wind, PV, battery, and diesel microgrid using a power management algorithm and particle swarm method. They consider both cost and reliability, where the latter is measured as probability of loss of power supply. Zheng et al. [83] present a multi-objective optimization model that generates operational, or dispatch, decisions for a large-scale electric grid connected to heating and cooling systems. They use a multi-objective group search optimizer, with objectives of economy and reliability. While demonstrated for large energy systems, the method could also be applied to microgrids. McIlvenna et al. [84] similarly optimize the control (but not sizing) of residential microgrids for improved reliability.

While previous work focuses on reliability, less work addresses resilience; the former focuses on routine, short-duration outages, while the latter examines lower probability, higher impact events. Our application treats one aspect of resilience, specifically, the ability of critical facilities to withstand disruptions in electric service using on-site backup power systems. In this context, resilience can be quantified as hours of outage, load not served, and/or costs incurred because of the outage Murphy et al. [79]. Previous research models resilience using a single-objective, cost minimization function, and a constraint requiring that the full critical load must be sustained for all outage hours at minimum life cycle cost Cook et al. [85]. However, this definition assumes that

there is no value to meeting a portion of the critical load. The actual critical load at any given site can often be adjusted through changes in operating conditions, such as shedding or shifting. Therefore, we quantify resilience in terms of the percent of load served during outage hours Murphy et al. [79].

We apply this approach to a wastewater treatment plant that purifies effluent collected via sewers from homes, businesses and industry for discharge or reuse. Previous efforts applying optimization to wastewater treatment have concentrated on operational control to reduce costs Zadorojniy et al. [86] and to improve efficiency Revollar et al. [87]. Others have focused on cost minimization incorporating renewable energy and combined heat and power on-site Gruber-Glatzl et al. [88]. Cook et al. [85] evaluate opportunities to incorporate on-site distributed energy resources for cost savings and backup power.

Given the importance of both cost and resilience for these plants, we develop a multi-objective optimization model to balance cost and resilience, where resilience is measured as the percent of load served during all hours of the outage Murphy et al. [79]. The contributions of this work are (i) a multi-objective optimization model that considers cost and resilience; (ii) incorporation of load shedding potential in resilience optimization; and, (iii) the application of this work to a real-world energy system.

3.4 Site Description

The Northside wastewater treatment plant treats an average of 10.4 million gallons per day of effluent, ranging from a low of 8.8 million gallons per day in January, on average, to a high of 11.9 million gallons per day, on average, in September. Cape Fear Public Utility Authority spent \$468,000 on 8,280,000 kilowatt-hours (kWh) of electricity purchases in 2019, amounting to an average cost of \$0.056/kWh for an average load of 945 kW. They purchase electricity from Duke Energy Progress under the Large General Service Real Time Pricing Rate Duke Energy Progress [89] by which Duke Energy Progress sets a Customer Baseline Load; all energy consumption below the Customer Baseline Load is billed at the Large General Service Time of Use Rate, and all consumption above the Customer Baseline Load is billed at a lower real-time pricing rate, which varies by hour and averages \$0.032/kWh. Figure 3.1 shows the total load and Customer Baseline Load, and Table B.5 provides the electric utility rate (see Appendix). Two diesel

generators with 25,320 gallons of diesel fuel storage yield emergency backup power.

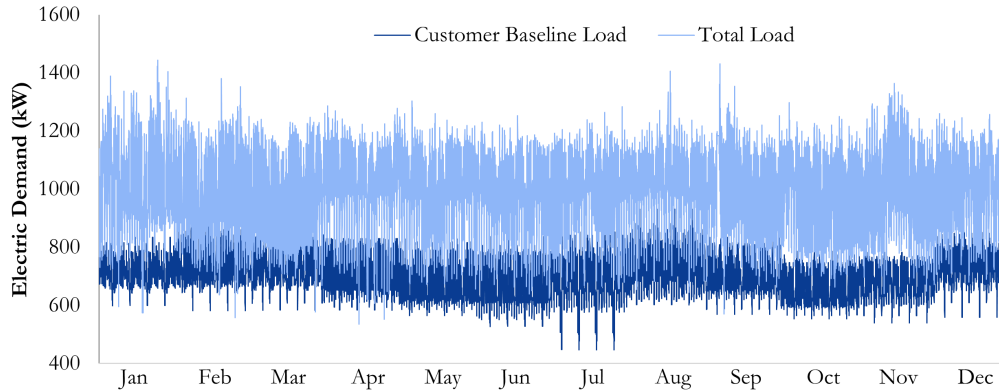


Figure 3.1 2019 Northside wastewater treatment plant electric demand

The Northside plant includes an anaerobic digester, which decomposes organic materials in the absence of oxygen, producing methane gas as a by-product. In 2019, the plant generated 66.8 million standard cubic feet of methane gas (also called biogas), which is used to mix digester sludge and provide fuel for the low-pressure hot-water boiler system. Approximately 53% of the gas was used on site in 2019, and the excess was flared (see Figure 3.2), representing an underutilized, and free, energy resource for the site. Figure 3.3 shows (a) the anaerobic digesters, (b) the hot water boiler system, and (c) excess gas flaring.

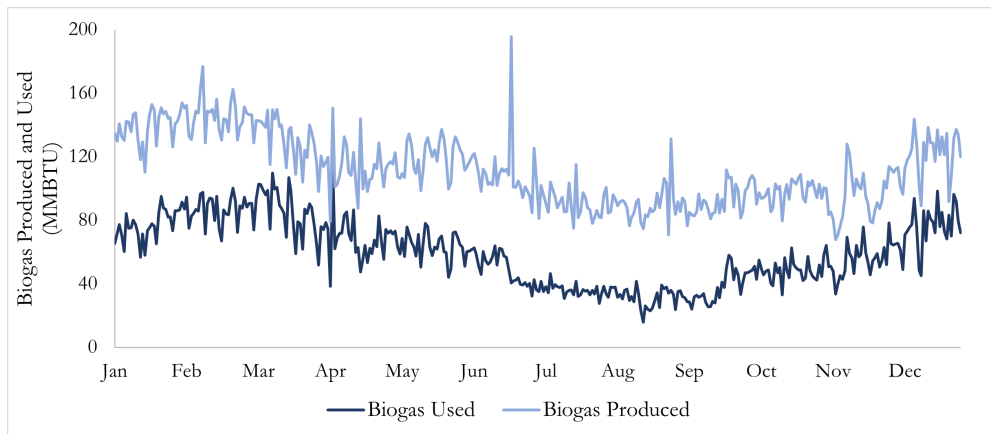
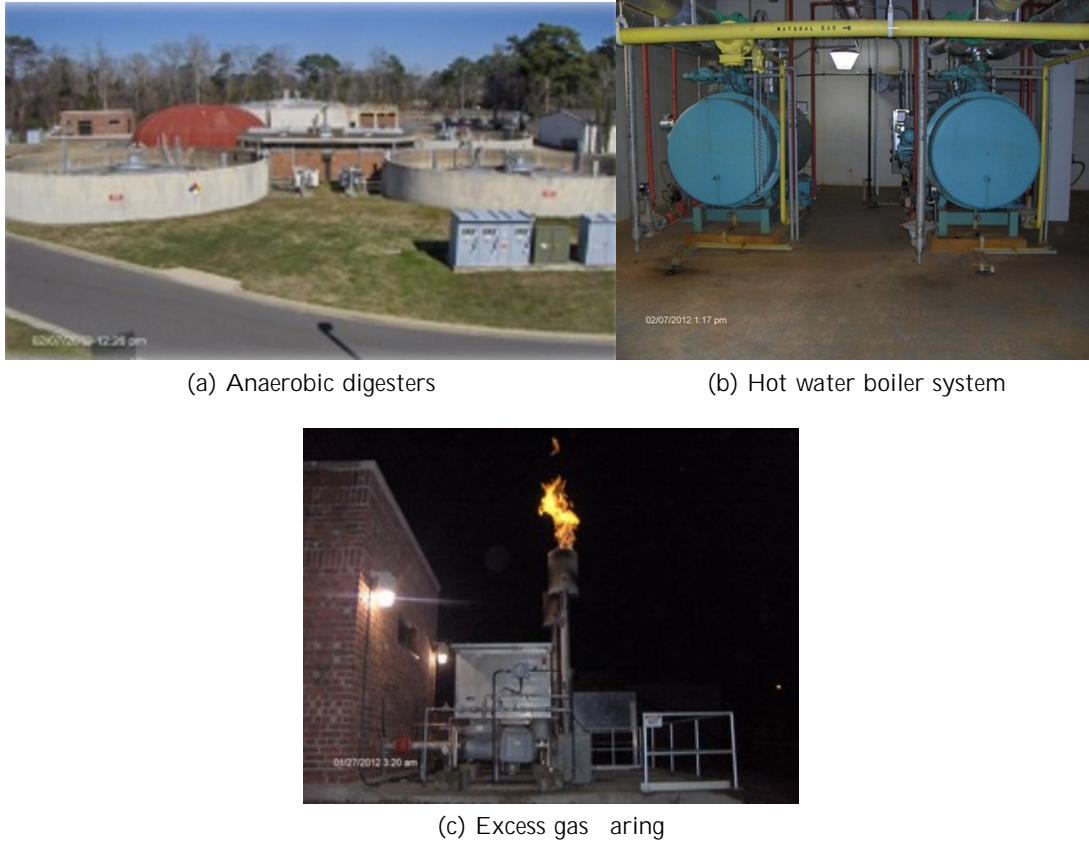


Figure 3.2 2019 Northside wastewater treatment plant biogas production and use



(a) Anaerobic digesters

(b) Hot water boiler system

(c) Excess gas burning

Figure 3.3 Northside wastewater treatment plan anaerobic digestion system. Source: CFPUA [1]

We explore opportunities to use combined heat and power, solar, and storage to reduce energy costs and increase resilience at the site. We evaluate an internal combustion gas engine with combined heat and power, solar PV, and battery storage. The Appendix provides additional data describing the solar resource, cost and performance assumptions for the systems considered, and economic parameters for the analysis. System sizes recommended are typical of commercially available system sizes. Typical combined heat and power system sizes can be found in the Department of Energy’s Combined Heat & Power eCatalog DOE [90].

3.5 Methodology

REopt LiteTM is a mixed-integer linear programming model that evaluates the economic viability of grid-connected combined heat and power, solar, and battery storage for a building or a campus Anderson et al. [8]. The model minimizes discounted cashflow associated with costs and

savings over the analysis period (typically, 25 years) while adhering to constraints on fuel use, system operations, system capacities, load balancing, grid sales, rate tariffs, and a variety of other interoperability and logical restrictions. It recommends an optimally sized mix of renewable energy, conventional generation, and storage technologies, while simultaneously optimizing the corresponding operating strategy. Figure 3.4 shows the model’s inputs and outputs.

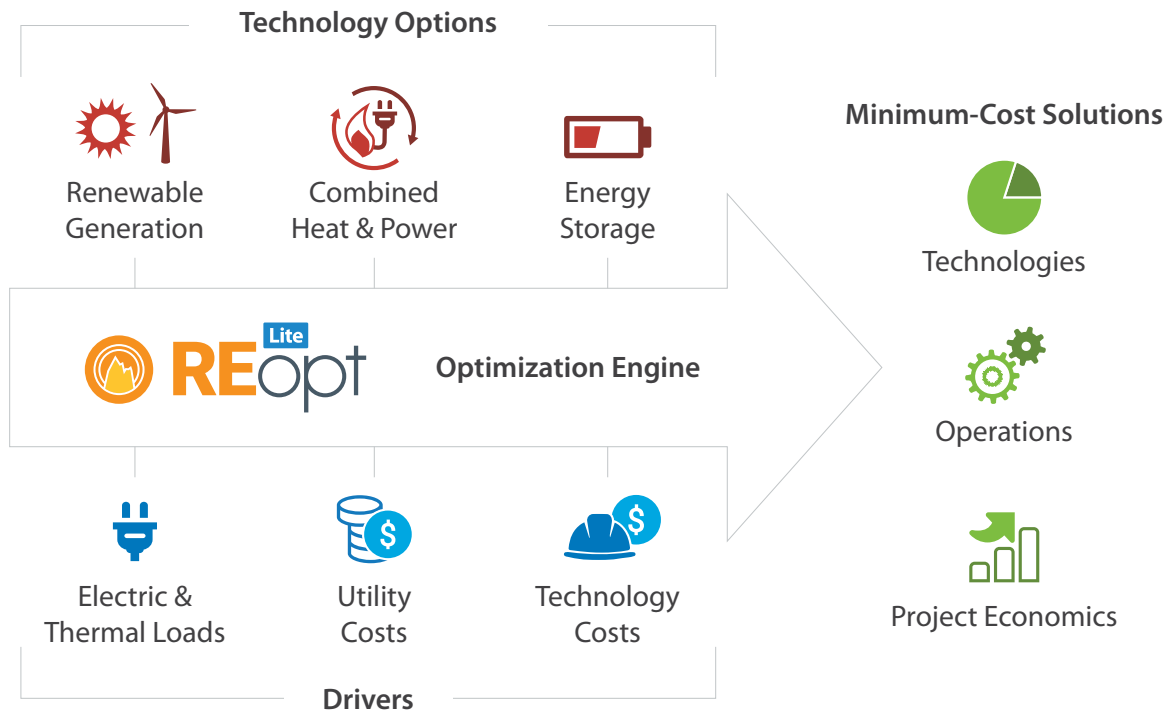


Figure 3.4 The REopt Lite model inputs include renewable energy, combined heat and power, and energy storage technology options (in red), and loads, utility costs, and technology costs (in blue). Outputs (in green) encompass recommended technology sizes, operations strategy, and project economics.

Initially developed as an internal model at the National Renewable Energy Laboratory in 2007, the model was later deployed as a public web tool and application programming interface. The model is licensed by the National Renewable Energy Laboratory under a permissive BSD-3 open source license, and can be used and modified by anyone free of charge. Its user base has grown to over 40,000, and includes renewable energy developers, energy consultants, utilities, building owners and researchers worldwide. For example, the utility Duke Energy uses the model to

identify customers who can save money by installing solar PV and batteries. The National Rural Electric Cooperative Association uses the model in a microgrid design tool available to more than 900 members to identify opportunities for renewable energy-powered microgrids in cooperative territories. Commercial companies use REopt to evaluate opportunities for cost effective PV, wind, storage, and ground source heat pumps at their properties. For example, Time Warner Cable identified 46 MW of renewable energy projects at 306 sites that would generate 10.5% of their annual energy consumption and save \$37 million over 25 years Richards et al. [91]. Verizon Wireless identified cost-effective opportunities and then issued the U.S. telecommunication industry’s first Green Bond, a \$1 billion offering to fund implementation of renewable energy, energy efficiency, and water measures NREL [92]. REopt has also been used to assess opportunities at universities, including Luther College, which installed a 950 kW PV and 370 kW storage system Anderson and Elgqvist [93]. The U.S. Department of Defense used the model to evaluate the economic and technical viability of distributed renewable energy and storage systems at sites around the world. REopt analysis led to development of 262 MW of renewable energy at Army and Navy bases Anderson [94], including, at Fort Carson, a 2 MW; 8 MWh battery, the largest in the Army at the time of its installation Elgqvist and Christiansen [95]. The model has also been used to evaluate renewable energy opportunities internationally, including assessing renewable energy microgrid opportunities in Sub-Saharan Africa Booth et al. [96].

While past REopt analyses have primarily informed solar and storage implementation, the model now considers combined heat and power. We describe how the model was used to evaluate such a system designed to provide both economic savings and increased resilience. We modify the objective of REopt Lite to minimize both life cycle cost of energy and load shed (i.e., not served) during the outage. Resilience is measured by the amount of load shed during the outage; if no load is shed, the system is 100% resilient. Typically, reducing load shed (and thus increasing resilience) requires larger, more expensive generation and storage systems with increased life cycle cost. Therefore, increasing resilience and reducing cost are competing objectives.

[10] provide a basic formulation of the model into which [9] integrate combined heat and power. For the purposes of this paper, and to maintain consistency with previous work, we refer to this basic model (with combined heat and power) as (\mathcal{R}). Our model (\mathcal{R}) modifies (\mathcal{R}) by adding sets, parameters and variables, as well as updating the objective function and constraints

corresponding mathematically to resilience or utility modifications. The focus of this work is on the application of the resilience modifications; however, the utility rate tariff structure requires a non-trivial modification to (\mathcal{R}) presented in the referenced literature. We outline the updates in the sections below, and the Appendix contains the associated mathematical formulation. The modified code is available from the authors upon request.

3.5.1 Resilience Modifications

The formulation (\mathcal{R}) seeks to measure resilience according to the amount of electric load met or unmet during a specified grid outage. We introduce a variable that represents the difference between the total electric load served during the grid outage and the critical load, the latter of which is defined as the amount of power needed to maintain key operations such as treating and processing effluent during an outage.

We extend the objective given in (\mathcal{R}) to a multi-objective function that seeks to minimize life cycle cost while at the same time minimizing load shed during the grid outage. We introduce scaling parameters for both the life cycle cost and the load shed to adjust the relative weighting of cost and resilience. Appropriate selection of the magnitude of these scalars is dependent on factors such as utility and technology costs, as well as desired amount of load shed. Scalar values that do not sufficiently penalize load shed result in solutions that overly favor life cycle costs. Conversely, values that overly penalize load shed can result in solutions that meet the entire outage load with little consideration of life cycle costs.

We add a constraint which restricts the critical load parameter to be greater than or equal to the difference between the sum of all energy not dispatched by installed technologies and the added load shed variable, and then vary the target amount of load-shed during outage, as defined by the deviation between load demanded and load met during said outage. Because outages are often unplanned, we add a constraint that ensures that the model does not use its perfect foresight to fully charge the battery in the time step before the outage occurs. Using a parameter that represents the maximum state-of-charge of the battery storage system at the time step during which the outage begins, we restrict the maximum state-of-charge to 50% of its energy capacity.

3.5.2 Utility Rate Tariff Modifications

The REopt formulation (\mathcal{R}) models three components of the utility rate tariff: energy purchases, monthly demand, and time-of-use demand. Energy purchases fall into different tiers, in which energy is priced at a lower rate up to a certain amount of consumption, and then at subsequently higher rates for each tier. In the base model, tiers are applied on a monthly basis. The convex nature of the pricing tiers permits a straight forward implementation. Conversely, the case study site operates on a more complex utility tariff in which the (more expensive) time-of-use pricing rates apply to all energy purchased up to the contracted customer base load before the (cheaper) real-time pricing rates are accessed. In the modified formulation (\mathcal{R}'), we introduce a binary decision variable, indexed both by hour and by tier, that ensures higher cost time-of-use pricing tiers are filled before accessing lower cost real-time pricing tiers. This results in the addition of 17,520 binary variables relative to the formulation (\mathcal{R}), which increases the difficulty associated with solving the model.

Monthly demand is the largest total demand across all of the off-peak hours less the largest time-of-use demand over the on-peak hours. A *facilities demand charge* captures the power used in excess of the contracted demand. We add a variable that represents the maximum of the sum of all demand in all pricing tiers over all off-peak hours in a given month. We add two constraints to model the monthly demand charges. The first computes the maximum demand in a given month and the second computes the difference between the maximum demand over all hours and the maximum demand in the off-peak hours. Time-of-use demand consists of two components, on-peak and off-peak. We add a variable to capture the largest recorded demand in all periods (on- and off-peak). The on-peak demand is the maximum demand registered in the on-peak hours of the current month. The off-peak demand, referred to in the tariff as the excess billing demand, is the maximum demand registered in the off-peak hours of the current month less the on-peak billing demand. These demand charges only apply to the time-of-use pricing tiers and are agnostic to the real-time pricing tier demand. A constraint captures this difference. The total contribution of the off-peak demand is comparatively small and does not significantly affect model solutions.

3.5.3 Scenarios

For the system design optimization, we use a 7.46-day outage starting on September 20th, 2019 at 6pm, chosen to correspond to the average number of hours of interruption experienced by Duke Energy Progress customers in North Carolina in 2019 EIA [97], and to occur at the peak-load hour of the year (representing a worst-case outage). Additionally, this period falls during the June-November hurricane season, when outages are likely to occur.

We evaluate four scenarios of interest to Cape Fear Public Utility Authority (hereafter referred to as Cape Fear). The first models their existing system, and provides the baseline against which we compare other options. This existing, or business-as-usual, system does not fully use the free, on-site biogas resource, and relies on diesel fuel which is often in short supply during grid outages. The second evaluates adding only combined heat and power to take advantage of the free on-site biogas. This is an option Cape Fear considered eight years ago, but did not to pursue due to poor economics; now, the utility would like to understand how costs and benefits of this option may have changed with current utility prices and technology costs. After seeing the results of the first two scenarios, Cape Fear requested a third and fourth scenario to explore additional technology options beyond combined heat and power to further reduce cost, increase renewable energy use, and further reduce reliance on diesel fuel. The third scenario considers additional technologies (PV and battery) which could provide additional cost savings and emissions reductions to meet sustainability goals such as North Carolina's Renewable Energy and Energy Efficiency Portfolio Standard. The final option evaluates how the site could sustain its load during a grid outage without diesel generation in order to reduce reliance on fuel re-supply chains that are often interrupted during natural disasters, and to conserve fuel for other critical infrastructure sites. In summary, the four scenarios are:

1. *Business-As-Usual*: In this scenario, the site purchases energy from the electric utility when the grid is available, and uses emergency backup diesel generators during the outage.
2. *Combined Heat and Power-Only*: This scenario considers only combined heat and power (along with the existing utility grid and diesel generators), which can be powered both by the free biogas generated in the on-site anaerobic digesters and by natural gas purchased from the utility.

3. *All Technologies*: This scenario considers a hybrid combined-heat-and-power system which matches this with solar photovoltaics and battery storage (along with the existing utility grid and diesel generators).
4. *No Diesel*: This scenario assumes that the site does not use diesel generators, which eliminates its dependence on diesel fuel, but includes the options of combined heat and power, solar photovoltaics, battery storage, and the existing utility grid.

For each scenario, we consider a no-outage case to understand the economics and performance of the system during normal operating conditions, and a seven-day outage case to evaluate economics and performance during major events resulting in extended grid-outage periods. In order to understand the trade-off between cost and resilience, we solve the model multiple times with varying objective function scaling parameters. This results in solutions that serve varying amounts of electric load during the grid outage.

3.6 Results

With no changes, in the *Business-As-Usual* scenario, Cape Fear will spend \$9.7M over 25 years (in 2021 dollars) in utility costs to power the Northside wastewater treatment plant (see Table 3.1). The existing diesel generators can sustain the full load during an annual seven-day outage at a lifecycle cost of \$10.5M, an increase of \$864,000 (8.9%) over 25 years compared to the *Business-as-Usual* no-outage case, as shown in Table 3.2. This solution requires no upfront capital investment, but relies heavily on diesel fuel that may be needed to power other critical infrastructure sites during outages, requiring 14,055 gallons of fuel to power the plant during the week-long outage.

Instead of continuing with the *Business-as-Usual* scenario, Cape Fear could install a 518 kW-combined-heat-and-power system at an upfront capital cost of \$1.4 million. Powered primarily by the free on-site biogas, this system would provide 42% of the site's electricity, off-setting utility purchases and reducing annual utility costs by 31% and life cycle energy costs by 2.4% (\$235,000 over 25 years) relative to the *Business-as-Usual* no-outage case. If paired with existing diesel generators, the combined-heat-and-power-diesel system could sustain the full load during a seven-day outage at lower life cycle cost than a diesel generator alone, saving the site

\$623,000 compared to the diesel-only solution in the *Business-as-Usual* seven-day outage case. Additionally, this would reduce diesel use substantially by 50% from 14,055 gallons to 7,009 gallons per year, increasing resilience by reducing dependence on limited diesel fuel supplies. However, this solution requires a \$1.4 million capital investment.

Table 3.1 System Sizes and Economics for No-Outage Case

	BAU	CHP Only	All Tech.	No Diesel
CHP System Size (kW)	0	518	486	1160
PV System Size (kW)	0	0	50	0
Storage System Size (kW; kWh)	0; 0	0; 0	60; 100	89; 275
Biogas Burned by CHP (MMBTU)	0	38,870	38,261	40,636
Natural Gas Burned by CHP (MMBTU)	0	322	271	417
Energy Purchased from Utility (kWh)	8,747,501	5,060,556	5,064,374	4,788,343
Total Annual Electricity Cost (\$)	470,524	323,911	315,960	329,903
Capital Cost (\$)	0	1,398,600	1,514,500	3,525,985
Life Cycle Cost (\$)	9,662,890	9,427,595	9,361,888	11,777,590
Net Present Value (\$)	0	235,295	301,002	-2,114,700
Increase in Life Cycle Costs (%)	0	-2.4%	-3.1%	21.9%

Note: BAU: business-as-usual; CHP: combined heat and power; Tech: Technologies; MMTBU: million British thermal units

Table 3.2 System Sizes and Economics for Seven-Day Outage Case

	BAU	CHP Only	All Tech.	No Diesel
Combined-heat-and-power System Size (kW)	0	518	486	1160
Photovoltaics System Size (kW)	0	0	50	0
Storage System Size (kW; kWh)	0; 0	0; 0	60; 100	89; 275
Diesel System Size (kW)	1,250	731	762	0
Biogas Burned by CHP (MMBTU)	0	38,818	38,224	40,619
Natural Gas Burned by CHP (MMBTU)	0	672	522	2,060
Diesel Fuel Use (gallons)	14,055	7,009	7,352	0
Energy Purchased from Utility (kWh)	8,562,539	4,940,360	4,947,968	4,747,349
Total Annual Electricity Cost (\$)	464,876	319,205	312,498	324,471
Capital Cost (\$)	0	1,398,600	1,514,500	3,385,122
Life Cycle Cost (\$)	10,526,777	9,903,464	9,863,124	11,904,211
Net Present Value (\$)	-	623,313	663,653	-1,377,434
Increase in Life Cycle Costs (%)	0%	-5.9%	-6.3%	13.1%

If we consider a hybrid system composed of combined heat and power, photovoltaics, and battery, as shown in the *All Technologies* scenario, Cape Fear can further reduce life cycle energy costs compared to the *CHP Only* scenario. Adding a 50 kW photovoltaics system and a 60 kW;

100 kWh battery system to a 486 kW-combined-heat-and-power system at a total capital cost of \$1.5 million decreases annual utility costs by 33% and life cycle energy costs by 3.1% (\$301,000 over 25 years) compared to the *Business-as-Usual* scenario, an additional \$66,000 in life cycle energy savings compared to the combined-heat-and-power system alone. The combined-heat-and-power system provides 41% of the site’s energy needs, with less than 1% coming from photovoltaics. If paired with the existing diesel generators, the combined hybrid combined heat and power-diesel system could sustain the full load during a seven-day outage while saving the site \$664,000 compared to the diesel-only solution in the *Business-as-Usual* seven-day outage case. Additionally, this would reduce diesel use by 48% from 14,055 gallons to 7,352 gallons per year, again increasing resilience by reducing dependence on limited diesel fuel supplies.

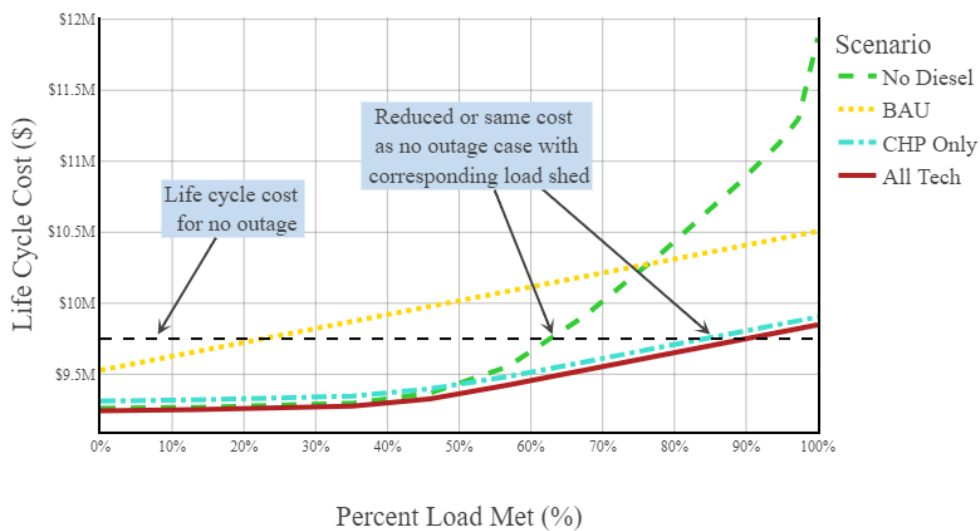


Figure 3.5 If load can be reduced during the outage by storing and deferring wastewater treatment, required system sizes and costs decrease

Completely eliminating diesel fuel use while sustaining the full load during an outage requires a much larger 1,160 kW combined-heat-and-power system (comprised of two 580 kW units) with an 89 kW; 275 kWh battery to meet the load during peak hours, with a capital cost of \$3.4 million. Because much of the 1,160 kW combined-heat-and-power system capacity is often un-used during lower load hours, it does not substantially offset utility purchases relative to the smaller combined-heat-and-power systems in the *Combined-heat-and-power Only* or *All Technologies* scenarios. It provides 46% of the site’s energy needs, versus 41-42% in the previous

scenarios. The utility savings do not offset the much larger capital investment, resulting in a \$1.4 million increase in life cycle cost of energy, compared to the cost associated with the diesel-only solution. While this solution eliminates reliance on diesel fuel, it comes at a significant cost.

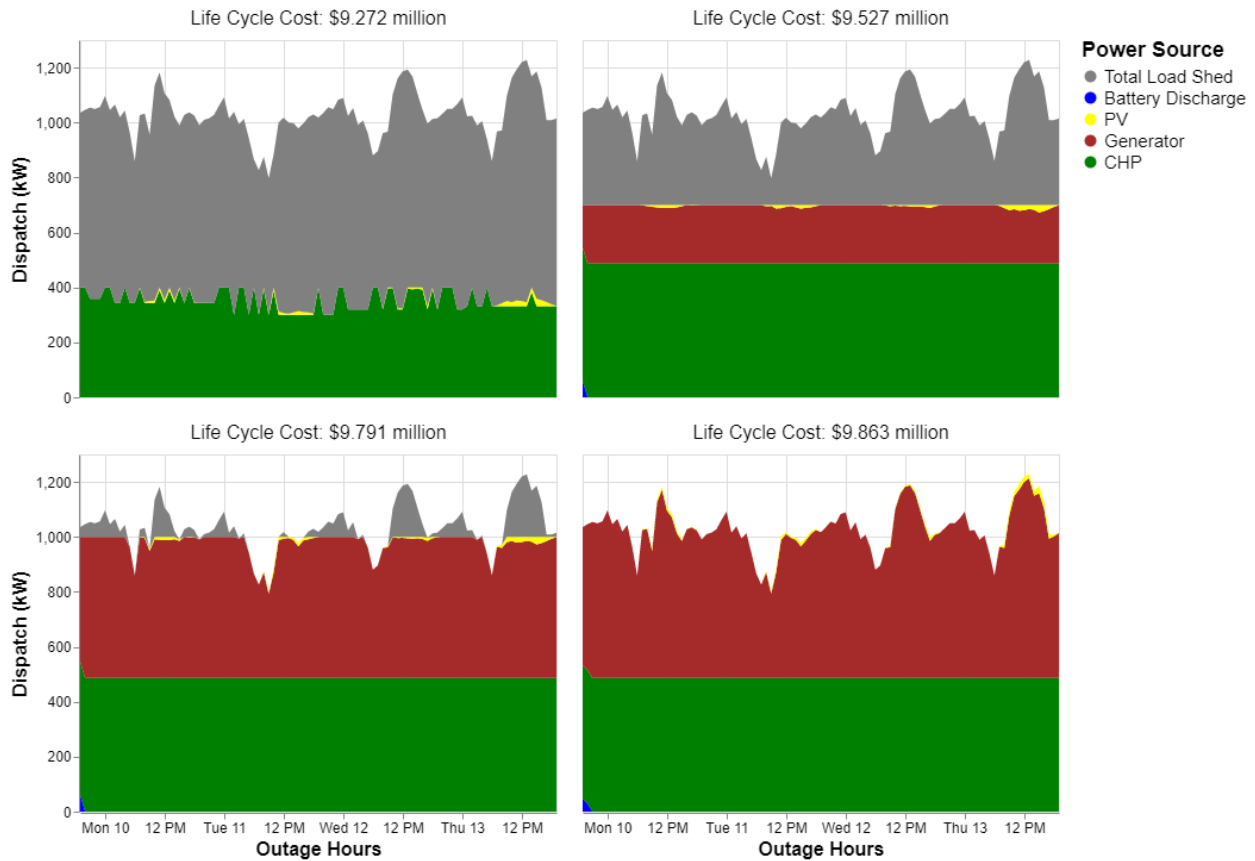


Figure 3.6 Peak loads are shed to reduce the required combined-heat-and-power and generator sizes, resulting in reduced life cycle cost, for the *All Technologies* seven-day outage case.

Although completely eliminating diesel fuel use while sustaining the full load is not cost-effective, if loads can be reduced by 40% during the outage, 60% of the load can be met and diesel generation can be eliminated with no increase in life cycle cost, as denoted by the “No Diesel” line in Figure 3.5. When all technologies are considered, a combination of combined heat and power, photovoltaics, storage, and diesel generation can meet 80% of the critical load with no cost increase, as denoted by the “All Tech.” line in Figure 3.5. Figure 3.6 shows how load can be shed across all hours to reduce system sizes, and therefore life cycle cost, for the *All Technologies* seven-day outage case. A smaller combined-heat-and-power, photovoltaics, and battery system supplies approximately one-third of the load at a life cycle cost of \$9.272 million in the upper left

graph of Figure 3.6. To meet at least two-thirds of the load at lowest cost, a diesel generator must be added to the technology mix, at a life cycle cost of \$9.527 million in the upper right graph of Figure 3.6. Increasing amounts of load are met by increasing the diesel generation capacity and fuel use until the full load is met at a life cycle cost of \$9.863 million, as shown in the lower left graph of Figure 3.6 and in Table 3.2. Figure 3.7 shows that diesel fuel consumption can also be lowered by reducing the percentage of load met. Approximately 50% of the load can be met by the *All Technologies* solution with very little diesel consumption.

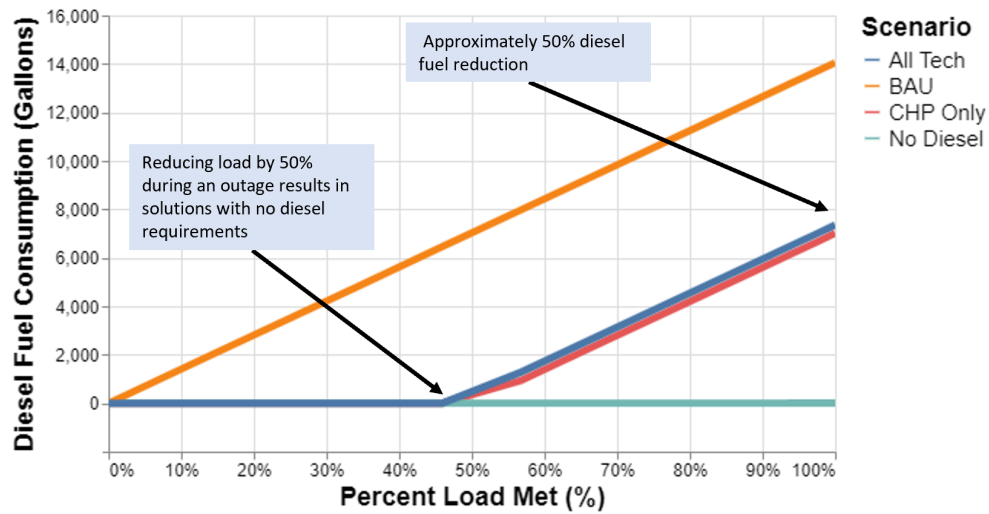


Figure 3.7 A hybrid combined-heat-and-power system in the *All Technologies* seven-day outage case reduces diesel consumption by 50% relative to the *Business-as-Usual* scenario when meeting the full load. Diesel consumption can be further reduced in the *Business-as-Usual*, *CHP Only*, and *All Technologies* scenarios by shedding load.

3.7 Conclusion

This work provided Cape Fear decision makers the information needed to make investment decisions in the face of competing objectives. The primary benefit is resilience; the combined heat and power system provides a resilient source of on-site power in case of a grid outage, helping to reduce dependence on diesel fuel and providing a redundant backup power source to the diesel generators. This benefits not only Cape Fear, but also the utility and its other customers, because the utility can prioritize restoration of other customers if they know the wastewater treatment plant has reliable backup power. Reduced dependence on diesel is particularly important during longer outages where the site would require re-supplies of diesel fuel to continue operating.

The system also provides economic and sustainability benefits. The savings are modest (at most 3% for the hybrid configuration), primarily due to the site's low utility rate (averaging \$0.05/kWh), as well as the additional standby charge the site incurs if combined heat and power is installed. The combined-heat-and-power system contributes toward sustainability goals by reducing carbon emissions (a reduction of 22% in the *All Technologies* case). The reduced emissions resulting from the combined-heat-and-power system also provide broader social benefits including reduced public health costs, reduced impact on climate change, and job creation for the construction, operation, and maintenance of the system.

Balancing these benefits is the significant capital expenditure required to build the system (\$1.5 million in the *All Technologies* case), and the increased complexity of owning and operating a power generation system at the wastewater treatment plant. These results enabled Cape Fear to consider the economic and resilience costs and benefits quantified in this study, as well as other more qualitative costs and benefits as they decided whether to implement a combined-heat-and-power system. They ultimately elected to allocate funds for implementation of a combined-heat-and-power system in fiscal year 2023.

Many critical infrastructure sites must weigh the need for increased resilience against the cost of resilience investments. The REopt model has been widely used by building owners to inform deployment of distributed energy systems that power critical infrastructure sites around the world, including at U.S. Department of Defense bases and telecommunication hubs. The case study presented here was used to inform hybrid combined-heat-and-power implementation

decisions at Cape Fear’s Northside wastewater treatment plant. Future work will apply this method to other critical infrastructure sites in North Carolina and beyond, and develop methods to generalize the results to be applicable to different sites. We also intend to expand this method to balance additional objectives beyond cost and resilience, including minimizing impacts on the climate and on health.

3.8 Acknowledgements

This work was authored by the National Renewable Energy Laboratory, operated by Alliance for Sustainable Energy, LLC, for the U.S. Department of Energy (DOE) under Contract No. DE-AC36-08GO28308. Funding was provided by the U.S. Department of Energy Advanced Manufacturing Office. The authors would like to thank Isaac Panzarella, Christina Kopitopoulou, and Simon Sandler of North Carolina State University and Matt Hourihan and Elizabeth Severt of Cape Fear Public Utility for analysis data and review. The authors also thank Alex Zolan, Bill Becker, Chris Hampel, Bruce Hedman, and Patti Garland for review of the results, Anne Hampson and Bob Gemmer (Advanced Manufacturing Office, DOE) for funding this work, and the Colorado School of Mines Advanced Energy Systems program for their support. The views expressed in the article do not necessarily represent the views of the DOE or the U.S. Government. The U.S. Government retains and the publisher, by accepting the article for publication, acknowledges that the U.S. Government retains a nonexclusive, paid-up, irrevocable, worldwide license to publish or reproduce the published form of this work or allow others to do so, for U.S. Government purposes.

CHAPTER 4

OPTIMIZING MICROGRID DEPLOYMENT FOR COMMUNITY RESILIENCE

Modified from a paper submitted to *Operations Research with Engineering* James Grymes^{8;9},
Alexandra Newman^{8;}, Destenie Nock¹⁰, Zana Cranmer¹¹

4.1 Abstract

The ability to (re)establish basic community infrastructure and governmental functions, such as medical and communication systems, after the occurrence of a natural disaster rests on a continuous supply of electricity. Traditional energy-generation systems consisting of power plants, transmission lines, and distribution feeders are becoming more vulnerable, given the increasing magnitude and frequency of climate-related natural disasters. We investigate the role that fuel cells, along with other distributed energy resources, play in post-disaster recovery efforts. We present a mixed-integer, non-linear optimization model that takes load and power-technology data as inputs and determines a cost-minimizing design and dispatch strategy while considering operational constraints. The model fails to achieve gaps of less than 15%, on average, after two hours for realistic instances encompassing five technologies and a year-long time horizon at hourly fidelity. Therefore, we devise a multi-phase methodology to expedite solutions, resulting in run times to obtain the best solution in fewer than two minutes; after two hours, we provide proof of near-optimality, i.e., gaps averaging 5%. Solutions obtained from this methodology yield, on average, an 8% decrease in objective function value and utilize fuel cells three times more often than solutions obtained with a straight-forward implementation employing a commercial solver.

4.2 Introduction and Background

Climate-related events that contribute to power disruptions are becoming more widespread. In 2021, the U.S. encountered 20 separate billion-dollar weather- and climate-related disasters, almost all of which impacted the ability to deliver reliable electricity to communities. The U.S.

⁸Operations Research with Engineering Graduate Program,

⁹Primary researcher and author

¹⁰Engineering and Public Policy, Carnegie Mellon University

¹¹Natural and Applied Sciences, Bentley University

Department of Energy defines reliability as the ability of the system or its components to withstand instability, uncontrolled events, cascading failures, and/or unanticipated loss of system components. The Federal Energy Regulatory Commission defines resilience as “the capacity to anticipate, adapt to, and rapidly recover from disruptive incidents.”

An independent group of scientists and communicators who research climate change reports a 67% increase in major power outages between the first and second decades of the 2000s [98]; Figure 4.1 reflects the costs associated with increased climate-related disasters. The average annual cost over the five-year period between 2017 and 2021 constituted \$148.4 billion, a new record [99]. The Department of Energy [100] estimates that power outages cost the U.S. economy \$150 billion per year and disruptions to power infrastructure are more attributable to climate-related events than any others (Figure 4.2). To protect large-scale infrastructure, utilities often deploy power safety shutoff measures which, without backup power generation, threaten the safety and well-being of residents. Thus, having a policy that provides reliable, affordable electricity in post-disaster recovery efforts will become more pressing, especially because the number of natural disasters is expected to rise [101, 102].

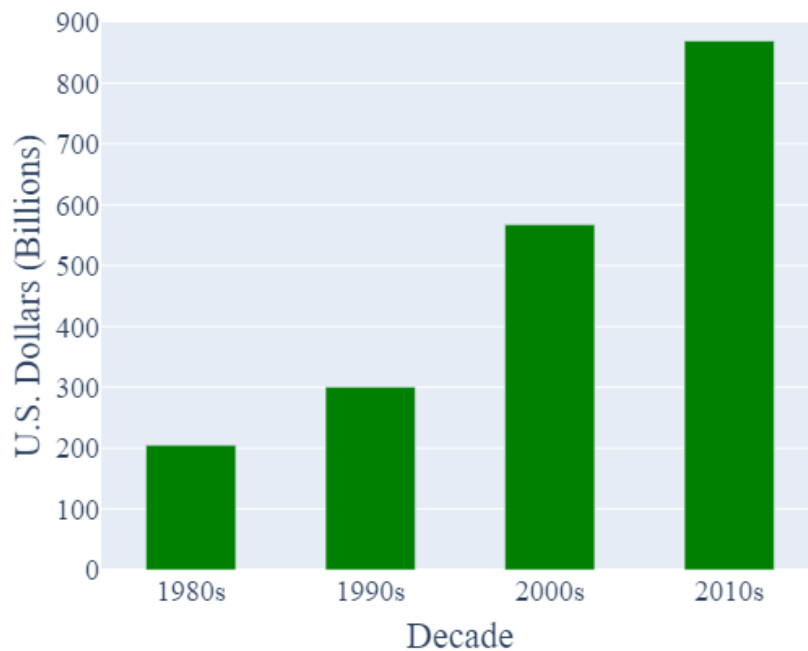


Figure 4.1 Climate-related disaster costsClimate-related disaster costs by decade [99]. See Appendix C.1 for a description of types of costs included.

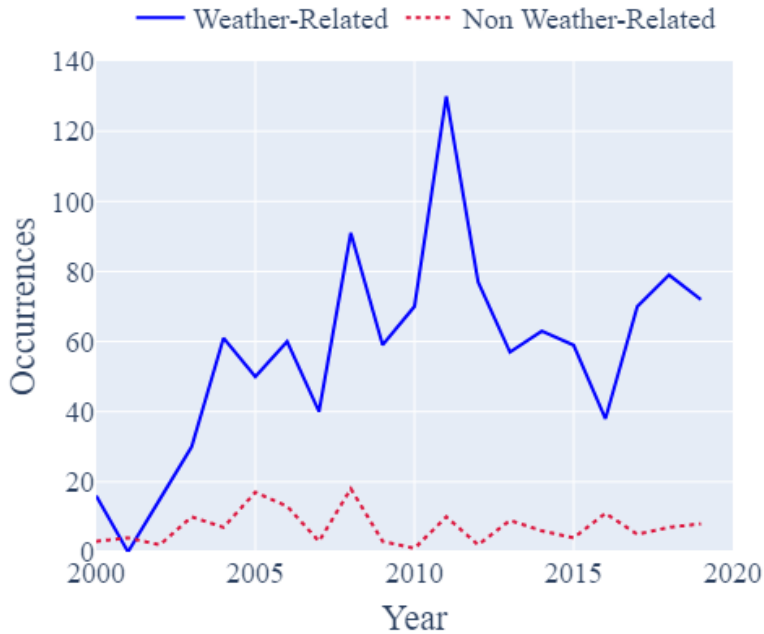


Figure 4.2 Power outages in 2020 Number of power outages affecting more than 50,000 customers [103].

Often, the nature and severity of natural disasters require residents to *shelter-in-place* rather than to evacuate. Examples of the latter include hurricanes and large-scale fires during which the deployment of rescue and response teams to the impacted area is a higher priority than maintaining persistent power [104]. Wildfires are particularly menacing due to their non-predictive nature. Climate-related impacts, such as droughts and heatwaves, have increased global wildfire risk [22, 105, 106]. In 2017, over 71,000 wildfires burned 10 million acres and more than 12,000 structures [107]. Within the U.S., 29 million Americans live with the significant potential for extreme wildfires [108]. Fire-related events pose risks to both the power generation and the distribution system, which include transmission and distribution lines [109]. The area impacted by wildfires often encompasses multiple types of power system architectures in which the effects differ by the level (i.e., electricity delivery and generation) of electrical equipment. At low-voltage (i.e., residential) delivery, a fire may cause system components to fail; conversely, high-voltage transmission components may be more resilient [110]. Some electrical service disruptions are due to preventative measures enacted by the utility service to prevent wildfires. For example, in 2019, Pacific Gas and Electric’s planned power shutoffs left an estimated 2.7

million people devoid of electricity, possibly the state’s largest planned blackout ever [111].

In addition to economic implications, there are social implications related to vulnerable populations (e.g., the elderly and those with electricity-dependent health risks) such as their inability to evacuate [112–114]. In 2017, over 65% of victims in the Northern Californian fire were over the age of 65 [114]. Regardless of whether power outages are caused by fire-related damage to the power system (i.e., generation and transmission) or are due to preventative measures, communities depend on energy for infrastructure such as hospitals.

Due to the dependence of many first-world countries on electricity for communication, healthcare, and water purification, efforts at the federal level are directed toward reducing electrical downtime. Many utilities are investing in distributed generation to improve network reliability and resilience with proper consideration of technology mix, size, and placement. Abiodun et al. [115] document how distributed generation can enhance power system resilience and improve energy equity. However, conventional microgrids, which often include technologies such as diesel generators, produce unhealthy exhaust, resulting in those with preexisting health conditions suffering consequences from resulting air pollution exposure. Fuel cells address this concern in that they run without emitting fumes, particulates, or carbon monoxide; and, because of this, fuel cells can be housed within a building, protecting it from some climate-disaster-related risks.

We develop an optimization model that prescribes an appropriate configuration and size of a distributed generation system to provide communities, in an environmentally sound way, with critical services during an electrical service disruption. Figure 4.3 depicts a traditional microgrid consisting of fossil-fuel powered combined-heat-and-power systems, reciprocating engine generators, and solar power combined with electrical storage [116]. The microgrid market in the U.S., with 10 gigawatts of installed capacity in 2022, is projected to grow 19% annually through 2027, with disaster mitigation being a primary use case [117].

While microgrids provide electricity resilience, threats to these types of systems include physical destruction to solar panels (through wind, fire, and hail), damage to electrical storage systems from extreme temperatures, and harmed fuel delivery systems [118]. Donaldson et al. [110] show that the presence of distributed roof-top solar and wind turbines has increased the exposure of electricity generation equipment to wildfires. The corresponding risk continues to

grow as more homes (and, subsequently, electrical infrastructure) are built using renewable technologies and at the wildland-urban interface. Deliberate consideration of technologies, their vulnerabilities, and their construction mitigates these threats. For example, Anderson et al. [21] show that during a hurricane-induced outage, the inclusion of combined-heat-and-power technologies at a wastewater treatment facility increases the overall resilience of the system through its ability to burn on-site biofuel. The same benefit would not be realized with a traditional microgrid. Beigzadeh et al. [119] demonstrate that fuel cells can deliver on-demand energy sourced from industrial-waste biogas, syngas, biofuel, and gasified biomass. The ability to operate with on-site fuel yields a microgrid design with solid oxide fuel cells that possess the ability to continuously operate even if the fuel supply is disrupted. We incorporate solid oxide fuel cell technology into microgrid design to reduce these vulnerabilities and to ensure that dependable energy sources exist.

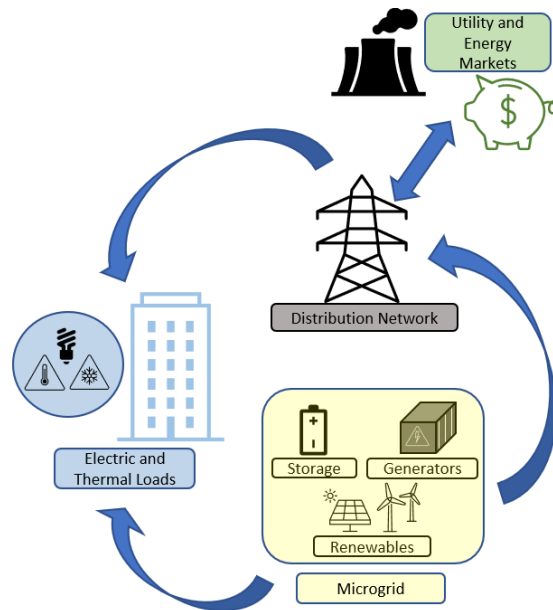


Figure 4.3 A representative microgrid and energy system.

4.3 Literature Review

There is an abundance of literature that addresses microgrid design, microgrid dispatch, and power system reliability and resilience. The fundamental gap in our knowledge and ability to deploy these technologies stems from a void of techno-economic microgrid optimization models

addressing energy resilience and environmentally friendly, deployable technologies such as fuel cells. HOMER (Hybrid Optimization Model for Electric Renewables), a widely used design and dispatch program, is a simulation model that, for a year-long demand profile, uses fixed dispatch strategies and ranks resulting solutions based on life-cycle cost [120, 121]. Some models employ prescriptive (optimization) methods; we highlight a few examples. A mixed integer program with wind power, batteries, and generators produces results comparable to HOMER’s [122]; however, their model generates the following solutions sequentially: (i) procurement resulting from running the mixed-integer program for a curtailed time horizon; and, (ii) dispatch following from a data mining algorithm to determine an operations strategy for the entire year given procurement from (i).

A two-phase approach fails to coordinate dispatch decisions and procurement strategies. Another techno-economical model, REopt[®] [123], is a cost-minimizing deterministic mixed-integer linear program that yields an optimal design and dispatch of distributed energy resources, including gas-turbines, renewables, and energy storage systems, to meet a set of predefined electrical, thermal, and cooling loads. While this model determines design and dispatch concurrently, it does not include solid oxide fuel cells, nor does it consider the non-linearities associated with thermal storage.

Pruitt et al. [2] develop a nonconvex, mixed-integer, nonlinear program to describe the design and dispatch of a distributed generation system of combined heat and power using solid oxide fuel cells for commercial buildings for a time horizon of one year at hourly fidelity. This model does not incorporate utility-related outages and omits technologies such as gas-turbine combined-heat-and-power systems and backup diesel generators; solutions to instances with time horizons that extend beyond a month are cost-minimizing only when all power is sourced exclusively from the grid. Some authors explore similar frameworks and reduce complexity by shortening the time horizon Morais et al. [124] or by using identical daily demands [125]. Other optimization models that incorporate solid oxide fuel cells as part of their system either: (i) omit the design or detailed dispatch component [126, 127], and/or (ii) use heuristics, rather than exact techniques, to determine a solution [128, 129]. Arefifar et al. [130] optimize microgrid design under considerations of reliability and supply security. Shokoohi et al. [131] examine controls in smart grids in line with Lin et al. [132], who review various strategies in the implementation of

power system resilience. To lessen the health impacts and damages associated with, for example, wildfires, Pacific Gas and Electric (California’s largest public utility) has proposed to deploy decentralized generation such as solar panels and diesel generators [133]. Similarly, Scioletti et al. [134] examine such a microgrid including batteries, and Goodall et al. [135] extend this system to capture battery fade. However, these applications miss an opportunity to utilize emerging, clean technologies, such as solid oxide fuel cells, to support critical entities such as hospitals and community centers.

Our research contributes to the literature by creating cost-minimizing, distributed generation solutions, including solid oxide fuel cells, while considering utility-service disruptions attributable to a natural disaster-induced outage. Specifically, our focus is disasters that result in a significant portion of the population remaining in place and relying on energy for sustainment and recovery. Our optimization framework considers how fuel cells, combined with other distributed generation, can reduce electrical outage time post-wildfire and support community rebuilding. We first describe individual components and then present a mathematical formulation of the entire system. The resulting output is a cost-minimizing system that prescribes the size of the solid oxide fuel cells, as well as conventional, renewable, and co-generational technologies, to provide planners with viable resilience solutions. We embellish a design and dispatch optimization model through enhancements that include: (i) additional generational technologies, (ii) new procurement costs, (iii) modifications to the electrical storage systems, and (iv) technology-specific modeling assumptions. We expand knowledge and capabilities in the disaster-response-and-recovery literature by creating a tool that can analyze and evaluate the value of different technology mixes (i.e., solar and storage, fuel cells, and gas-turbine generators) for a microgrid. Our model accounts for on-site heating loads to demonstrate the co-generational contributions of the technology mix. We capture the temporal and seasonal nature of energy demand, and create a cost-benefit framework for the responsible civic organization. We investigate the specific contribution that solid oxide fuel cells make in delivering energy services due to their co-generational capability and ability to be sourced by a variety of fuel types, including bio-waste [136]. We provide decision-makers with solutions that would allow electric utilities to respond to disasters (i.e., wildfires and earthquakes) that have a high probability of causing blackouts.

4.4 Modeling the Energy System

Our optimization model, (P^{θ}), extended from Pruitt et al. [2], investigates how microgrids bring reliability and resilience to communities post-disaster (Figure 4.4). We incorporate a grid-related outage and additional co-generational technologies. We consider a simulated set of electrical loads, of various quantities, for a distribution feeder. The installed microgrid is co-located at a building site with a thermal load. We incorporate characteristics of the technologies, such as efficiencies and start-up requirements. We utilize basic utility rate structures that include both energy and peak demand charges. The objective minimizes total cost, consisting of the capital, operations and maintenance (O&M), and operational costs of the acquired technologies, as well as the existing costs resulting from demand met by the utility and on-site hot-thermal energy system, typically, a boiler. We include an emissions penalty in the objective function. Design variables associated with fuel cells are general integers to assist with modeling the hourly operation of the system. We relax integrality on all other procurement variables. We assume that all design decisions are made at the beginning of the time horizon. The model includes both linear and non-linear constraints. We present the full mathematical formulation (P^{θ}) in Section 4.4.1.

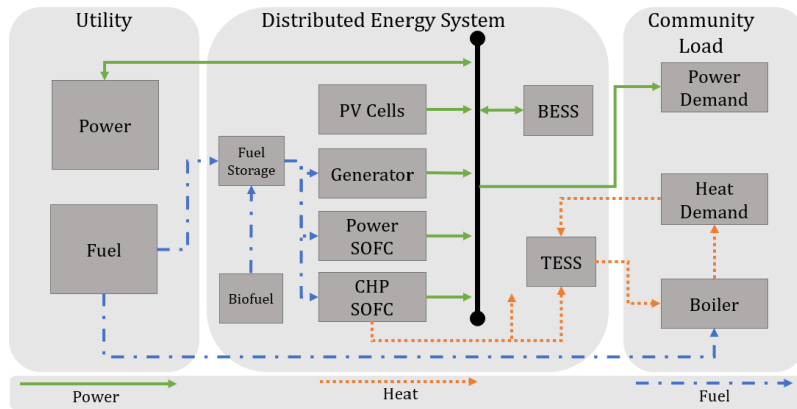


Figure 4.4 Distributed Energy System modified from Pruitt et al. [2]

Note: CHP: Combined heat and power, BESS: Battery Electric Storage System, TESS: Thermal Energy Storage System, PV: Photovoltaic

We utilize capital and lower-case letters to distinguish variables and parameters, respectively. We use script capital letters to distinguish sets, subsets, and indexed sets. Additionally, notation with check and hat decorations describes flows in and out of an entity, respectively. Variables X ,

Y , and Z represent continuous, integer, and binary quantities, respectively.

4.4.1 Mathematical Formulation

Sets

K	Technology cost segments
J	Power producing technologies
M	Months of year
T	Time steps

Subsets and indexed Sets

J^S	J	Solid oxide fuel cell technologies
J^{CHP}	J	Combined heat and power technologies
J^R	J	Renewable technologies
J^B	J	Heat-only producing technologies
J^E	J	Electrical producing technologies
T_m	T	Time steps in month m
T^g	T	Time steps when the utility is available

Time and demand parameters

Δ	Demand time steps	[hours]
d_t^h	Heating load in time step t	[kW]
d_t^e	Electric load in time step t	[kW]

Cost and emission parameters

j	Annualized variable capital cost of technology j	[\$/unit]
j_k^a	Annualized fixed installation cost of technology j in size segment k	[\$]
b	Annualized variable capital cost of electric battery	[\$/kWh]
w	Annualized variable capital cost of water storage	[\$/gal]
c_j^{om}	Operation and maintenance cost of technology j	[\$/kWh]
c_t^b	Utility energy cost (including emissions penalty) in time step t	[\$/kWh]
c_t^s	Utility energy purchase price in time step t	[\$/kWh]
c_t^g	Utility gas cost (including emissions penalty) in time step t	[\$/kWh]

Power generation and storage parameters

b_{jk}	Maximum power rating of technology j in cost segment k	[kW]
e_j^-	Maximum electricity efficiency for technology j	[fraction]
e_j^+	Minimum electricity efficiency for technology j	[fraction]
\bar{e}_b^j	Maximum electricity efficiency for technology electrical storage	[fraction]
\hat{k}_j	Power rating of technology j	[kW/unit]

f_j^b	y -intercept for fuel of technology j	[unitless]
f_j^m	Fuel burn slope of technology j	[unitless]
f_{jt}^p	Production factor of technology j in time step t	[fraction]
j	Maximum turn-down of technology j	[fraction]
j	Amount of fuel needed to start up technology j	[kWh/unit]
\underline{s}	Minimum capacity of electrical storage system	[fraction]
\bar{s}	Maximum capacity of electrical storage system	[fraction]
j	Start-up time for each technology j to reach maximum turn-down (j)	[hours]

Heat generation and storage parameters

	Ambient heat loss for water	[fraction]
	Arbitrary temperature for which there is no thermal loss	[C]
h_j	Thermal efficiency for technology j	[fraction]
j	Exhaust gas output for technology j	[kg/kWh]
h^e	Specific heat of exhaust	[kWh/(kg C)]
h^w	Specific heat of water	[kWh/(gal C)]
$-$	Maximum water storage capacity	[gal]
$-$	Minimum water storage capacity	[gal]
\hat{j}	Average exhaust temp from hot-thermal-producing technology j	[C]
\sim	Average return water temperature to water storage tank	[C]
$-$	Maximum allowed temperature of water in the system	[C]
$-$	Minimum allowed temperature of water in the system	[C]

Continuous variables

X^w	Volume of water storage tank	[gal]
X^{ba}	Amount of electrical storage procured	[kWh]
\hat{X}_t^u	Power purchased from the utility in time step t	[kW]
\hat{X}_t^s	Power sold to the utility in time step t	[kW]
\bar{X}_m^u	Peak power purchased from the utility in month m	[kW]
X_{jt}^p	Power produced by each technology j in time step t	[kW]
\hat{X}_t^b	Power into electrical storage system in time step t	[kW]
\hat{X}_t^o	Power out of electrical storage system in time step t	[kW]
X_t^{psc}	State of charge of electrical storage system in time step t	[kWh]
X_{jt}^{ef}	Electric efficiency of each technology j in time step t	[fraction]
X_{jt}^f	Fuel consumed by technology j in time step t	[kW]
\hat{X}_{jt}	Flow rate of fluid into thermal storage from technology j in time step t	[kg/hour]
\hat{X}_t	Flow rate of water out of thermal storage in time step t	[gal/hour]
X_t^t	Temperature of water in storage in time step t	[C]

Integer variables

Y_j^a	Number of each technology j procured	[units]
Y_{jt}^{op}	Number of each technology j operating in time step t	[units]
Y_{jt}^{to}	Increased number of each technology j operating from $t-1$ to t	[units]

Binary variables

Z_{jk}^{ak}	1 if generating technology j in segment k is procured, 0 otherwise	[binary]
Z^w	1 if additional water storage capacity is procured, 0 otherwise	[binary]
\hat{Z}_t^{\sim}	1 if water storage tank is above $(\sim +)$ in time step t , 0 otherwise	[binary]
\hat{Z}_t^{\wedge}	1 if water storage tank is above $(\hat{\text{boiler}})$ in time step t , 0 otherwise	[binary]

Objective function (See Section 4.4.2.1)

$$\begin{aligned}
(P^0) \text{ minimize } & \underbrace{b X^{ba} + \sum_{j \in J^2; k \in K} a_{jk} Z_{jk}^{ak} + \sum_j Y_j^a + w(X^w -)}_{\text{Capital Costs}} \\
& + \Delta \sum_{j \in J^E; t \in T} c_j^{om} X_{jt}^p + \sum_{j \in J^S; t \in T} c_t^g (\sum_j Y_{jt}^{to} + \Delta X_{jt}^f) \\
& + \Delta \sum_{t \in T} \underbrace{c_t^p \hat{X}_t^u + \sum_m c_m^d \hat{X}_m^u}_{\text{O\&M Costs}} + \Delta \sum_{t \in T} \underbrace{c_t^s \check{X}_t^u}_{\text{Fuel Costs}} \\
& + \Delta \sum_{j \in J^B; t \in T} \underbrace{(\sum_j c_j^{om} + c_t^g) X_{jt}^f}_{\text{Grid Purchase}} \\
& + \underbrace{\sum_{j \in J^B; t \in T} c_{jt}^b X_{jt}^b}_{\text{Grid Sales}} \\
& + \underbrace{\sum_{j \in J^B; t \in T} c_{jt}^b X_{jt}^b}_{\text{Existing Boiler Cost}}
\end{aligned} \tag{4.1}$$

Load balancing (See Section 4.4.2.2)

$$(h^{-b} \hat{X}_t^b - \check{X}_t^b) + \sum_j X_{jt}^p + (\hat{X}_t^u - \check{X}_t^u) = d_t^p \quad \forall t \in T^g \tag{4.2a}$$

$$(h^{-b} \hat{X}_t^b - \check{X}_t^b) + \sum_{j \in J^E} X_{jt}^p = d_t^p \quad \forall t \in T \setminus T^g \tag{4.2b}$$

$$h^w (\hat{X}_t^{\sim} - \check{X}_t^{\sim}) + \sum_j \hat{X}_t^{\wedge} - \sum_j \check{X}_t^{\wedge} = d_t^h \quad \forall j \in J^B; t \in T \tag{4.2c}$$

Utility operations (See Section 4.4.2.3)

$$\bar{X}_m^u \quad \hat{X}_t^u \quad \delta m \quad 2 M; t \quad 2 T_m \quad (4.3a)$$

$$\check{X}_t^u \quad \hat{X}_t^u \quad \delta m \quad 2 M \quad (4.3b)$$

$$t \quad 2 T_m \quad t \quad 2 T_m$$

Power capacity (See Section 4.4.2.4)

$$X_{jt}^p \quad f_{jt}^p \hat{k}_j Y_j^a \quad \delta j \quad 2 J^R; t \quad 2 T \quad (4.4a)$$

$$j \hat{k}_j Y_{jt}^{op} \quad X_{jt}^p \quad \hat{k}_j Y_j^{op} \quad \delta j \quad 2 J^E \quad n J^R; t \quad 2 T \quad (4.4b)$$

$$Y_{jt}^{op} \quad Y_j^a \quad \delta j \quad 2 J^S; t \quad 2 T \quad (4.4c)$$

$$\hat{k}_j Y_j^a \quad \bar{b}_{jk} Z_{jk}^{ak} \quad \delta j \quad 2 J; k \quad 2 K \quad (4.4d)$$

$$Z_{jk}^{ak} \quad 1 \quad \delta j \quad 2 J \quad (4.4e)$$

$$k \quad 2 K$$

Electricity efficiency (See Section 4.4.2.5)

$$X_{jt}^{ef} = \frac{j^-}{1} \frac{j^-}{j} \quad \frac{j^-}{\hat{k}_j(1-j)} \quad \frac{j^-}{Y_{jt}^{op}} \quad \delta j \quad 2 J^S; t \quad 2 T \quad (4.5)$$

Fuel consumption (See Section 4.4.2.6)

$$X_{jt}^f = \frac{X_{jt}^p}{X_{jt}^{ef}} \quad \delta j \quad 2 J^S; t \quad 2 T \quad (4.6a)$$

$$X_{jt}^f = f_j^b \hat{k}_j Y_j^{op} + f_j^m X_{jt}^p \quad \delta j = J^E \quad n(J^S [J^R]); t \quad 2 T \quad (4.6b)$$

$$X_{jt}^f = \frac{h^w \hat{X}_t(j \quad X_t^f)(1 \quad \hat{Z}_t)}{h_j} \quad \delta t \quad 2 T; j \quad 2 J^B \quad (4.6c)$$

Start-up (See Section 4.4.2.7)

$$Y_{j;t+}^{op} \quad Y_{jt}^{op} \quad Y_{j;t+}^{to} \quad \delta j \quad 2 J^S; t \quad 2 T : t < jTj \quad j \quad (4.7)$$

Power storage (See Section 4.4.2.8)

$$X_{t+1}^{bsc} \quad X_t^{bsc} = \Delta(-^b \check{X}_t^b \quad \hat{X}_t^b) \quad \delta t \quad 2 T : t < jTj \quad (4.8a)$$

$$\underline{s} X^{ba} \quad X_t^{bsc} \quad \bar{s} X^{ba} \quad \delta t \quad 2 T \quad (4.8b)$$

$$X_1^{bsc} = X_{jTj}^{bsc} \quad (4.8c)$$

Heat capacity (See Section 4.4.2.9)

$$\check{X}_{jt} = \sum_{j \in J} X_{jt}^f - \sum_{j \in J} X_{jt}^{CHP}; t \in T \quad (4.9)$$

Heat storage (See Section 4.4.2.10)

$$X_{t+1}^t - \rho (1 - \check{Z}_t^t) X_t^t = \frac{\sum_{j \in J} \Delta_j^h h^e \check{X}_{jt}(\hat{j} - X_t^t) - \Delta h^w \hat{X}_t(X_t^t - \check{X}_t^t)}{h^w X^w} \quad \forall t \in T : t < |T| \quad (4.10a)$$

$$X_t^t - \check{X}_t^t - (\hat{X}_t^t - \check{X}_t^t) Z^w \quad \forall t \in T \quad (4.10b)$$

$$\check{Z}_t^t - X_t^t - \check{X}_t^t + (\hat{X}_t^t - \check{X}_t^t) \check{Z}_t^t \quad \forall t \in T \quad (4.10c)$$

$$(\hat{X}_t^t - \check{X}_t^t)(1 - \hat{Z}_t^t) - X_t^t - \hat{X}_t^t - (\hat{X}_t^t - \check{X}_t^t) \hat{Z}_t^t \quad \forall t \in T; j \in J^B \quad (4.10d)$$

$$- X^w - \quad (4.10e)$$

$$Z^w = X_{j \in J}^a Y_j^a \frac{\max_{t \in T} f d_t^P g}{\min_{j \in J} f k_j g} Z^w \quad (4.10f)$$

Non-negativity and integrality

$$X^w; X^{ba} \geq 0 \quad (4.11a)$$

$$X_{jt}^f; X_{jt}^p; X_{jt}^{ef}; \check{X}_{jt} \geq 0 \quad \forall j \in J; t \in T \quad (4.11b)$$

$$\bar{X}_m^u \geq 0 \quad \forall m \in M \quad (4.11c)$$

$$\hat{X}_t^u; \check{X}_t^u; \check{X}_t^b; \hat{X}_t^b; X_t^{bsc}; \hat{X}_t; X_t^t \geq 0 \quad \forall t \in T \quad (4.11d)$$

$$Y_j^a \geq 0; \text{integer} \quad \forall j \in J \quad (4.11e)$$

$$Y_{jt}^{op}; Y_{jt}^{to} \geq 0; \text{integer} \quad \forall j \in J; t \in T \quad (4.11f)$$

$$Z^w \text{ binary} \quad (4.11g)$$

$$\check{Z}_t^t; \hat{Z}_t^t \text{ binary} \quad \forall t \in T \quad (4.11h)$$

$$Z_{jk}^{ak} \text{ binary} \quad \forall j \in J; k \in K \quad (4.11i)$$

4.4.2 Discussion of Formulation

We describe, in detail, the objective function and constraint set.

4.4.2.1 Objective function

The objective function minimizes costs associated with fixed and variable procurement, operation and maintenance, power generation, and the net utility charge. Procurement includes both size-dependent capital cost (variable) and installation (fixed), which may incorporate the construction of tailored equipment housing units and the emplacement of piping and cables. The

fixed cost segments are increasing and therefore convex, precluding binary logic to ensure placement in the appropriate cost segment. Binary variable Z_{jk}^{ak} enforces the piecewise-linear installation cost. The way in which load is met is influenced by the fuel cost and grid purchase terms in the objective function and controlled through various constraints in set (4.6).

We use a standard annualized cost computation, which includes the use of a capital recovery factor [120]:

$$C_j = \frac{i(1+i)^{N_j}}{(1+i)^{N_j} - 1} \bar{c}_j \quad \forall j \in \mathcal{J} \quad (4.12)$$

where i is the annualized real discount rate, N_j is the expected lifetime, in years, of technology j and \bar{c}_j is the net present capital cost of technology j . Although expression (4.12) only includes the technologies in set \mathcal{J} , this formula is extended to the electrical storage system as well.

4.4.2.2 Load Balancing

Constraint (4.4.1) balances electrical load with the sum of: the amount of net power deployed from the storage system, the power dispatched from all electrical power systems, and the net power purchased from the utility. We relax, from equality, this constraint by ensuring that the net power produced by the microgrid and purchased from the utility meets or exceeds the electrical load. We introduce a gas turbine generator with and without combined-heat-and-power capabilities to the set \mathcal{T}^e , in addition to fuel cells and photovoltaic panels. Constraint (4.2b) restricts the grid interaction during utility service disruptions, requiring all loads to be met with the microgrid. We enforce constraint (4.2c) through a set of bi- and tri-linear terms in which the on-site heating load is met through a mixture of hot and cold water. If the water temperature in the tank is above \hat{T}_{Boil} , then thermal demand is met through the product of variable water flow out of the tank and the temperature gradient above the delivery temperature. Otherwise, the flow out becomes fixed and is determined by equation (4.13). As the temperature of the water in the storage tank increases, the flow of water out decreases; and, therefore, the fuel needed to power the boiler decreases [2].

$$\hat{X}_t = \frac{d_t^h}{h^w(\hat{T}_{\text{Boil}} - T^d)} \quad \forall t \in \mathcal{T} \quad (4.13)$$

4.4.2.3 Utility Operations

Constraint (4.3a) is the linearization of equation (4.14), which captures the peak power purchased in month m . Constraint (4.3b) restricts energy arbitrage and enforces net metering, typical for grid-connected systems.

$$\bar{X}_m^u = \max_{t \in T_m} \hat{X}_t^u \quad \forall m \in M \quad (4.14)$$

4.4.2.4 Power Capacity

Constraint (4.4a) restricts the power output of renewable technology j to be less than or equal to the product of the capacity of the procured system and the production factor in hour t . Constraint (4.4b) ensures that the power output of non-renewable, electric-producing technology j is between the minimum required turn-down and the maximum amount of available power in hour t . The former level requires the fuel cell to produce sufficient power at its minimum required temperature. Constraint (4.4c) restricts the number of operational fuel cells to be no more than the number acquired. Constraint (4.4d) dictates that the chosen power rating is assigned to the correct installation cost segment. Constraint (4.4e) limits the selection to at most one segment.

4.4.2.5 Electrical Efficiency

We model electrical efficiency as a decreasing function of the average output of the operational fuel cells through constraint (4.5). In this case, as the power output increases, the electrical efficiency of the system decreases. We assume that all fuel cells of type j operate identically. The tradeoff, however, is the inclusion of additional bi-linear terms that include the product of a continuous variable and a general integer variable. The variable efficiency is bounded between $\underline{\eta}_j$ and $\bar{\eta}_j$ for fuel cell technology j [2].

4.4.2.6 Fuel Consumption

Constraint (4.6a) ensures that the amount of fuel consumed by fuel cell type j in time period t is equal to the quotient of the total power produced and the average variable efficiency; this constraint creates $\sum_j X_j^p$ additional bi-linear terms. We implement constraint (4.6b) to compute the fuel needed to produce $X_{j,t}^p$ kW of power for both the standard electrical and

combined-heat-and-power generators. We use the linear formulation consisting of the sum of the marginal contribution of fuel per kW ($f_j^m X_{jt}^p$) and the product of the y -intercept (f_j^p) and the capacity of fuel cells operating in a given hour ($\hat{k}_j Y_{jt}^{op}$). We implement constraint (4.6c) to calculate the fuel used to power the boiler as the quotient of the amount of thermal energy dispatched and the boiler efficiency. If the water temperature is above the delivery temperature, then no fuel is consumed [2].

4.4.2.7 Start-up

The coarseness of time fidelity precludes the necessity of power-ramping constraints; that is, fuel cell operation can fluctuate between the maximum power rating and minimum turn-down within a single time step. However, when activated, solid oxide fuel cells must reach a designated temperature prior to producing power. The parameter τ_j dictates the number of time steps to reach operational temperature from ambient. Therefore, we include constraint (4.7) to ensure that if the number of fuel cells in operation in time period $t + \tau_j$ is greater than the number of fuel cells operational in time period t , then Y_{jt}^{to} assumes the value of the difference; otherwise, its value is 0. This models the number of fuel cells required to turn on in time period t and ensures that we capture the amount of time and fuel necessary to bring the fuel cell from ambient to operational temperature prior to dispatching power.

4.4.2.8 Power Storage

Constraint (4.8a) requires that the difference in states of charge between time steps t and $t + 1$ equal the net energy dispatched from the storage system in time period t . We incorporate a constant electrical efficiency loss for charging the battery. Constraint (4.8b) dictates that the battery's state of charge is restricted to between the minimum and maximum allowable limit of the procurement variable. Constraint (4.8c) requires equality of the electrical storage system's beginning and ending state of charge.

4.4.2.9 Heat Capacity

In our system, fuel cells with combined-heat-and-power capabilities provide the added benefit of utilizing the thermal exhaust produced by the fuel cell to heat water in the storage tank. Constraint (4.9) dictates that the amount of exhaust flow is a function of the fuel consumed by the

co-generational fuel cell. We utilize an inequality to allow for curtailment of the thermal energy in time periods in which the inclusion of the exhaust would force the water temperature to exceed its allowable limit. The added co-generational benefit does not apply to diesel-powered generation.

4.4.2.10 Heat Storage

Constraint (4.10a) governs the temperature differential between time periods. We (i) account for a constant heat loss due to thermal conduction; (ii) add the thermal energy provided by the exhaust heat from the various combined-heat-and-power systems; and, (iii) subtract the thermal energy dispatched to meet the heating load. Constraint (4.10b) limits the temperature to \bar{T} if a storage tank is required and to \tilde{T} otherwise. Constraint (4.10c) dictates that if the water temperature is arbitrarily close (ϵ) to the return water temperature (\tilde{T}), we do not apply the heat loss due to thermal conduction (described in constraint (4.10a)). Constraint (4.10d) governs the binary variable \hat{Z}_t^\dagger used to determine if the water temperature is above or below the delivery temperature (\hat{T}_{Boil}). Constraint (4.10f) serves two purposes: (i) it requires the procurement of additional water storage system capacity if a combined-heat-and-power system is procured; and, (ii) it limits the number of acquired combined-heat-and-power systems to the maximum power demand. Constraint (4.10e) bounds the capacity of the water storage system [2].

4.5 Solution Methodology

The formulation (P^θ) is a mixed-integer nonlinear program that includes continuous, binary, and integer variables, as well as constraints with non-linear terms. State-of-the-art global optimizers yield gaps of greater than 10% after more than two hours of solution time. Therefore, we present, in this section, our methods to expedite solutions to realistic instances of (P^θ).

Standard approaches to expedite solutions include: (i) scaling to reduce the magnitude between the largest and smallest values for each data set; (ii) conversion of tri-linear to bi-linear terms and the introduction of auxiliary variables and constraints to create exact linearizations of the product of binary and continuous variables; and, (iii) a bound tightening procedure [2].

Through scaling, we reduce the number of orders of magnitude in the data by four. We use standard techniques [137] to create exact linearizations of eligible non-linear terms, i.e., nonlinear terms involving the product of at least one discrete variable in which said linearization yields

favorable results (see Table 4.1). By executing the bound-tightening algorithm, we reduce the difference between the upper and lower bounds by more than 50% for select variables.

Table 4.1 Type and quantity of non-linear terms in the constraint set and how they are modified after performing standard linearization techniques [137].

†: The case of the product of a continuous and an *integer* (vice binary) variable requires additional model elements for its linearization, and testing yields unfavorable results.

Type	Term	Quantity	Constraint	Transformation
Bi-linear	$\tilde{Z}_t^t X_t^t$	jTj	(4.2c)	Linear
	$\tilde{Z}_t^t \hat{X}_t$	jTj	4.6c	
	$Y_{jt}^{\text{op}} X_{jt}^{\text{ef}}$	$jJ^S j jTj$	(4.5) [†]	No change
	$X_{jt}^{\text{ef}} X_{jt}^t$	$jJ^S j jTj$	(4.6a)	
	$\hat{X}_t X_t^t$	jTj	(4.2c), (4.6c), (4.10a)	
	$X_t^w X_t^t$	jTj	(4.2c)	
Tri-linear	$\hat{Z}_t^t \hat{X}_t X_t^t$	jTj	(4.6c)	Bi-linear
	$\tilde{Z}_t^t X_t^w X_t^t$	jTj	(4.2c)	

Table 4.2 Size of (P^b) in terms of set cardinality.

Model Component	Characteristic	Number
Variables	Continuous	$jTj (8 + 3jJj) + jMj + 2$
	Integer	$jTj (jJj + 1)$
	Binary	$2jTj + jJj jKj + 1$
Constraints	Linear	$6jTj (1 + jJj) + jJj (1 + jKj) + jMj$
	Non-linear	$jTj (jJj + 1)$

The full formulation of (P^b), after the linearizations reflected in Table 4.1, has a size reflected in Table 4.2 and includes $5jTj + 2jJ^S j jTj$ bi-linear terms. We refer to the method of solving (P^b) using techniques (i)-(iii), outlined in the prior paragraph, as method (\mathbf{M}^b), the **baseline** method. While the implementation of (\mathbf{M}^b) yields optimality gap improvements of approximately 2%, on average, after two-hour solve time, we are still unable to generate solutions with less than a 10% gap.

Ultimately, complications arise in two sets of constraints: (i) those ensuring that the thermal energy produced through the co-generational technologies and the boiler is sufficient to heat the water in the storage system and meet the hot thermal load (see Table 4.3: row (P^b)-Thermal); and, (ii) those governing the fuel consumption and the efficiency associated with the solid oxide

fuel cells (see Table 4.3: row (P^{\cdot})-Electric). Therefore, we present an enhanced, three-phase solution methodology (M^e) using linear approximations depicted in Figure 4.5.

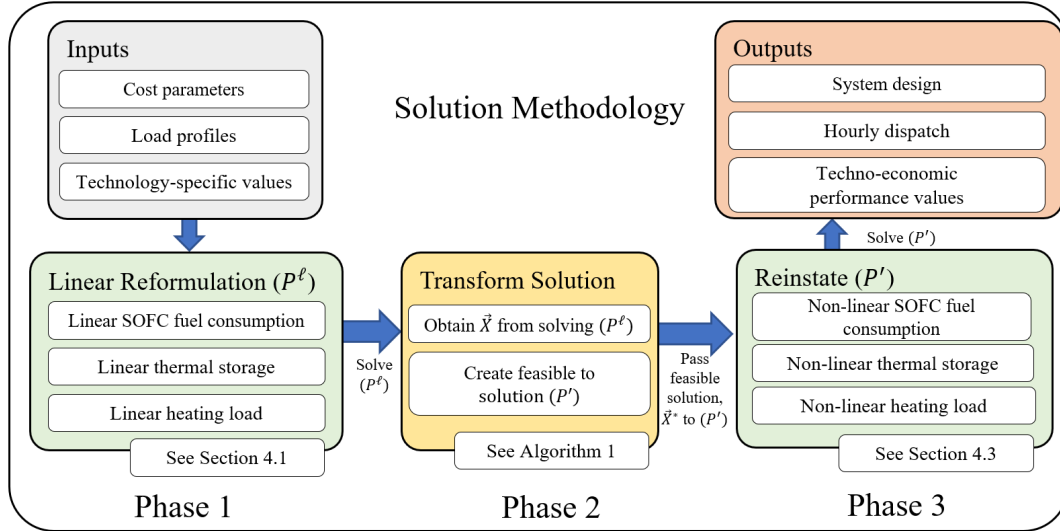


Figure 4.5 Three-phase methodology to generate feasible solutions to (P^0) with improved solutions and optimality gaps.
 Note: SOFC - Solid oxide fuel cell

4.5.1 Linear Reformulation (Phase 1)

Phase 1 modifies (P^0) by creating linear approximations for constraints in the “no change” and “bi-linear” rows found in Table 4.1. We refer to this reformulation as (P^ℓ). Figure 4.6 depicts a fuel consumption curve, representing a 10kW fuel cell system used in the model (P^0), and a linear approximation of that curve.

The solid, red line results from the combination of constraints (4.5) and (4.6a), while the dashed, blue line is a piece-wise linear approximation. Without loss of generality, Figure 4.6 shows two segments, but the approximation could be made with an arbitrary number of S segments. However, more segments, though potentially providing a more accurate approximation, create additional integer variables and can slow model solve time.

The linear approximation creates a conservative characterization of the system in that the resulting solution is an over-estimation of fuel consumption, resulting in a higher cost of fuel per unit energy produced for the solid oxide fuel cell than when employing the non-linear fuel curve used in (P^0). The increased amount of fuel consumed for a commensurate amount of power results

in a larger contribution of thermal energy to the heating load. Therefore, the approximation overestimates the total cost, and employing it results in a restriction of our original model (P^0).

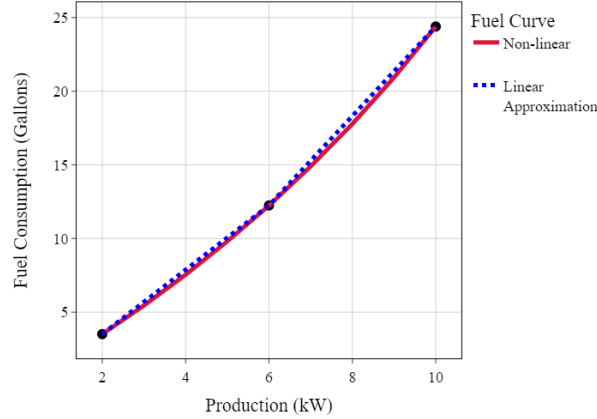


Figure 4.6 Comparison of piece-wise linear and non-linear fuel consumption of a representative solid oxide fuel cell with two segments.

Notation required in model (P^1):

Notation	Description	Units
S	Linear approximation segments	
b_{js}^f	y -intercept for linearization of fuel curve for technology j in segment s	[gal]
m_{js}^f	Marginal fuel consumption of technology s for segment s	[gal/kW]
l_{js}	Lower bound of power output of technology j in segment s	[kW]
u_{js}	Upper bound of power output of technology j in segment s	[kW]
Z_{jst}^{op}	1 if technology j is operating in segment s , in time period t and 0 otherwise	[binary]
X_{jst}^{ps}	Amount of power dispatched from technology j in segment s in time period t	[kW]

Fuel cell constraints present in (P^1):

$$X_{jt}^f = m_{js}^f X_{jst}^{ps} + b_{js}^f Y_{jt}^{op} \quad \forall j \in J^S; s \in S; t \in T \quad (4.15a)$$

$$X_{jst}^{ps} \leq l_{js} Y_{jt}^{op} \quad \forall j \in J^S; s \in S; t \in T \quad (4.15b)$$

$$X_{jst}^{ps} \leq u_{js} Y_{jt}^{op} + M(1 - Z_{jst}^{op}) \quad \forall j \in J^S; s \in S; t \in T \quad (4.15c)$$

$$X_{jst}^{ps} \leq M Z_{jst}^{op} \quad \forall j \in J^S; s \in S; t \in T \quad (4.15d)$$

$$X_{jt}^p = \sum_{s \in S} X_{jst}^{ps} \quad \forall j \in J^S; t \in T \quad (4.15e)$$

$$\sum_{s \in S} Z_{jst}^{op} \leq 1 \quad \forall j \in J^S; t \in T \quad (4.15f)$$

$$Z_{jst}^{\text{op}} \quad Y_{jt}^{\text{op}} \quad \delta_j \quad \forall j \in J^S; s \in S; t \in T \quad (4.15g)$$

Instead of non-linear fuel consumption as a function of the variable efficiency and power output, (P^i) represents fuel consumption as a linear function of power output and a fixed fuel intercept. Constraint (4.15a) governs the fuel consumed by the solid oxide fuel cell and is a linear combination of the power produced and an appropriately selected intercept if the fuel cell is operating in segment s , and 0 otherwise. Constraints (4.15b)-(4.15d) require that the power produced by technology j in time period t is restricted between the appropriate lower and upper bound of segment s . We use constraint (4.15e) to consolidate power from all segments. Constraint (4.15f) limits the power output to at most one segment, and constraint (4.15g) restricts the binary variable to 0 if there are no operational fuel cells. We replace constraints (4.5) and (4.6a) with constraints (4.15a)-(4.15g).

The other sources of non-linearities reside in the thermal load balance constraint (4.2c) and in the water tank temperature constraint (4.10a). We devise a way to approximate these constraints with a linear equation that satisfies the thermal load as a convex combination of energy from the boiler and exhaust heat produced by the solid oxide fuel cell (4.16a). The associated notation and model modifications are found in Table 4.3 and in constraints (4.16a)-(4.16c).

Linear thermal storage notation:

Notation	Description	Units
$\tilde{\Delta}$	Incremental increase of water storage tank size	[gal]
X_t^{hts}	Amount of heat sent to storage in time period t	[kWh]
X_t^{hfs}	Amount of heat dispatched from storage in time period t	[kWh]

Linear thermal energy constraints:

$$\sum_{j \in J^{\text{CHP}}} h_j^e X_{jt}^f + \sum_{j \in J^{\text{B}}} X_{jt}^f + (X_t^{\text{hfs}} - X_t^{\text{hts}}) = d_t^h \quad t \in T \quad (4.16a)$$

$$X_t^{\text{tsc}} = (1 - \alpha) X_{t-1}^{\text{tsc}} + X_t^{\text{hts}} - X_t^{\text{hfs}} \quad t \in T \quad (4.16b)$$

$$X_t^{\text{tsc}} \leq X^w \quad t \in T \quad (4.16c)$$

To account for thermal storage, we add variables X_t^{hts} and X_t^{hfs} which model the heat to and from, respectively, the thermal storage system. Constraint (4.16a) ensures that the heating load is

met through a linear combination of thermal energy from the co-generational solid oxide fuel cell, thermal energy generated by the boiler, and thermal energy from the storage system. We account for energy lost in storage through a parameter λ . Constraint (4.16b) balances the thermal energy in storage, and constraint 4.16c restricts the energy in storage to the capacity of the system. We replace the constraints found in row (P^θ) of Table 4.3 with the constraints in rows labeled (P^ζ) to create a mixed-integer linear model.

Table 4.3 Constraint numbers with associated quantities required to transform (P^θ) into (P^ζ) . The constraints in each of the rows corresponding to a particular model are mutually exclusive.

Model	Energy Type	Constraints	Quantity
(P^θ)	Electric	(4.5), (4.6a)	$2jJj - jTj$
	Thermal	(4.2c), (4.6c), (4.9), (4.10a)-(4.10e)	$jTj(6 + jJj)$
(P^ζ)	Electric	(4.15a)-(4.15g)	$jJj - jTj(5jSj + 1)$
	Thermal	(4.16a)-(4.16c)	$3jTj$

4.5.2 Transform Solution (Phase 2)

We solve the linear program (P^ζ) utilizing state-of-the-art software and obtain a solution to which we refer as \mathcal{X} . Utilizing the heuristic described in Algorithm 4, we obtain from \mathcal{X} solution \mathcal{X}^* , which is feasible for (P^θ) . We first initialize the variable values according to \mathcal{X} from (P^ζ) . We then compute the solid oxide fuel cell efficiency and fuel consumption in each time period using the power produced by the associated technology. We then determine the variable values, such as exhaust flow from the fuel cell and water temperature, corresponding to the thermal load and thermal storage constraints. We establish a starting temperature and related binary variables \hat{Z}_t^+ and \check{Z}_t^+ . With this information and the amount of exhaust $(\hat{X}_{j,t})$ from combined heat and power technology j , we compute the remaining variable values. For those associated with thermal storage, we include a condition to handle a solution resulting in a temperature that exceeds $\bar{\tau}$. In those instances, we increase the volume of the hot water storage tank by $\bar{\tau}$ and re-compute the variable values. Lastly, we update variable bounds using information obtained by the solution (\mathcal{X}^*) . If combined-heat-and-power technologies are not a component in the fixed design, the computation of variables related to thermal load becomes explicit, as shown by **Function 2** found in Algorithm 4.

Algorithm 4 Induce feasibility in (P^h) from a solution to (P^c) .

Comments (\triangleright) reflect which restored constraint is made feasible.

Require: X^c, X^h

for $j \in J^S; t \in T$ do

$$X_{jt}^{ef*} = \begin{cases} \frac{j^e - j^e}{1 - j^e} \frac{X_{jt}^p}{Y_{jt}^{op*}} & \text{if } Y_{jt}^{op*} > 0 \\ \text{---} & \text{otherwise} \end{cases} \quad . \text{ Constraint (4.5)}$$

$$X_{jt}^{f*} = \begin{cases} \frac{X_{jt}^{p*}}{X_{jt}^{ef*}} & \text{if } Y_{jt}^{op*} > 0 \\ 0 & \text{otherwise} \end{cases} \quad . \text{ Constraint (4.6a)}$$

for $j \in (J^S \setminus J^{CHP}); t \in T$ do

$$\beta_j^* X_{jt}^* = j X_{jt}^{f*} \quad . \text{ Constraint (4.9)}$$

if $\sum_{j \in J^{CHP}} Y_j^a > 0$ then

$$X_1^{t*} = \frac{+\hat{j}}{2} \quad . \text{ Set the initial temperature to the mid-point}$$

$$X^{w*} = \text{---} \quad . \text{ Constraint (4.10e)}$$

$X = \text{Thermal}(X)$

while $\max_{t \in T} X_t^g > \text{---}$ do $\quad . \text{ Constraint (4.10b)}$

$$\begin{cases} X^{w*} = X^{w*} + \sim \\ \text{---} - \text{---} + \sim & \text{if } X^{w*} > \text{---} \end{cases} \quad . \text{ Constraint (4.10e)}$$

$X = \text{Thermal}(X)$

else

$X = \text{No CHP}(X)$

Function 1 - Creates feasibility for thermal energy constraints with combined-heat-and-power

```

function Thermal( $X$ )
  for  $t \geq 2$   $T$  do
     $\hat{Z}_t^*$  = 1 if  $X_t^* \leq 0$  otherwise . Constraint (4.10c)
     $\tilde{Z}_t^*$  = 1 if  $X_t^* \geq 0$  otherwise . Constraint (4.10d)
     $\hat{X}_t^*$  =  $\frac{d_t^h}{h^w(\hat{\lambda}_j)}$  . Constraint (4.2c)
     $X_{jt}^*$  =  $\frac{h^w \hat{X}_t^* (\hat{\lambda}_j X_t^*) (1 - \hat{Z}_t^*)}{h_j}$   $j = \text{Boiler}$  . Constraint (4.6c)
     $X_{t+1}^*$  =  $(1 - \tilde{Z}_t^*) X_t^* + \frac{\sum_{j \in \text{CHP}} h_j h^e X_{jt}^* (\hat{\lambda}_j X_t^*)}{(h^w X^{w*})} - h^w \hat{X}_t^* (X_t^*)$  . Constraint (4.10a)
  return  $X$ 

```

Function 2 - Creates feasibility for thermal energy constraints without combined-heat-and-power

```

function No CHP( $X$ )
   $X_t^* \leq 0$   $\forall t \geq 2$   $T$  . Constraints (4.10a), (4.10b)
  for  $t \geq 2$   $T$  do
     $\hat{Z}_t^*$  = 0 . Constraint (4.10c)
     $\tilde{Z}_t^*$  = 0 . Constraint (4.10d)
     $\hat{X}_t^*$  =  $\frac{d_t^h}{h^w(\hat{\lambda}_j)}$  . Constraint (4.2c)
     $X_{jt}^*$  =  $\frac{h^w(\hat{\lambda}_j) \hat{X}_t^*}{h_j}$   $j = \text{Boiler}$  . Constraint (4.6c)
  return  $X$ 

```

4.5.3 Return of the Original Formulation (P^0) (Phase 3)

We reconstitute (P^0) by performing replacements of constraints in Table 4.3 consistent with transforming (P^1) into (P^0). We use the solution obtained in **Phase 2** as a feasible starting point for (P^0). The solution to this problem provides an improvement over our initial feasible solution and, as a second-order effect, tightens the lower bound. To ensure that the resulting solution is feasible for (P^0), we assume that we have access to sufficient fuel for the boiler and to solid oxide fuel cells; we also assume that we can procure an appropriately sized hot water tank, which is necessary to maintain the water temperature within the allowable limits. The variables we update through Algorithm 4 are only found in the constraints we reinstate during **Phase 3**; through proper ordering of variable determination, we ensure their feasibility. The remaining constraints,

which are feasible to (P^1) , remain feasible with respect to (P^0) .

4.6 Inputs and Results

We solve (P^0) utilizing the process described in Section 4.5. This section describes the input data, provides the performance of the model in terms of solution quality and run time, and analyzes one such solution. Model (P^0) consists of a variety of inputs, including technology-specific data, electrical production factors, and electrical and heating loads.

4.6.1 General Inputs

Table 4.4 provides parameter values for technologies other than fuel cells [138]. (Section 4.6.2 describes inputs related to solid oxide fuel cells.)

Table 4.4 Technology input values (not including solid oxide fuel cells). The lithium-ion battery has a two-hour power rating.

Technology	Capital Cost	O&M	Lifetime (years)
Photovoltaic	\$1,592/kW	\$17/ (kW year)	20
Lithium Ion Battery	\$775/kWh	-	10
Generator	\$500/kW	10/(kW year)	20
CHP System	\$500/kW	0.019/kWh	20

CHP: Combined heat and power

We obtain all 16 distinct hourly electric load profiles for a representative year compiled by the National Renewable Energy Lab from the Open Energy Data Initiative website. This dataset was developed by the National Renewable Energy Lab’s Distributed Energy Systems Integration group as part of a study on high penetrations of distributed solar photovoltaics [3]. Table C.1 in Appendix C.2 provides details. We choose to highlight a moderate suburban community combined with a light rural area (R1-1247-2) to show how a microgrid consisting of solid oxide fuel cells can add resilience to communities at risk of fire-related utility service disruptions. Figure 4.7 is a snapshot of case R1-1247-2 [139].

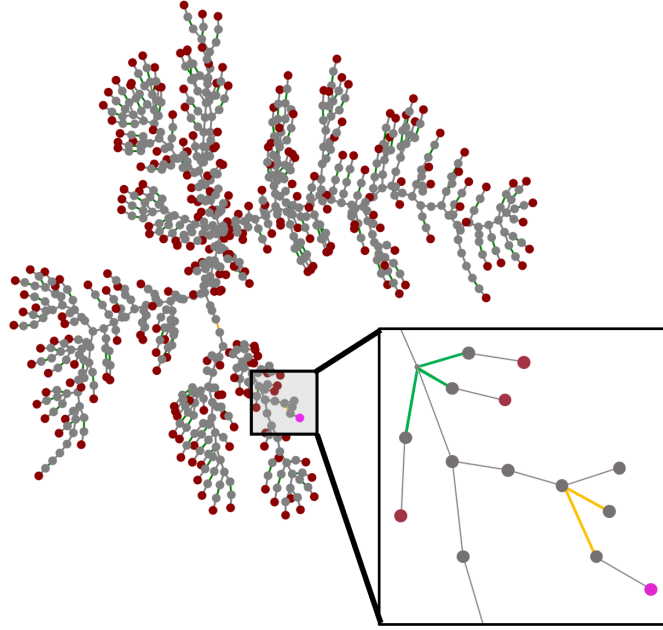


Figure 4.7 R1-12.47-2 Taxonomy Feeder. Magenta represents the slack bus (the power source of the distribution network), while dark red depicts the loads that require power. Green links are transformers; orange links are switches; and gray links and nodes are triplex lines and connections, respectively.

Figure 4.8 depicts the load profile R1-1247-2. The oval in the figure shows the time period in which the natural disaster occurs and the corresponding unavailability of utility services. The dark blue color (outlined by the oval) shows that, for this particular instance, we reduce the demand to a predetermined “critical load” during the service disruption. We generate heating loads from the EnergyPlus[®] simulation software hosted by the National Renewable Energy Lab using a combination of five building types: hospital, hotel, apartment, large office, and supermarket. Figure 4.9 depicts a heat map of the thermal load at hourly fidelity. For the photovoltaic production factors f_{jt}^p , we use data obtained from the *PVWatts Tool* [140] given in Figure 4.10. We annotate the time of year the utility outage occurs to highlight the amount of solar irradiance available. The installed photovoltaic capacity for a resilience model is influenced by the outage time period selected.

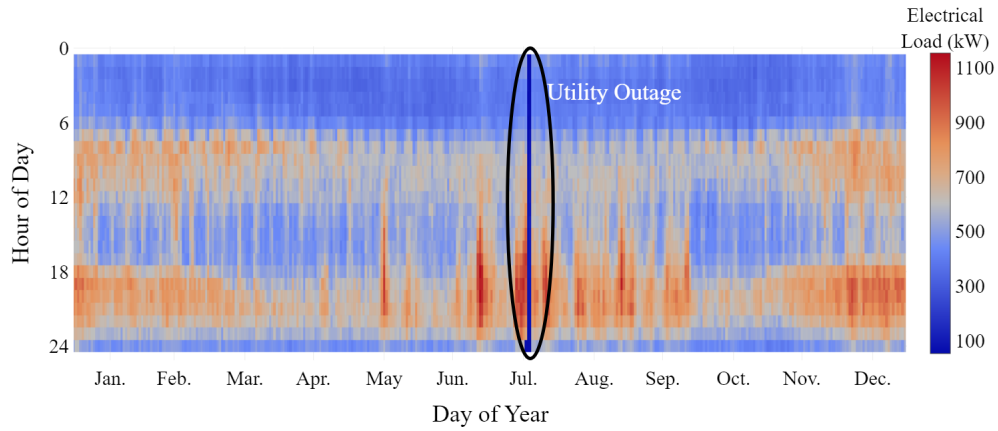


Figure 4.8 Example load profileElectric load profile for distribution feeder R1-1247-2, given by the network graph in Figure 4.7, shown with a utility service disruption.

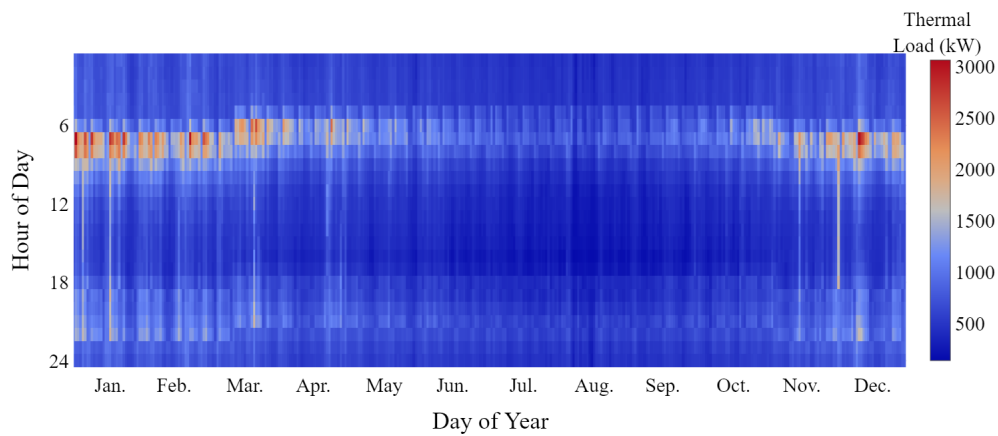


Figure 4.9 Hot thermal load profile derived from the EnergyPlus[®] simulation software, representing a collection of building types, including a hospital, hotel, apartment, large office, and supermarket.

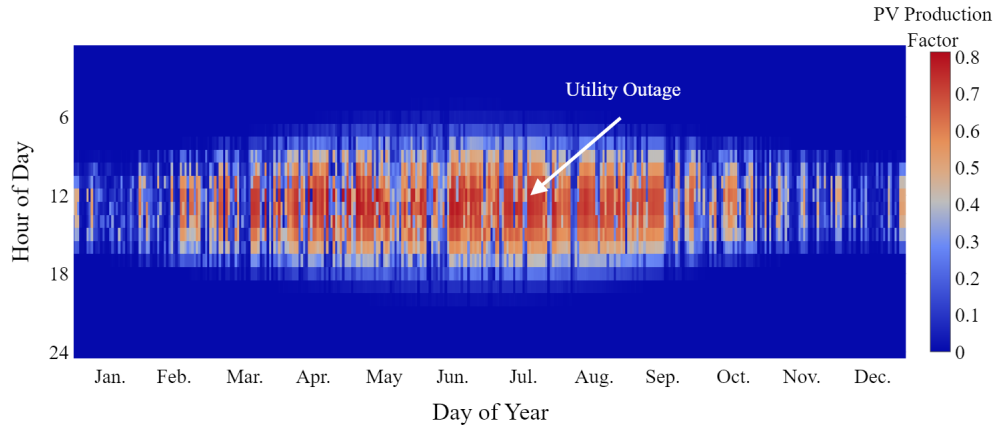


Figure 4.10 Estimated electricity production of a grid-connected roof- or ground-mounted photovoltaic system installed in Richmond, CA. The arrow shows the approximate timeframe of the modeled utility service disruption.

4.6.2 Solid Oxide Fuel Cell Inputs

The U.S. Energy Information Administration [141], Battelle Memorial Institute [142, 143], and Whiston et al. [144] offer costs associated with equipment, installation, stack, heat recovery, and inverters. We conduct analysis using system sizes from 10 to 250kW. Cost values in this range are similar though minor differences exist between the 10-25kW range [142] and the 100-250kW range [143]. A drawback of high-temperature solid oxide fuel cells is the cost associated with the stacks whose replacement is necessary, in part, due to the stress of operating at high temperatures [144]. Specifically, over time, the high-temperature gradients degrade the system. We therefore consider a conservative start-up (from ambient temperature) time of three hours [145] which assumes a heating rate of approximately 5°C per minute [146]; in this way, we emphasize system reliability over fast start up. We incorporate fixed operations and maintenance (O&M) costs, including the cost of replacing the stack, reformer, and inverter after five years. System lifetime is assumed to be 10-20 years, depending on the source. Stack lifetime is assumed to be five years [141], [142, 143] and [144].

Costs are separated into three categories (high, medium, and low). The high-capital-cost case assumes elevated equipment price and sales markup. Additionally, we consider variations by decade which are attributable to the assumption that an inverse relationship exists between production and price. We include a cost with sales markup for combined heat and power heat

recovery equipment and assume a 5% discount rate. See Appendix C.3 for a more detailed description of the economic data.

We also update the efficiency parameters (η_j and η_{-j}) and start-up time ($t_{j, start}$). To determine parameter values of interest, we vary parameter values and solve the model to establish that, other than costs, the efficiency parameters and start-up time impact fuel cell operational behavior the most. Beigzadeh et al. [119] report electrical efficiencies of solid oxide fuel cells between 57% and 72%, depending on the type of fuel used; the lower value corresponds to gasified biomass and the higher to natural gas. Additionally, we confirm, through discussion with commercial partners, that deployed systems realize electrical efficiencies of around 60%. We use conservative values to account for both lifecycle system degradation and the utilization of biofuel. However, an end-user of our framework could choose to modify these values as the technology continues to mature. Table 4.5 reflects parameter values that differ from Pruitt et al. [2].

Table 4.5 Values used for power-only and combined-heat-and-power solid oxide fuel cells.

Parameter	Description	Value	
		$j = \text{CHP}$	$j = \text{Power}$
η_j^e	Maximum electricity efficiency	54%	54%
η_{-j}^e	Minimum electricity efficiency	60%	60%
$t_{j, start}$	Start-up time for each technology j to reach η_j	3 hours	3 hours
η_j	Maximum turn-down	20%	20%
c_j^{cap}	Capital cost	\$3,360/kW	\$2,800/kW
c_j^{om}	O&M cost	\$0.024/kWh	\$0.020/kWh

4.6.3 Model Inputs from Solution-Expediting Methodologies

Figure 4.11 shows how the bound tightening procedure [2] produces desired reductions in the feasible region for variables involved in bi-linear terms. These reductions allow the spatial branch-and-bound algorithm to find better solutions and to tighten bounds more easily.

We compare the size of models (P^{full}) and (P^{reduced}), for the inputs used, in Table 4.6. Model (P^{full}) contains over 275,000 constraints, of which 52,000 involve non-linear terms. The reduced size and complexity of (P^{reduced}) relative to (P^{full}) affords us with the ability to generate good solutions quickly, with which we can then initialize the original monolith.

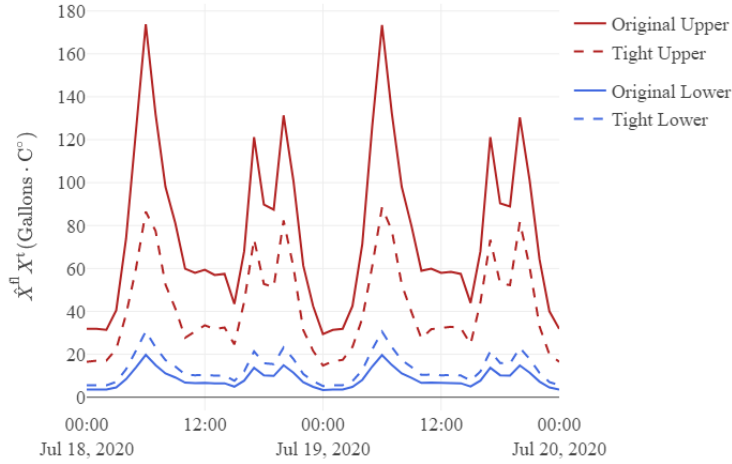


Figure 4.11 Improvement from bound-tightening procedure for the auxiliary, bi-linear variable \hat{X}_{jt}^d . \hat{X}_{jt}^d reduces the magnitude between the upper and lower bound by 57%, as an example.

Table 4.6 Average size and structure of models (P^b) and (P^c) . The (P^c) column shows the percent increase or decrease in size relative to (P^b) .

Category	Type	(P^b)	(P^c)
Variables	Total	232,034	-15%
	Continuous	179,478	-20%
	Discrete	52,556	0%
Constraints	Total	275,897	0%
	Linear	223,339	24%
	Non-linear	52,558	-100%

4.6.4 Solution Quality

Solving (P^b) using (M^e) yields solutions, on average, five times faster than solving (P^b) using (M^b) . Table 4.7 shows results for a one-year time horizon. In general, (M^e) generates an 8% improvement in the objective function value and over a 50% improvement in the optimality gap after a two-hour solve time limit. In only one of the 16 instances did (M^b) return the first solution faster; however, even in this case, the solution obtained by (M^e) is superior.

Table 4.7 Comparison of solutions solving (P^0) with and without the solution obtained from (P^1). Objective function values and optimality gap after two hours of run time, and time until the first feasible solution is obtained. Δ : Reduction between methods (M^b) and (M^e)

Case	Objective Function Value Decrease (\$)			Optimality Gap Reduction (%)			Time to First Solution (Seconds)		
	(M^b)	(M^e)	% Δ	(M^b)	(M^e)	% Δ	(M^b)	(M^e)	Δ
R1-1247-2	1,012,986	931,014	8	15	7	50	178	56	122
R1-1247-3	745,548	692,023	7	14	7	48	253	56	197
R1-1247-4	2,164,754	1,906,774	12	18	7	62	377	73	304
R1-2500-1	1,556,543	1,412,495	9	16	7	54	503	63	440
R2-1247-1	4,483,279	4,112,745	8	13	5	61	845	63	782
R2-1247-2	3,269,277	2,971,911	9	15	6	58	298	60	238
R2-2500-1	7,825,518	7,379,453	6	10	4	57	748	68	680
R3-1247-2	4,085,636	3,790,034	7	13	6	54	1,042	63	979
R4-1247-2	1,744,135	1,589,823	9	15	7	53	288	47	241
R4-2500-1	1,914,215	1,742,076	9	15	7	55	295	75	220
R5-1247-1	6,076,208	5,414,754	11	15	5	68	471	69	402
R5-1247-2	4,500,123	4,165,739	7	13	6	56	911	73	838
R5-1247-4	4,470,154	4,017,051	10	15	5	64	232	69	163
R5-1247-5	4,165,565	3,835,660	8	13	5	58	313	181	132
R5-2500-1	7,932,270	7,272,899	8	12	4	66	240	356	(116)
R5-3500-1	5,425,448	5,078,233	6	11	5	56	425	75	350
Average Across All Cases			8	14	6	58	464	90	373

4.6.5 Solution Implications

To assess the financial benefits of distributed generation, we compare the solution with no distributed generation to that with an installed microgrid capable of servicing a critical load during a utility service disruption. In order to create an equitable comparison, we omit the energy cost during the service disruption. Table 4.8 depicts the resulting values for all 16 load profiles, along with the fraction of demanded power serviced from the utility in the presence of a microgrid. In all cases, the cost to meet the demanded electrical load with distributed generation is less than that associated with the “No Microgrid” solution. Along with cost savings of 8.3%, on average, across the 16 cases, the customer also benefits from added reliability and resilience by being able to service the electrical load during power disruptions to the utility.

Table 4.8 Solution comparison between purchasing all electricity from the utility versus installing a microgrid that is capable of meeting a 48-hour outage occurring during the highest electrical demand period.

Case	Annualized Lifecycle Cost (\$)		Δ (%)	Grid Utilization (%)
	No Microgrid	Microgrid		
R1-1247-2	1,007,933	929,337	-8.5	12.4
R1-1247-3	731,736	690,028	-6.0	6.5
R1-1247-4	2,115,108	1,903,575	-11.1	13.1
R1-2500-1	1,545,364	1,408,578	-9.7	8.1
R2-1247-1	4,419,348	4,101,889	-7.7	10.8
R2-1247-2	3,239,292	2,969,497	-9.1	15.2
R2-2500-1	7,916,373	7,366,441	-7.5	15.2
R3-1247-2	4,058,615	3,775,831	-7.5	8.9
R4-1247-2	1,731,984	1,587,963	-9.1	24.0
R4-2500-1	1,910,583	1,740,579	-9.8	20.3
R5-1247-1	5,832,474	5,402,292	-8.0	13.8
R5-1247-2	4,503,345	4,154,198	-8.4	7.4
R5-1247-4	4,343,550	4,009,787	-8.3	16.6
R5-1247-5	4,136,660	3,831,042	-8.0	21.5
R5-2500-1	7,763,028	7,263,047	-6.9	19.7
R5-3500-1	5,448,520	5,071,643	-7.4	20.3

Table 4.9 reflects the dispatched amount of each technology as a percentage of the total power consumed throughout the year. All remaining power is met by the utility. For almost all 16 cases, the co-generational fuel cell dominates the other technologies in dispatched power, providing approximately 58% of demanded annual power, with an additional 25% coming from the power-only fuel cell. Additionally, because this is a hybrid system of solid oxide fuel cells, photovoltaics, and electrical storage, the diesel generator is not consistently relied on to provide power. This mix of installed technologies also enhances system reliability in that there is not a single point of failure. An additional benefit of the installed microgrid is sustaining possible disruptions in fuel supply. Solid oxide fuel cells have the ability to utilize bio-fuels and, therefore, if strategically located at a site that produces bio-waste, the fuel cell would have access to low-cost fuel that is sourced on-site. This type of setup would reduce the dependency on utility-provided fuel sources while increasing the overall resilience and reliability of the system.

Figure 4.12 compares, for two representative instances (R1-1247-2 and R1-1247-4), solutions returned by (\mathbf{M}^b) and (\mathbf{M}^e) . These two instances differ by electric demand, in which the former services a smaller critical load during the outage than the latter. The area between the two

dashed red lines represents the grid outage. We require the model to service the fully demanded electric and heating load during the disruption. Plots (a) and (c) show the solution returned by (\mathbf{M}^b), in which the solver is unable to leverage the benefit of a combined-heat-and-power solid oxide fuel cell, resulting in larger objective function values (shown in Table 4.7). Instead, the solution installs an oversized photovoltaic system and a backup diesel generator. While this is an acceptable alternative to adding resilience to the system, the solution favors traditional methods. Plots (b) and (d) reflect solutions obtained by (\mathbf{M}^e) which correspond to comparatively smaller objective function values while leveraging co-generational technologies. Additionally, the solutions returned by (\mathbf{M}^e) do not result in curtailed power during the outage.

Table 4.9 Percent of total power consumed during the year by each type of installed technology in the microgrid. No solution includes the diesel generator. CHP: combined heat and power; SOFC: solid oxide fuel cell; PV: photovoltaics

Case	Dispatched Power (%)			
	CHP SOFC	Power SOFC	PV	Utility
R1-1247-2	88	0	0	12
R1-1247-3	89	0	5	6
R1-1247-4	86	0	1	13
R1-2500-1	84	0	8	8
R2-1247-1	47	35	8	10
R2-1247-2	65	20	0	15
R2-2500-1	25	57	3	15
R3-1247-2	51	36	4	9
R4-1247-2	76	0	0	24
R4-2500-1	80	0	0	20
R5-1247-1	35	51	1	13
R5-1247-2	45	45	3	7
R5-1247-4	48	36	0	16
R5-1247-5	51	28	0	21
R5-2500-1	26	55	0	19
R5-3500-1	38	42	0	20
Average	59	25	2	14

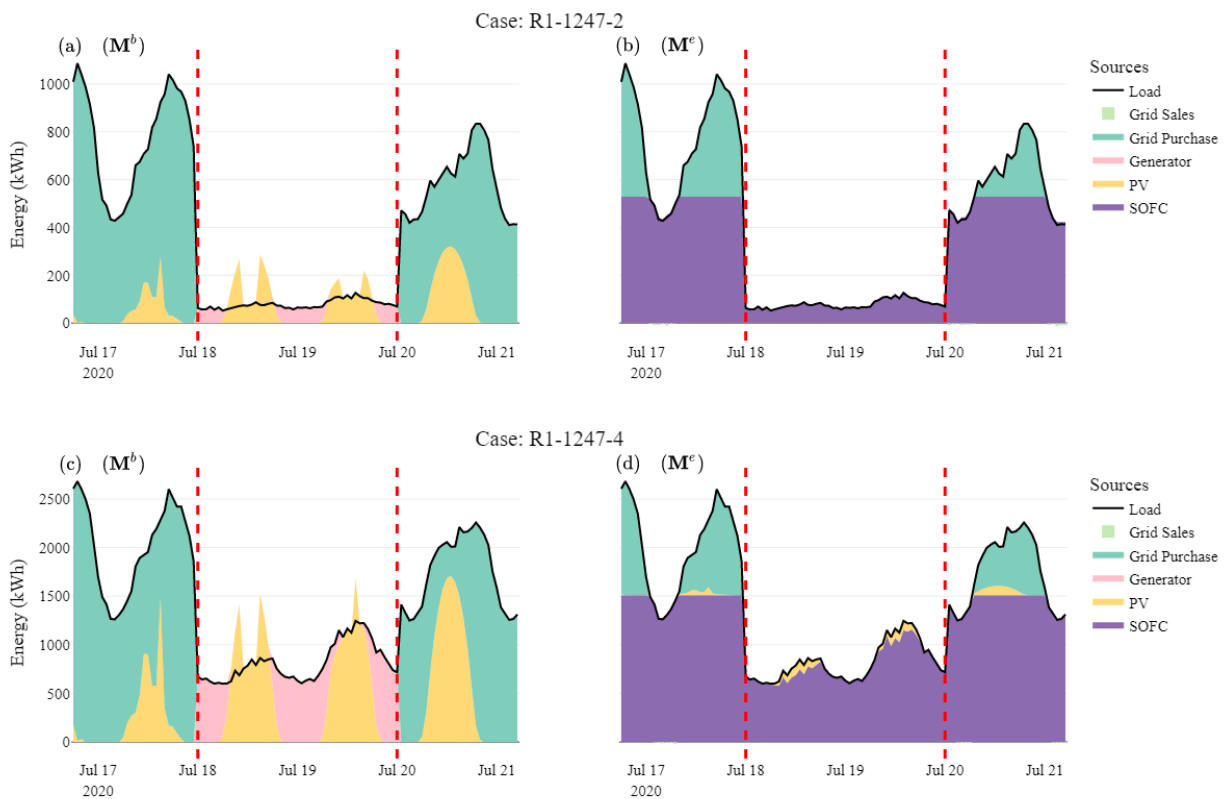


Figure 4.12 Power output by technology type from a combination of microgrid and utility. Dashed lines show the start and end of the utility service disruption. Omitted from the plots are electrical storage operations: while they are part of the configuration, they are not utilized during the depicted time frame. Grid sales are present directly preceding the outage but are difficult to discern.

4.7 Conclusion

This work demonstrates an optimization-based framework for creating solutions that enhance community resilience during outages by increasing the reliability of the electrical infrastructure. We present a mixed-integer, non-linear optimization model that incorporates many distributed energy resource technologies. Our model (P^{θ}) is a member of a class of problems (mixed-integer nonlinear programs) that often present challenges for commercial optimization solvers. Therefore, we create a methodology capable of quickly generating solutions with better objective function values.

The framework presented affords civic and governmental organizations the ability to develop alternate solutions to meet their electric power needs during a utility service disruption and to provide critical services in post-disaster recovery. Additionally, we show the benefit of incorporating solid oxide fuel cells into a microgrid design, due, in part, to its minimal emissions, dependable power supply, and ability to consume multiple fuel types.

4.8 Acknowledgments

This work is a collaborative effort between the Colorado School of Mines, Carnegie Mellon University, Bentley University, and industry partners, in particular, Martin Hering from Robert Bosch LLC. We acknowledge contributions from Dr. Amritanshu Pandey of the University of Vermont and Arnav Gautam from Carnegie Mellon University for their assistance in modeling and representing the distribution network. We are also grateful for the technical expertise of Dr. Jack Brouwer of the University of California-Irvine regarding the fuel cells. The project is funded by the National Science Foundation grant number 2053856.

CHAPTER 5

CONCLUSION

The combination of reduced costs and the need for more reliable power has led to a surge in microgrid utilization. Microgrids are relatively small power systems, typically located close to demanded loads, that can operate with or without the grid (macrogrid). These benefits include, but are not limited to, (i) reduced energy costs, (ii) incorporation of renewable energy sources and diminished emissions, (iii) improved energy resilience and independence, and (iv) enhanced efficiency from a reduction in power-line losses and increased co-generational benefits.

Commercial and open-source tools exist to assist planners in developing and analyzing possible microgrid configurations. However, these tools possess shortcomings, such as the inability to assess multiple scenarios due to run time issues, the absence of resilience metrics to provide planners with multiple courses of action, and omitted technologies.

This work begins by applying a custom *Matheuristic* for designing and dispatching a distributed energy system. In Chapter 2, we define the system and the specific complexities that challenge optimization software and develop a methodology that decouples each problematic component. The original formulation (\mathcal{P}), solved with commercial optimization software, is unable to yield optimal, and sometimes feasible, solutions in fewer than two minutes. The procedure leverages a genetic algorithm that explores the state space of competing microgrid configurations, a time-dependent policy for scheduling the combined-heat-and-power system, and a mathematical optimization model that determines the economic dispatch to minimize production and utility costs. This chapter details the model and methodology we use. Additionally, we show an improvement in solution time and objective function value for a practical time limit (two minutes). This improvement affords two main benefits. First, it allows practitioners to analyze various inputs in a reasonable amount of time without sacrificing quality. Second, the model is a component of an online web tool; therefore, timely solutions are critical. Our methodology ensures, at a minimum, a feasible solution in fewer than 20 seconds and in all tested cases returns a solution within 5% of the best available solution in fewer than two minutes.

Chapter 3 creates a framework to provide the North Carolina waste-water treatment facility the information needed to make investment decisions in the face of competing objectives. We embellish the REopt[®] techno-economic mixed-integer linear formulation to include resilience metrics. We create a multi-objective optimization model to balance the tradeoffs between minimizing cost and maximizing resilience. Specifically, we are interested in modeling utility service disruptions resulting from damage caused by hurricanes and coastal flooding. Additionally, we consider potential disruptions to the diesel fuel supply, which powers the “business-as-usual” backup generation. We create an array of solutions to provide competitive options to our clients. Microgrids reduce dependence on diesel which is particularly important during longer outages when the site would require re-supplies of diesel fuel to continue operating. We show economic and resilience benefits associated with microgrid procurement. In addition to decreasing utility dependence, the site can reduce its carbon emissions by 22%, reducing public health and climate-related impacts.

Finally, Chapter 4 combines ideas from Chapters 2 and 3 to create an optimization-based framework that enhances community resilience during outages by increasing the reliability of the electrical infrastructure. We define an energy system that includes emerging co-generational technologies not present in the other works. The formulation introduces non-linearities to represent the physical system. Owing to the optimization model’s non-linearities, we develop a methodology that can produce better solutions than traditional commercial solvers. Specifically, our procedure yields an average objective function value reduction of 8% and over a 58% reduction in the optimality gap. Additionally, on average, we expedite solutions four-fold for the instances we test, allowing governmental organizations to implement affordable and sustainable measures that enhance the community’s energy resilience and reliability.

REFERENCES

- [1] CFPUA. Wastewater treatment plant anaerobic gas utilization. *Personal communication*, 2013.
- [2] Kristopher A. Pruitt, Sven Leyffer, Alexandra M. Newman, and Robert J. Braun. A mixed-integer nonlinear program for the optimal design and dispatch of distributed generation systems. *Optimization and Engineering*, 15(1):167–197, Mar 2014. ISSN 1573-2924. doi: 10:1007/s11081-013-9226-6.
- [3] Kevin P. Schneider, Yousu Chen, David P. Chassin, Robert G. Pratt, David W. Engel, and Sandra E. Thompson. Modern grid initiative distribution taxonomy final report. Technical Report PNNL-18035, 1040684, Pacific Northwest National Lab, Nov 2008. URL <http://www.osti.gov/servlets/purl/1040684/>.
- [4] Charles Fant, Brent Boehlert, Kenneth Strzepek, Peter Larsen, Alisa White, Sahil Gulati, Yue Li, and Jeremy Martinich. Climate change impacts and costs to US electricity transmission and distribution infrastructure. *Energy*, 195:116899, 2020.
- [5] Roshanak Nateghi, Seth Guikema, and Steven M. Quiring. Power outage estimation for tropical cyclones: Improved accuracy with simpler models. *Risk Analysis*, 34(6):1069–1078, 2014. doi: <https://doi.org/10:1111/risa:12131>. URL <https://onlinelibrary.wiley.com/doi/abs/10:1111/risa:12131>.
- [6] Sayanti Mukherjee and Roshanak Nateghi. Climate sensitivity of end-use electricity consumption in the built environment: an application to the state of Florida, United States. *Energy*, 128:688–700, 2017.
- [7] Fauzan Hanif Jufri, Victor Widiputra, and Jaesung Jung. State-of-the-art review on power grid resilience to extreme weather events: Definitions, frameworks, quantitative assessment methodologies, and enhancement strategies. *Applied Energy*, 239:1049–1065, 2019. ISSN 0306-2619. doi: <https://doi.org/10:1016/j.apenergy:2019:02:017>.
- [8] Kate Anderson, Dan Olis, Bill Becker, Linda Parkhill, Nick Laws, Xiangkun Li, Sakshi Mishra, Ted Kwasnik, Andrew Jeffery, Emma Elgqvist, et al. REopt Lite user manual. Technical report, National Renewable Energy Lab, Golden, CO (United States), 2021.
- [9] Jusse Hirwa, Oluwaseun Ogunmodede, Alexander Zolan, and Alexandra Newman. Optimizing Design and Dispatch of a Renewable Energy System with Combined Heat and Power. *Optimization and Engineering*, accepted, 2021.
- [10] Oluwaseun Ogunmodede, Kate Anderson, Dylan Cutler, and Alexandra Newman. Optimizing design and dispatch of a renewable energy system. *Applied Energy*, 287:116527, 2021.

- [11] David Feldman, Robert Margolis, Paul Denholm, and Joseph Stekli. Exploring the potential competitiveness of utility-scale photovoltaics plus batteries with concentrating solar power, 2015–2030. Technical report, National Renewable Energy Laboratory, Golden, CO (United States), 2016.
- [12] Mudathir Funsho Akorede, Hashim Hizam, and Edris Pouresmaeil. Distributed energy resources and benefits to the environment. *Renewable and Sustainable Energy Reviews*, 14(2):724–734, 2010.
- [13] Aziz Saif, Shafi K Khadem, Michael F Conlon, and Brian Norton. Impact of distributed energy resources in smart homes and community-based electricity market. *IEEE Transactions on Industry Applications*, 59(1):59–69, 2022.
- [14] Stephanie Lenhart and Kathleen Araújo. Microgrid decision-making by public power utilities in the United States: A critical assessment of adoption and technological profiles. *Renewable and Sustainable Energy Reviews*, 139:110692, 2021.
- [15] Tom Lambert, Paul Gilman, and Peter Lilienthal. Micropower system modeling with HOMER. *Integration of Alternative Sources of Energy*, 1(1):379–385, 2006.
- [16] Michael Stadler, Markus Groissböck, Gonçalo Cardoso, and Chris Marnay. Optimizing distributed energy resources and building retrofits with the strategic DER-CAModel. *Applied Energy*, 132:557–567, 2014.
- [17] Kathleen Krahn. Behind-the-meter solar+ storage modeling tool comparison. Technical report, National Renewable Energy Laboratory, Golden, CO (United States), 2019.
- [18] Wai Lip Theo, Jeng Shiun Lim, Wai Shin Ho, Haslenda Hashim, and Chew Tin Lee. Review of distributed generation (DG) system planning and optimisation techniques: Comparison of numerical and mathematical modelling methods. *Renewable and Sustainable Energy Reviews*, 67:531–573, 2017.
- [19] Haochen Zhang, Shaowei Cai, Chuan Luo, and Minghao Yin. An efficient local search algorithm for the winner determination problem. *Journal of Heuristics*, 23(5):367–396, Oct 2017. ISSN 1572-9397. doi: 10:1007/s10732-017-9344-y.
- [20] Luis Flores-Luyo, Agostinho Agra, Rosa Figueiredo, and Eladio Ocaña. Heuristics for a vehicle routing problem with information collection in wireless networks. *Journal of Heuristics*, 26(2):187–217, Apr 2020. ISSN 1572-9397. doi: 10:1007/s10732-019-09429-6.
- [21] Kate Anderson, James Grymes, Alexandra Newman, and Adam Warren. North Carolina water utility builds resilience with distributed energy resources. *INFORMS Journal on Applied Analytics*, Sep 2022. ISSN 2644-0865. doi: 10:1287/inte:2022:1136. URL <https://pubsonline.informs.org/doi/full/10:1287/inte:2022:1136>.

- [22] Alexander J. Zolan, Michael S. Scioletti, David P. Morton, and Alexandra M. Newman. Decomposing loosely coupled mixed-integer programs for optimal microgrid design. *INFORMS Journal on Computing*, 33(4):1300–1319, Oct 2021. ISSN 1091-9856. doi: 10:1287/ijoc:2020:0955.
- [23] Sadiq Sait and Habib Youssef. *Iterative Computer Algorithms with Applications in Engineering*. Wiley, 01 2000.
- [24] Babak Jeddi, Yateendra Mishra, and Gerard Ledwich. Dynamic programming based home energy management unit incorporating pvs and batteries. In *2017 IEEE Power & Energy Society General Meeting*, page 1–5, Jul 2017. doi: 10:1109/PESGM:2017:8273925.
- [25] Meng Xu, Rui Wang, Peng Zhao, and Xia Wang. Fast charging optimization for lithium-ion batteries based on dynamic programming algorithm and electrochemical-thermal-capacity fade coupled model. *Journal of Power Sources*, 438:227015, Oct 2019. ISSN 0378-7753. doi: 10:1016/j.jpowsour:2019:227015.
- [26] Richard Bellman. *Dynamic Programming*. Princeton University Press, Princeton, NJ, USA, 1 edition, 1957.
- [27] Ming Niu, Can Wan, and Zhao Xu. A review on applications of heuristic optimization algorithms for optimal power flow in modern power systems. *Journal of Modern Power Systems and Clean Energy*, 2(4):289–297, Dec 2014. ISSN 2196-5420. doi: 10:1007/s40565-014-0089-4.
- [28] James D. Foster, Adam M. Berry, Natasha Boland, and Hamish Waterer. Comparison of mixed-integer programming and genetic algorithm methods for distributed generation planning. *IEEE Transactions on Power Systems*, 29(2):833–843, Mar 2014. ISSN 1558-0679. doi: 10:1109/TPWRS:2013:2287880.
- [29] K. Hara, M. Kimura, and N. Honda. A method for planning economic unit commitment and maintenance of thermal power systems. *IEEE Transactions on Power Apparatus and Systems*, PAS-85(5):427–436, May 1966. ISSN 0018-9510. doi: 10:1109/TPAS:1966:291680.
- [30] Chung-Li Tseng. *On power system generation unit commitment problems*. Ph.d., University of California, Berkeley, United States – California, 1996. URL <https://www.proquest.com/docview/304265345/abstract/2773B7D2C0A7420EPQ/1>.
- [31] Jorge Valenzuela and Alice E. Smith. A seeded memetic algorithm for large unit commitment problems. *Journal of Heuristics*, 8(2):173–195, Mar 2002. ISSN 1572-9397. doi: 10:1023/A:1017960507177.
- [32] Tiew-On Ting, M.V.C. Rao, C.K. Loo, and S.S. Ngu. Solving unit commitment problem using hybrid particle swarm optimization. *Journal of Heuristics*, 9(6):507–520, Dec 2003. ISSN 1572-9397. doi: 10:1023/B:HEUR.0000012449:84567:1a.

- [33] M. Nazari-Heris, B. Mohammadi-Ivatloo, and G. B. Gharehpetian. A comprehensive review of heuristic optimization algorithms for optimal combined heat and power dispatch from economic and environmental perspectives. *Renewable and Sustainable Energy Reviews*, 81: 2128–2143, Jan 2018. ISSN 1364-0321. doi: 10:1016/j.rser:2017:06:024.
- [34] Ali Sulaiman Alsagri and Abdulrahman A. Alrobaian. Optimization of combined heat and power systems by meta-heuristic algorithms: An overview. *Energies*, 15(1616):5977, Jan 2022. ISSN 1996-1073. doi: 10:3390/en15165977.
- [35] Fukang Ren, Xiaozhen Lin, Ziqing Wei, Xiaoqiang Zhai, and Jianrong Yang. A novel planning method for design and dispatch of hybrid energy systems. *Applied Energy*, 321: 119335, Sep 2022. ISSN 0306-2619. doi: 10:1016/j.apenergy:2022:119335.
- [36] Akbar Maleki, Fathollah Pourfayaz, and Mohammad Hossein Ahmadi. Design of a cost-effective wind/photovoltaic/hydrogen energy system for supplying a desalination unit by a heuristic approach. *Solar Energy*, 139:666–675, Dec 2016. ISSN 0038-092X. doi: 10:1016/j.solener:2016:09:028.
- [37] Michael S. Scioletti, Alexandra M. Newman, Johanna K. Goodman, Alexander J. Zolan, and Sven Leyffer. Optimal design and dispatch of a system of diesel generators, photovoltaics and batteries for remote locations. *Optimization and Engineering*, 18(3), May 2017. ISSN 1389-4420. doi: 10:1007/s11081-017-9355-4.
- [38] Gavin Goodall, Michael Scioletti, Alex Zolan, Bharatkumar Suthar, Alexandra Newman, and Paul Kohl. Optimal design and dispatch of a hybrid microgrid system capturing battery fade. *Optimization and Engineering*, 20(1):179–213, March 2019. ISSN 1573-2924. doi: 10:1007/s11081-018-9404-7.
- [39] C.H. Lo and M.D. Anderson. Economic dispatch and optimal sizing of battery energy storage systems in utility load-leveling operations. *IEEE Transactions on Energy Conversion*, 14(3):824–829, Sep 1999. ISSN 1558-0059. doi: 10:1109/60:790960.
- [40] Masoud Zebarjadi and Alireza Askarzadeh. Optimization of a reliable grid-connected pv-based power plant with/without energy storage system by a heuristic approach. *Solar Energy*, 125:12–21, Feb 2016. ISSN 0038-092X. doi: 10:1016/j.solener:2015:11:045.
- [41] Aida Fazliana, Azah Mohamed, Hussain Shareef, M.Z.C. Wanik, and Ahmad Ibrahim. Optimal sizing and placement of distributed generation in distribution system considering losses and thdv using gravitational search algorithm. *Przegląd Elektrotechniczny*, 89: 132–136, Apr 2013.
- [42] Ming Shu, Shizhong Wu, Tong Wu, Zhonglin Qiao, Nai Wang, Fei Xu, A. Shanthini, and Bala Anand Muthu. Efficient energy consumption system using heuristic renewable demand energy optimization in smart city. *Computational Intelligence*, 38(3):784–800, 2022. ISSN 1467-8640. doi: 10:1111/coin:12412.

- [43] Adam N. Letchford, Qiang Ni, and Zhaoyu Zhong. A heuristic for fair dynamic resource allocation in overloaded ofdma systems. *Journal of Heuristics*, 26(1):21–32, Feb 2020. ISSN 1572-9397. doi: 10:1007/s10732-019-09422-z.
- [44] Karla B. Freitas, Márcio S. Arantes, Claudio F. M. Toledo, and Alexandre C. B. Delbem. MIQP model and improvement heuristic for power loss minimization in distribution system with network reconfiguration. *Journal of Heuristics*, 26(1):59–81, Feb 2020. ISSN 1572-9397. doi: 10:1007/s10732-019-09421-0.
- [45] Luca Moretti, Marco Astolfi, Claudio Vergara, Ennio Macchi, José Ignacio Pérez-Arriaga, and Giampaolo Manzolini. A design and dispatch optimization algorithm based on mixed integer linear programming for rural electrification. *Applied Energy*, 233–234:1104–1121, Jan 2019. ISSN 0306-2619. doi: 10:1016/j.apenergy:2018:09:194.
- [46] Nima Nikmehr and Sajad Najafi-Ravadanegh. Optimal operation of distributed generations in micro-grids under uncertainties in load and renewable power generation using heuristic algorithm. *IET Renewable Power Generation*, 9(8):982–990, 2015. ISSN 1752-1424. doi: 10:1049/iet-rpg:2014:0357.
- [47] Vittorio Maniezzo, Thomas Stützle, and Stephan Voß. *Matheuristics: Hybridizing Metaheuristics and Mathematical Programming*, volume 10 of *Annals of Information Systems*. Springer US, Boston, MA, 2010. ISBN 978-1-4419-1305-0. doi: 10:1007/978-1-4419-1306-7. URL <https://link.springer.com/10:1007/978-1-4419-1306-7>.
- [48] Nicolas Dupin and El-Ghazali Talbi. Matheuristics to optimize refueling and maintenance planning of nuclear power plants. *Journal of Heuristics*, 27(1):63–105, Apr 2021. ISSN 1572-9397. doi: 10:1007/s10732-020-09450-0.
- [49] Joyce McLaren, Seth Mullendore, Nicholas Laws, and Kate Anderson. Identifying potential markets for behind-the-meter battery energy storage: A survey of U.S. demand charges. Technical report, National Renewable Energy Lab, Golden, CO (United States), 2017.
- [50] Rachid Chelouah and Patrick Siarry. A continuous genetic algorithm designed for the global optimization of multimodal functions. *Journal of Heuristics*, 6:191–213, Jun 2000. doi: 10:1023/A:1009626110229.
- [51] Boxin Tang. Orthogonal array-based latin hypercubes. *Journal of the American Statistical Association*, 88(424):1392–1397, Dec 1993. ISSN 0162-1459. doi: 10:1080/01621459:1993:10476423.
- [52] Volker Nissen. *A Brief Introduction to Evolutionary Algorithms from the Perspective of Management Science*, chapter 2.3, pages 165–210. Springer, Dec 2017. ISBN 978-3-319-64393-9. doi: 10:1007/978-3-319-64394-6_8. journalAbbreviation: Innovative Research Methodologies in Management: Volume I: Philosophy, Measurement and Modelling.

- [53] Gilbert Syswerda. Uniform crossover in genetic algorithms. In *International Conference on Genetic Algorithms*, 01 1989.
- [54] Gurobi Optimization, LLC. Gurobi Optimizer Reference Manual, 2023. URL <https://www.gurobi.com>.
- [55] Elizabeth D. Dolan and Jorge J. More. Benchmarking optimization software with performance profiles. *Mathematical Programming*, 91(2):201–213, Jan 2002. ISSN 1436-4646. doi: 10:1007/s101070100263.
- [56] NOAA. Billion dollar weather and climate disasters: Overview, 2018. URL <https://www.ncdc.noaa.gov/billions/>.
- [57] Eliza Hotchkiss. How solar PV can support disaster resiliency, 2015. URL <https://www.nrel.gov/state-local-tribal/blog/posts/how-solar-pv-can-support-disaster-resiliency.html>.
- [58] Kate Anderson, Nicholas D Laws, Spencer Marr, Lars Lisell, Tony Jimenez, Tria Case, Xiangkun Li, Dag Lohmann, and Dylan Cutler. Quantifying and monetizing renewable energy resiliency. *Sustainability*, 10(4):933, 2018.
- [59] Jeffrey Marqusee, William Becker, and Sean Ericson. Resilience and economics of microgrids with PV, battery storage, and networked diesel generators. *Applied Energy*, in press, 2021.
- [60] Kate Anderson, Kari Burman, Travis Simpkins, Erica Helson, and Lars Lisell. New York Solar Smart DG Hub-Resilient Solar Project: Economic and resiliency impact of PV and storage on New York critical infrastructure. Technical report, National Renewable Energy Lab, Golden, CO (United States), 2016.
- [61] Eliza Hotchkiss, A Dane, and C Komomua. Resilience roadmap: A collaborative approach to multi-jurisdictional planning, 2016. URL <https://www.nrel.gov/resilience-planning-roadmap/>.
- [62] Narayan Bhusal, Michael Abdelmalak, Md Kamruzzaman, and Mohammed Benidris. Power system resilience: Current practices, challenges, and future directions. *IEEE Access*, 8: 18064–18086, 2020.
- [63] Sahil Chinoy. The places in the US where disaster strikes again and again, 2018. *New York Times*.
- [64] Mansur Ali Jisan, Shaowu Bao, Leonard J Pietrafesa, Dongliang Shen, Paul T Gayes, and Jason Hallstrom. Hurricane Matthew (2016) and its impact under global warming scenarios. *Modeling Earth Systems and Environment*, 4(1):97–109, 2018.
- [65] Srikanto Paul, Dawit Ghebreyesus, and Hatim O Sharif. Brief communication: Analysis of the fatalities and socio-economic impacts caused by hurricane florence. *Geosciences*, 9(2):58, 2019.

- [66] Michael E Mann and Kerry A Emanuel. Atlantic hurricane trends linked to climate change. *Eos, Transactions American Geophysical Union*, 87(24):233–241, 2006.
- [67] EPA. Energy efficiency in water and wastewater facilities, 2013. URL <https://www.epa.gov/sites/production/files/2015-08/documents/wastewater-guide.pdf>.
- [68] Arian Aghajanzadeh, Craig Wray, and Aimee McKane. Opportunities for automated demand response in California wastewater treatment facilities. Technical report, Lawrence Berkeley National Lab, Berkeley, CA, 2015.
- [69] Srinivas Bollapragada, Brandon Owens, and Steve Taub. Practice summaries: An optimization model to support renewable energy investment decisions. *Interfaces*, 41(4):394–395, 2011.
- [70] Madeleine Udell and Oliver Toole. Optimal design of efficient rooftop photovoltaic arrays. *INFORMS Journal on Applied Analytics*, 49(4):281–294, 2019.
- [71] Martina Fischetti, Jesper Runge Kristoffersen, Thomas Hjort, Michele Monaci, and David Pisinger. Vattenfall optimizes offshore wind farm design. *INFORMS Journal on Applied Analytics*, 50(1):80–94, 2020.
- [72] Samira Fazlollahi and François Maréchal. Multi-objective, multi-period optimization of biomass conversion technologies using evolutionary algorithms and mixed integer linear programming (MILP). *Applied Thermal Engineering*, 50(2):1504–1513, 2013.
- [73] Di Zhang, Sara Evangelisti, Paola Lettieri, and Lazaros G Papageorgiou. Optimal design of CHP-based microgrids: Multiobjective optimisation and life cycle assessment. *Energy*, 85:181–193, 2015.
- [74] Lixia Kang and Yongzhong Liu. Multi-objective optimization on a heat exchanger network retrofit with a heat pump and analysis of CO₂ emissions control. *Applied Energy*, 154:696–708, 2015.
- [75] Tobias Falke, Stefan Krengel, Ann-Kathrin Meinerzhagen, and Armin Schnettler. Multi-objective optimization and simulation model for the design of distributed energy systems. *Applied Energy*, 184:1508–1516, 2016.
- [76] Qiong Wu, Hongbo Ren, Weijun Gao, and Jianxing Ren. Multi-objective optimization of a distributed energy network integrated with heating interchange. *Energy*, 109:353–364, 2016.
- [77] Marialaura Di Somma, Bing Yan, Nicola Bianco, Peter B Luh, Giorgio Graditi, Luigi Mongibello, and Vincenzo Naso. Multi-objective operation optimization of a distributed energy system for a large-scale utility customer. *Applied Thermal Engineering*, 101:752–761, 2016.

- [78] Michael CW Kintner-Meyer, Juliet S Homer, Patrick J Balducci, and Mark R Weimar. Valuation of electric power system services and technologies. Technical report, Pacific Northwest National Lab, Richland, WA (United States), 2017.
- [79] Caitlin Murphy, Elizabeth L Hotchkiss, Katherine H Anderson, Clayton P Barrows, Stuart M Cohen, Sourabh Dalvi, Nicholas D Laws, Jeffrey B Maguire, Gordon W Stephen, and Eric J Wilson. Adapting existing energy planning, simulation, and operational models for resilience analysis. Technical report, National Renewable Energy Lab, Golden, CO (United States), 2020.
- [80] Mohammad H Moradi and A Khandani. Evaluation economic and reliability issues for an autonomous independent network of distributed energy resources. *International Journal of Electrical Power & Energy Systems*, 56:75–82, 2014.
- [81] Kaile Zhou, Shanlin Yang, Zhiqiang Chen, and Shuai Ding. Optimal load distribution model of microgrid in the smart grid environment. *Renewable and Sustainable Energy Reviews*, 35:304–310, 2014.
- [82] Hanieh Borhanazad, Saad Mekhilef, Velappa Gounder Ganapathy, Mostafa Modiri-Delshad, and Ali Mirtaheri. Optimization of micro-grid system using MOPSO. *Renewable Energy*, 71:295–306, 2014.
- [83] JH Zheng, JJ Chen, QH Wu, and ZX Jing. Multi-objective optimization and decision making for power dispatch of a large-scale integrated energy system with distributed DHCs embedded. *Applied Energy*, 154:369–379, 2015.
- [84] Amelia McIlvenna, Jim Ostrowski, Andrew Herron, Daniel King, Philip Irminger, Joshua Hambrick, and Ben Ollis. Practice summary: Improved reliability via optimization in residential microgrids. *INFORMS Journal on Applied Analytics*, 50(2):112–118, 2020.
- [85] Jeffrey Cook, Elizabeth Hotchkiss, Xiangkun Li, and Jesse Cruce. Planning for the storm: Considering renewable energy for critical infrastructure resilience. *Journal of Emergency Management*, 18(4):295–309, 2020.
- [86] Alexander Zadorojniy, Segev Wasserkrug, Sergey Zeltyn, and Vladimir Lipets. Unleashing analytics to reduce costs and improve quality in wastewater treatment. *INFORMS Journal on Applied Analytics*, 49(4):262–268, 2019.
- [87] S Revollar, R Vilanova, P Vega, M Francisco, and M Meneses. Wastewater treatment plant operation: simple control schemes with a holistic perspective. *Sustainability*, 12(3):768, 2020.
- [88] Wolfgang Gruber-Glatzl, Christoph Brunner, Sarah Meitz, and Hans Schnitzer. From the wastewater treatments plant to the turnstiles of urban water and district heat networks. *Frontiers in Sustainable Cities*, 2:60, 2020.

- [89] Duke Energy Progress. Duke Energy Progress rates, 2021. URL https://desitecoreprod-cd.azureedge.net/_/media/pdfs/for-your-home/rates/electric-nc/g11ncschedulelgsrtpdep.pdf?la=en&rev=eecd95b0956549a4ad88231b97d68a3b. Accessed: 6/26/21.
- [90] DOE. Combined heat & power ecatalog of recognized package CHP systems, 2019. URL <https://chp.ecatalog.lbl.gov/>. Accessed: 2022-01-29.
- [91] Allison Richards, Jodi Deprizio, Kate Anderson, Nick DiOrio, Emma Elgqvist, and Travis Simpkins. Portfolio analysis of renewable energy opportunities. In *Office of Scientific and Technical Information*. National Renewable Energy Lab, Golden, CO, 2016.
- [92] NREL. Reopt helps optimize telecommunications power for Verizon Wireless, 2018. URL <https://reopt.nrel.gov/projects/case-study-verizon.html>. Accessed: 2021-09-18.
- [93] Kate Anderson and Emma Elgqvist. NREL screens universities for solar and battery storage potential. Technical report, National Renewable Energy Laboratory, Golden, CO, 2017.
- [94] Kate Anderson. REopt screenings catalyze development of hundreds of megawatts of renewable energy for federal agencies. Technical report, National Renewable Energy Laboratory, Golden, CO, 2017.
- [95] Emma Elgqvist and Katy Christiansen. Behind-the-meter to front of the line: Prioritizing battery storage opportunities across a portfolio of sites. Technical report, National Renewable Energy Laboratory, Golden, CO, 2020.
- [96] Samuel Booth, Xiangkun Li, Ian Baring-Gould, Diana Kollanyi, Abishek Bharadwaj, and Peter Weston. Productive use of energy in African microgrids: Technical and business considerations. Technical report, National Renewable Energy Lab, Golden, CO, 2018.
- [97] EIA. Annual electric power industry report, form EIA-861 detailed data files. Technical report, U.S. Energy Information Agency, 2020.
- [98] Climate Central, 2020. URL <https://www.climatecentral.org/climate-matters/power-outages>.
- [99] Adam B. Smith. 2021 U.S. billion-dollar weather and climate disasters, 2021. URL <http://www.climate.gov/news-features/blogs/beyond-data/2021-us-billion-dollar-weather-and-climate-disasters-historical>.
- [100] Department of Energy. Department of Energy Report Explores U.S. Advanced Small Modular Reactors to Boost Grid Resiliency, 2018. URL <https://www.energy.gov/ne/articles/department-energy-report-explores-us-advanced-small-modular-reactors-boost-grid>.

- [101] Tania Schoennagel, Jennifer K. Balch, Hannah Brenkert-Smith, Philip E. Dennison, Brian J. Harvey, Meg A. Krawchuk, Nathan Mietkiewicz, Penelope Morgan, Max A. Moritz, Ray Rasker, Monica G. Turner, and Cathy Whitlock. Adapt to more wildfire in western North American forests as climate changes. *Proceedings of the National Academy of Sciences*, 114(18):4582–4590, 2017. doi: 10:1073/pnas:1617464114. URL <https://www.pnas.org/doi/abs/10:1073/pnas:1617464114>.
- [102] F. Stuart Chapin, Sarah F. Trainor, Orville Huntington, Amy L. Lovecraft, Erika Zavaleta, David C. Natcher, A. David McGuire, Joanna L. Nelson, Lily Ray, Monika Calef, Nancy Fresco, Henry Huntington, T. Scott Rupp, La’ona DeWilde, and Rosamond L. Naylor. Increasing wildfire in Alaska’s Boreal forest: Pathways to potential solutions of a wicked problem. *BioScience*, 58(6):531–540, Jun 2008. ISSN 0006-3568. doi: 10:1641/B580609.
- [103] U.S. Department of Energy. U.s. department of energy, form oe-417, 2023. URL https://www.oe.netl.doe.gov/OE417_annual_summary.aspx.
- [104] Ayberk Kocatepe, Mehmet Baran Ulak, Grzegorz Kakareko, Eren Erman Ozguven, Sungmoon Jung, and Reza Arghandeh. Measuring the accessibility of critical facilities in the presence of hurricane-related roadway closures and an approach for predicting future roadway disruptions. *Natural Hazards*, 95:615–635, 2019.
- [105] Ian P. Davies, Ryan D. Haugo, James C. Robertson, and Phillip S. Levin. The unequal vulnerability of communities of color to wildfire. *PLOS ONE*, 13(11):e0205825, Nov 2018. ISSN 1932-6203. doi: 10:1371/journal.pone.0205825.
- [106] W. Matt Jolly, Mark A. Cochrane, Patrick H. Freeborn, Zachary A. Holden, Timothy J. Brown, Grant J. Williamson, and David M. J. S. Bowman. Climate-induced variations in global wildfire danger from 1979 to 2013. *Nature Communications*, 6(11):7537, Jul 2015. ISSN 2041-1723. doi: 10:1038/ncomms8537.
- [107] Thomas Jenkins. Impacts of the 2017 wildfires in the United States, Mar 202018. URL <https://www.govinfo.gov/committee/house-transportation?path=/browsecommittee/chamber/house/committee/transportation>.
- [108] Natural disasters: California camp fire was world’s costliest in 2018, 2018. URL <https://www.usatoday.com/story/news/2019/01/08/natural-disasters-camp-fire-worlds-costliest-catastrophe-2018/2504865002/>.
- [109] Richard J Campbell. Weather-related power outages and electric system resiliency. *Congressional Research Journal*, 2012.
- [110] Daniel L. Donaldson, Manuel S. Alvarez-Alvarado, and Dilan Jayaweera. Power system resiliency during wildfires under increasing penetration of electric vehicles. In *2020 International Conference on Probabilistic Methods Applied to Power Systems (PMAPS)*, pages 1–6, 2020. doi: 10:1109/PMAPS47429:2020.9183683.

- [111] Emma Newburger. More than 2 million people expected to lose power in PG&E blackout as California wild res rage, Oct 2019. URL [https://www :cnn:com/2019/10/26/pge-will-shut-off-power-to-940000-customers-in-northern-california-to-reduce-wild re-risk:html](https://www.cnn.com/2019/10/26/pge-will-shut-off-power-to-940000-customers-in-northern-california-to-reduce-wild-re-risk.html).
- [112] Nathanael Greene and Roel Hammerschlag. Small and clean is beautiful: Exploring the emissions of distributed generation and pollution prevention policies. *The Electricity Journal*, 13(5):50{60, Jun 2000. ISSN 1040-6190. doi: 10.1016/S1040-6190(00)00118-4.
- [113] Who's at risk when the power goes out? the at-home electricity-dependent population in the United States, 2017. URL [https://journals :lww:com/jphmp/Abstract/2017/03000/Who_s_at_Risk_When_the_Power_Goes_Out__The_At_home.aspx](https://journals.lww.com/jphmp/Abstract/2017/03000/Who_s_at_Risk_When_the_Power_Goes_Out__The_At_home.aspx).
- [114] Palaiologos Palaiologou, Alan A. Ager, Max Nielsen-Pincus, Cody R. Evers, and Michelle A. Day. Social vulnerability to large wild res in the western USA. *Landscape and Urban Planning*. 189: 99-116, 189:99{116, 2019. doi: 10.1016/j.landurbplan.2019.04.006.
- [115] Kehinde Abiodun, Arnav Gautam, Alexandra Newman, Destenie Nock, and Amritanshu Pandey. The role of microgrids in advancing energy equity through access and resilience, 2022.
- [116] Center for Climate and Energy Solutions, 2020. URL [https://www :c2es:org/content/microgrids/](https://www.c2es.org/content/microgrids/).
- [117] Henrik Nilsson, 2023. URL [https://www :utilitydive :com/news/us-microgrid-market-wood-mackenzie/642341/](https://www.utilitydive.com/news/us-microgrid-market-wood-mackenzie/642341/).
- [118] Sakshi Mishra, Kate Anderson, Brian Miller, Kyle Boyer, and Adam Warren. Microgrid resilience: A holistic approach for assessing threats, identifying vulnerabilities, and designing corresponding mitigation strategies. *Applied Energy*, 264:114726, Apr 2020. ISSN 0306-2619. doi: 10.1016/j.apenergy.2020.114726.
- [119] Milad Beigzadeh, Fathollah Pourfayaz, Mahyar Ghazvini, and Mohammad H. Ahmadi. Energy and exergy analyses of solid oxide fuel cell-gas turbine hybrid systems fed by different renewable biofuels: A comparative study. *Journal of Cleaner Production*, 280: 124383, Jan 2021. ISSN 0959-6526. doi: 10.1016/j.jclepro.2020.124383.
- [120] Tom Lambert. HOMER[®] Energy Modeling Software, Version 00. Technical report, National Renewable Energy Lab. (NREL), Golden, CO (United States), 12 2000. URL [https://www :osti:gov/biblio/1231441](https://www.osti.gov/biblio/1231441).
- [121] Sha qur Rehman and Luai M. Al-Hadhrami. Study of a solar PV{diesel}battery hybrid power system for a remotely located population near Rafha, Saudi Arabia. *Energy*, 35(12): 4986{4995, 2010. ISSN 0360-5442. doi: [https://doi.org/10:1016/j:energy.201008:025](https://doi.org/10.1016/j.energy.2010.08.025).

- [122] Ali Saleh Aziz, Mohammad Faridun Naim Tajuddin, Moaid K. Hussain, Mohd Ra Adzman, Nur Ha zah Ghazali, Makbul A. M. Ramli, and Tekai Eddine Khalil Zidane. A new optimization strategy for wind/diesel/battery hybrid energy system. *Energy*, 239: 122458, 2022. ISSN 0360-5442. doi: <https://doi.org/10.1016/j.energy.2021.122458>.
- [123] Katherine H. Anderson, Dylan S. Cutler, Daniel R. Olis, Emma M. Elqvist, Xiangkun Li, Nicholas D. Laws, Nicholas A. DiOrio, and H. A. Walker. REopt: A platform for energy system integration and optimization. Technical Report NREL/TP-7A40-70022, National Renewable Energy Lab. (NREL), Golden, CO (United States), Sep 2017. URL <https://www.osti.gov/biblio/1395453>.
- [124] Hugo Morais, Peter Kadar, Pedro Faria, Zita A. Vale, and H.M. Khodr. Optimal scheduling of a renewable micro-grid in an isolated load area using mixed-integer linear programming. *Renewable Energy* 35(1):151{156, 2010. ISSN 0960-1481. doi: <https://doi.org/10.1016/j.renene.2009.02.031>. Citation Key: MORAIS2010151.
- [125] Jose L. Bernal-Agustn, Rodolfo Dufo-Lopez, and David M. Rivas-Ascaso. Design of isolated hybrid systems minimizing costs and pollutant emissions. *Renewable Energy* 31(14):2227{2244, Nov 2006. ISSN 0960-1481. doi: <https://doi.org/10.1016/j.renene.2005.11.002>.
- [126] Sajid Hussain Qazi, Mohd Wazir Mustafa, Umbrin Sultana, Nayyar Hussain Mirjat, Shakir Ali Soomro, and Nadia Rasheed. Regulation of voltage and frequency in solid oxide fuel cell-based autonomous microgrids using the whales optimisation algorithm. *Energies* 11(55):1318, May 2018. ISSN 1996-1073. doi: <https://doi.org/10.3390/en11051318>.
- [127] Marco Sorrentino, Antonio Adamo, and Gianmarco Nappi. Optimal sizing of an rSOC-Based renewable microgrid. *Energy Procedia* 159:237{242, 2019. ISSN 1876-6102. doi: <https://doi.org/10.1016/j.egypro.2018.12.063>. Citation Key: SORRENTINO2019237.
- [128] T. Vigneysh and N. Kumarappan. Autonomous operation and control of photovoltaic/solid oxide fuel cell/battery energy storage based microgrid using fuzzy logic controller. *International Journal of Hydrogen Energy*, 41(3):1877{1891, 2016. ISSN 0360-3199. doi: <https://doi.org/10.1016/j.ijhydene.2015.11.022>. Citation Key: VIGNEYSH20161877.
- [129] Qijun Deng, Xing Gao, Hong Zhou, and Wenshan Hu. System modeling and optimization of microgrid using genetic algorithm. In 2011 2nd International Conference on Intelligent Control and Information Processing, volume 1, page 540{544, Jul 2011. doi: <https://doi.org/10.1109/ICICIP.2011.6008303>.
- [130] Seyed Ali Are far, Yasser A.-R. I. Mohamed, and Tarek H. M. EL-Fouly. Optimum microgrid design for enhancing reliability and supply-security. *IEEE Transactions on Smart Grid*, 4(3):1567{1575, Sep 2013. ISSN 1949-3061. doi: <https://doi.org/10.1109/TSG.2013.2259854>.
- [131] Shores Shokoohi, Sajjad Golshannavaz, Rahmat Khezri, and Hassan Bevrani. Intelligent secondary control in smart microgrids: an on-line approach for islanded operations. *Optimization and Engineering*, 19:917{936, 2018.

- [132] Yanling Lin, Zhaohong Bie, and Aici Qiu. A review of key strategies in realizing power system resilience. *Global Energy Interconnection*, 1(1):70{78, 2018.
- [133] Backup power, 2023. URL https://www.pge.com/en_US/safety/electrical-safety/electric-generator-safety/electric-generator-safety.
- [134] Michael S Scioletti, Alexandra M Newman, Johanna K Goodman, Alexander J Zolan, and Sven Ley er. Optimal design and dispatch of a system of diesel generators, photovoltaics and batteries for remote locations. *Optimization and Engineering*, 18:755{792, 2017.
- [135] Gavin Goodall, Michael Scioletti, Alex Zolan, Bharatkumar Suthar, Alexandra Newman, and Paul Kohl. Optimal design and dispatch of a hybrid microgrid system capturing battery fade. *Optimization and Engineering*, 20:179{213, 2019.
- [136] Arianna Baldinelli, Linda Barelli, Gianni Bidini, and Giovanni Cinti. Micro-cogeneration based on solid oxide fuel cells: Market opportunities in the agriculture/livestock sector. *International Journal of Hydrogen Energy*, 46(16):10036{10048, 2021. ISSN 0360-3199. doi: <https://doi.org/10.1016/j.ijhydene.202004.226>. URL <https://www.sciencedirect.com/science/article/pii/S0360319920316372>. *Hydrogen and Fuel Cells*.
- [137] Egon Balas. An additive algorithm for solving linear programs with zero-one variables. *Operations Research*, 13(4):517{546, Aug 1965. ISSN 0030-364X. doi: 10.1287/opre.13:4:517.
- [138] Kate Anderson, Dan Olis, Bill Becker, Linda Parkhill, Nick Laws, Xiangkun Li, Sakshi Mishra, Andrew Je ery, Emma Elgqvist, Kathleen Krah, Dylan Cutler, Alex Zolan, Nick Muerdter, Rob Eger, Andy Walker, Chris Hampel, Gregg Tomberlin, and Amanda Farthing. *The REopt Web Tool User Manual*. Technical report, National Renewable Energy Laboratory, 2023.
- [139] Michael A. Cohen, 2013. URL http://emac.berkeley.edu/gridlabd/taxonomy_graphs/.
- [140] A. Dobos. PVWatts version 5 manual. Technical Report NREL/TP-6A20-62641, 1158421, National Renewable Energy Lab, Sep 2014. URL <http://www.osti.gov/servlets/purl/1158421/>.
- [141] U.S. Energy Information Administration. Distributed generation, battery storage, and combined heat and power system characteristics and costs in the buildings and industrial sectors. Technical report, U.S. Energy Information Administration, 2020.
- [142] Battelle Memorial Institute. Manufacturing cost analysis of 1, 5, 10 and 25 kW fuel cell systems for primary power and combined heat and power applications. Technical report, Battelle Memorial Institute, 2017.

- [143] Battelle Memorial Institute. Manufacturing cost analysis of 100 and 250 kW fuel cell systems for primary power and combined heat and power applications. Technical report, Battelle Memorial Institute, 2017.
- [144] Michael M. Whiston, Inês M. Lima Azevedo, Shawn Litster, Constantine Samaras, Kate S. Whitefoot, and Jay F. Whitacre. Paths to market for stationary solid oxide fuel cells: Expert elicitation and a cost of electricity model. *Applied Energy*, 304:117641, 2021. ISSN 0306-2619. doi: <https://doi.org/10.1016/j.apenergy.2021.117641>. URL <https://www.sciencedirect.com/science/article/pii/S0306261921010084>.
- [145] Harikishan R. Ellamla, Iain Staell, Piotr Bujlo, Bruno G. Pollet, and Sivakumar Pasupathi. Current status of fuel cell based combined heat and power systems for residential sector. *Journal of Power Sources* 293:312-328, Oct 2015. ISSN 03787753. doi: 10.1016/j.jpowsour.201505:050.
- [146] Ryan J. Milcarek, Michael J. Garrett, Thomas S. Welles, and Jeongmin Ahn. Performance investigation of a micro-tubular ammonia-assisted fuel cell stack with 3,000 rapid thermal cycles. *Journal of Power Sources* 394:86-93, 2018. ISSN 0378-7753. doi: <https://doi.org/10.1016/j.jpowsour.201805:060>. Citation Key: MILCAREK201886.
- [147] DOE AMO. Combined heat and power basics, 2017. URL <https://www.energy.gov/eere/amo/combined-heat-and-power-basics>. Accessed: 6/26/21.
- [148] Aron Dobos. PVWatts version 5 manual. Technical report, National Renewable Energy Lab, Golden, CO, 2014.
- [149] Laura J Vimmerstedt, Sertac Akar, Chad R Augustine, Philipp C Beiter, Wesley J Cole, David J Feldman, Parthiv Kurup, Eric J Lantz, Robert M Margolis, Tyler J Stehly, et al. 2019 annual technology baseline. Technical report, National Renewable Energy Lab, Golden, CO, 2019.
- [150] Charalampos Patsios, Billy Wu, Efstratios Chatzinikolaou, Daniel J Rogers, Neal Wade, Nigel P Brandon, and Phil Taylor. An integrated approach for the analysis and control of grid connected energy storage systems. *Journal of Energy Storage* 5:48-61, 2016.
- [151] Nicholas DiOrio, Aron Dobos, and Steven Janzou. Economic analysis case studies of battery energy storage with SAM. Technical report, National Renewable Energy Lab, Golden, CO, 2015.
- [152] Wood Mackenzie. U.S. energy storage monitor: Q3 2019 full report, 2019.
- [153] DSIRE. Database of state incentives for renewables and efficiency. North Carolina Clean Energy Technology Center, 2020. URL <https://www.dsireusa.org/>. Accessed: 6/29/2020.
- [154] Energy Information Administration. Annual energy outlook 2019 { electricity supply, disposition, prices, and emissions.}, 2019. URL <https://www.eia.gov/outlooks/aeo/data/browser/#/?id=3-AEO2019&cases=ref2019&sourcekey=0>. Accessed: 9/04/2020.

APPENDIX A

CHAPTER 2

A.1 Dynamic Programming Formulation and Algorithm

Notation

Sets	
S	Set of available states of charge
S_s^p	Set of available states of charge accessible by s
Parameters	
d_h	electrical demand in period h (kWh)
x^{bkWh}	size of electrical storage system (kWh)
x^{kW}	power rating of electrical storage system (kW)
x_0^{sc}	initial state-of-charge of the electrical storage system (kWh)
Variables	
X_{th}^{pts}	energy sent to storage by technology t in period h (kWh)
X_n^g	energy purchased in period h (kWh)
X_n^{sc}	state of charge of storage system in period h (kWh)
X_n^{dfs}	amount of energy discharged storage in period h (kWh)

Given the electrical storage system size (x^{bkWh}) we determine the appropriate set of discrete states of charge (S). Additionally, given the systems power rating (x^{kW}) we determine the states of charge accessible (S_s^p) by a previous state of charges. This restricts us to only feasible moves from one state to the next. Function (A.1a) returns the cost associated with producing and/or purchasing energy in time period h to move from current state of charges to s^n .

Equation (A.1b) defines the recursive relationship that returns the minimum cost of battery operation over each of the discrete states of charge. This function is also responsible for determining (greedily) the amount of energy that would be needed from production and/or from the utility. The cost function considers both energy and peak demand costs. Omitted from the math below are simple procedures to return the associated electrical production and purchasing variables (X_n^g and X_{th}^{pts}) associated with moving between states of charge. Figure Figure A.1 depicts a set of possible states-of-charge and associated state-space moves that are possible from hour h to hour $h + 1$.

Recursive Functions and Notation

$$\text{cost}(h; s; s^n) \tag{A.1a}$$

$$\text{opt}(h; s) = \min_{s^n \in S_s^p} f \text{cost}(h; s; s^n) + \text{opt}(h + 1; s^n)g \tag{A.1b}$$

Algorithm 5 Dynamic program procedure to determine optimal electrical storage operations. The functions `charge()`; `discharge()` return the minimum cost charging or discharging (respectively) strategy for a given x_h^f in hour h .

```

function
  Inputs:  S; Ssp; M ; Hm; dh
          . discretized states of charge,
          . states of charge accessible by previous state of charge,
          . months, hours in month m, electrical load in hour h

  Outputs: xhg; xhgts; xthpts; xhdfs
          . energy purchased from utility,
          . energy from grid to storage,
          . energy produced to storage, dispatched from storage

  Initialize Inputs
  for m ∈ M do
    for h ∈ Hm do
      for sp ∈ S do
        for sn ∈ Sspp do
          xhf = sn - sp
          if xhf > 0 then
            | xthpts; xhg; xhgts = charge(xhf; h)
          else
            | xhdfs; xhg = discharge(xhf; h)
          if Csp;h + cost(h; xthpts; xhg) < Csn;h+1 then
            | Update Cost Table
            | Update Traceback Table
  
```

Figure A.1 An illustrative example of the discretized state of charge and associated possible moves from hour h to hour $h + 1$.

APPENDIX B

CHAPTER 3

B.1 Technical and Economic Parameters

The technical and economic parameters used in the analysis are shown in Table B.1, Table B.2, Table B.3 and Table B.4.

Table B.1 Combined-Heat-and-Power Parameters

Parameter	Value	Reference
Prime mover type	Reciprocating engine	[-]
Size class	100-630 kW	DOE AMO [147]
Existing boiler efficiency	80%	DOE AMO [147]
Electric efficiency	36%	DOE AMO [147]
Thermal efficiency	41%	DOE AMO [147]
Prime mover minimum electric loading	50%	DOE AMO [147]
Biogas available	41,754 MMBTU/year	CFPUA [1]
Capital cost	\$2,700/kW	DOE AMO [147]
Operations & maintenance cost	\$0.0225/kWh	DOE AMO [147]
Biogas cost	\$0/kWh	CFPUA [1]
Incentives	None	[-]

Note : DOE: Department of Energy; AMO: Advanced Manufacturing Office; CFPUA: Cape Fear Public Utility Authority

Table B.2 Photovoltaic Parameters

Parameter	Value	Reference
Array type	Rooftop, Fixed	Dobos [148]
Array azimuth	180	Dobos [148]
Array tilt	10	Dobos [148]
DC-to-AC size ratio	1.2	Dobos [148]
System losses	14%	Dobos [148]
Capital cost	\$1,600/kW	Vimmerstedt et al. [149]
Operations & maintenance cost	\$16/kWh	Vimmerstedt et al. [149]
Incentives	None	[-]

Note : DC: direct current; AC: alternating current

Table B.3 Storage Parameters

Parameter	Value	Reference
Rectifier efficiency	96%	Patsios et al. [150]
Round-trip efficiency	97.5%	Patsios et al. [150]
Inverter efficiency	96%	Patsios et al. [150]
Minimum state of charge	20%	Patsios et al. [150]
Initial state of charge	50%	[-]
Battery life	10 years	DiOrio et al. [151]
Energy capacity cost	\$420/kWh	Wood Mackenzie [152]
Energy replacement cost	\$200/kWh	Wood Mackenzie [152]
Power capacity cost	\$840/kW	Wood Mackenzie [152]
Power replacement cost	\$410/kW	Wood Mackenzie [152]
Operations & maintenance cost	\$0/kW	[-]
Incentives	None	[-]

Table B.4 System-wide General Economic Parameters

Parameter	Value	Reference
Analysis period	25 years	Vimmerstedt et al. [149]
Net metering limit	1000 kW	DSIRE [153]
Wholesale rate	\$0/kWh	[-]
Host discount rate	4%	Vimmerstedt et al. [149]
Electricity cost escalation rate	2.3%	Energy Information Administration [154]
Fuel cost escalation rate	3.4%	Energy Information Administration [154]
Operations & maintenance cost escalation rate	2.5%	Vimmerstedt et al. [149]

B.2 Utility Rate

The utility rate is shown in Table B.5.

Table B.5 Duke Energy Progress Large General Service Real Time Pricing Rate [89]

	Value	Units	Applied to
Fixed charges			
Basic customer charge	200	\$/month	Not applicable
RTP administrative charge	165	\$/month	Not applicable
Large Load Curtailable Rider	50	\$/month	Not applicable
Energy charges			
CBL on-peak	0.04723	\$/kWh	CBL on-peak kWh
CBL o -peak	0.04203	\$/kWh	CBL o -peak kWh
RTP hourly energy charge adjustment	Varies	\$/kWh	RTP kWh
Rider adjustment incremental charge	0.00764	\$/kWh	RTP kWh
Demand-side management opt-out	-0.00063	\$/kWh	Total kWh
Energy efficiency opt-out	-0.00701	\$/kWh	Total kWh
Demand charges			
CBL on-peak kW summer	21.31	\$/kW	CBL on-peak kW
CBL on-peak kW rest of year	16.87	\$/kW	CBL on-peak kW
CBL o -peak excess kW	1.14	\$/kW	CBL o -peak minus CBL on-peak kW
Facilities demand charge	3.8	\$/kW	Total peak kW minus CBL on-peak kW minus CBL o -peak kW
Large load curtailable rider credit	-5.4	\$/kW	Average demand during CBL on peak
Standby charge			
CHP standby charge	4.36	\$/kW	CHP nameplate capacity

Note : CBL: customer baseline load; RTP: real-time price

B.3 Pricing

The real-time price is shown in Figure Figure B.1.

Figure B.1 Real-time price for 2019

B.4 Renewable Energy Resource

The solar resource is shown in Figure Figure B.2.

Figure B.2 Northside wastewater treatment plant solar production factor for a representative year.

B.5 Model Performance

Model (R) is implemented in AMPL and solved in AMPL/CPLEX version 12.10.0.0 on a Dell Power Edge R410 server with two Intel Xeon E5520s at 2.27 GHz 28GB RAM, and 1TB HDD. We tuned the mode to achieve the best average performance across all cases and scenarios using the values found in Table B.6.

Table B.6 Solver Settings

Setting	Value
branch	1
probe	3
mipemphasis	4
mipstartalg	2

The complexities added such as the multi-objective optimization and the new energy tari result in long solve times. In some instances we are unable to obtain anything better than an 8% optimality gap after 24 hours. Therefore, we use an iterative approach to generate near optimal solutions (< 1% optimality gap). In the rst iteration we solve the Linear Programming relaxation as well as tailored sizing parameters to generate distributed energy resource (DER) and electrical battery energy storage system (BESS) sizes. We then use the resulting system sizes as inputs in the second iteration along with enforcing integrality on a subset of the binary variables. The solution from the second iteration is used as a warm start for the third iteration. Additionally, in the third iteration, we x the system size variables associated with both the DERs and electrical BESS and enforce all integrality. The fourth and nal iteration uses the solution from the third iteration as a warm start and un xes all variables. The purpose of this iteration is to provide the solver an opportunity to polish the solution as well as obtain an appropriate lower bound for optimality gap assessment. We specify a max solve time of 600 seconds and a MIP Gap stopping criteria of 1% (whichever comes rst) for all four iterations. We compute the total solve time as the sum of solve times from all four iterations which are found in Table B.7.

Table B.7 Average Solve Times in Seconds

Case	BAU	CHP Only	All Tech.	No Diesel
No Outage	1.7	30.3	810.1	1351.1
Outage	1.8	82.5	813.3	1472.3

APPENDIX C

CHAPTER 4

C.1 Disaster Cost Components

More than one dozen public and private sector data sources help capture the total, direct costs (both insured and uninsured) of the weather and climate events. These costs include physical damage to residential, commercial, and municipal buildings; material assets (content) within buildings; time element losses such as business interruption or loss of living quarters; damage to vehicles and boats; public assets including roads, bridges, levees; electrical infrastructure and offshore energy platforms; agricultural assets including crops, livestock, and commercial timber; and wildfire suppression costs, among others. However, these disaster costs do not take into account losses to natural capital or environmental degradation; mental or physical healthcare-related costs, the value of a statistical life; or supply chain, contingent business interruption costs. Therefore, our estimates should be considered conservative with respect to what is truly lost, but cannot be completely measured due to a lack of consistently available data [99].

C.2 Taxonomy Feeders

Table C.1 Summary of distribution feeders used to create electrical load profile. Data obtained from the Open Energy Data Initiative https://openenergydata.org/datasets/les/968/pub/individual_profiles/ and sourced from work by Schneider et al. [3].

Feeder	Community Description	Annual Electrical Demand (kWh)
R1-1247-2	Moderate suburban and light rural	4,905,544
R1-1247-3	Small urban center	2,589,839
R1-1247-4	Heavy suburban	14,586,540
R1-2500-1	Light rural	9,577,933
R2-1247-1	Light urban	34,316,316
R2-1247-2	Moderate suburban	24,148,877
R2-2500-1	Moderate urban	64,973,641
R3-1247-2	Moderate urban	31,760,229
R4-1247-2	Light suburban and moderate urban	11,047,930
R4-2500-1	Light rural	12,409,270
R5-1247-1	Heavy suburban and moderate urban	47,010,268
R5-1247-2	Moderate suburban and heavy urban	35,584,108
R5-1247-4	Moderate suburban and urban	33,908,450
R5-1247-5	Moderate suburban and light urban	31,886,294
R5-2500-1	Heavy suburban and moderate urban	63,259,096
R5-3500-1	Moderate suburban and light urban	43,247,521

C.3 Additional Solid Oxide Fuel Cell Costs

Assumptions

- ^ U.S. Energy Information Administration [141] estimates "owner costs" though the applicability of those to this context is unclear: "typically include development costs, preliminary feasibility and engineering studies, environmental studies and permitting, legal fees, project management (including third-party management), insurance costs, infrastructure interconnection costs (e.g., gas, electricity), and owner's contingency."
- ^ O&M costs from U.S. Energy Information Administration [141] are orders of magnitude different from Battelle Memorial Institute [142] as the former estimates are much more inclusive.
- ^ High capital cost case assumes high equipment costs and a high sales markup.
- ^ Costs over time are based on the assumption that production volumes increase, reducing the costs of production.
- ^ Equipment cost includes the cost of heat recovery equipment for combined heat and power and sales markup.
- ^ Costs assume a 5% discount rate, but given current economic conditions, a higher value may be more appropriate and would increase the low and medium case fixed O&M.
- ^ With all sources pooled together, there was agreement that production volume matters for costs, but not system size (except at very small system sizes, 1 kW and 5 kW, which we do not consider in the model).
- ^ The levelized cost of energy (LCOE) estimates only factor in the electricity delivered, not the heat energy, assuming a 5% discount rate, a 10-year system lifetime, a 5-year stack and inverter replacement, and a capacity factor of 93%.

Based on these assumptions, we estimate fuel cell costs and report them in Table C.2.

Table C.2 Projected costs of solid oxide fuel cells.

Scenario Production (units/yr)		2020 100-500	2030 500-1k	2040 1k-10k	2050 10k-50k
Capital cost (\$/kW)	High	17,245	7,221	5,068	4,967
	Medium	5425	4318	3007	2712
	Low	2384	1946	1902	1813
Equipment cost (\$/kW)	High	16,000	6,000	3,896	3,818
	Medium	4800	3818	2557	2312
	Low	1984	1546	1502	1413
CHP equipment cost (\$/kW)	High*	934	795	731	692
	Medium	471	462	453	444
	Low	167	162	157	148
Installation cost (\$/kW)	High	1,245	1,221	1,172	1,149
	Medium	625	500	450	400
	Low*	400	400	400	400
FOM (\$/kW/yr)	High	318	318	318	318
	Medium	217	156	147	133
	Low	167	138	129	116
VOM (\$/kWh)	High	0.092	0.090	0.088	0.086
	Medium	0.047	0.046	0.045	0.044
	Low	0.002	0.002	0.002	0.002
LCOE _{ij} (\$/kWh)	High	0.405	0.244	0.207	0.204
	Medium	0.160	0.134	0.111	0.103
	Low	0.060	0.050	0.048	0.045

Note: *Represents cost values for systems of projected size of 50kW or less. CHP: combined heat and power, FOM: Fixed operations and maintenance cost, VOM: Variable operations and maintenance cost

LCOE_{ij} is the levelized cost of energy for technology_j, at a life expectancy of t_j , where AEP is the annual electricity production, and is computed as:

$$\text{LCOE}_{ij} = \frac{\sum_{j=1}^{t_j} \frac{i(1+i)^{N_j}}{(1+i)^{N_j} - 1} + \text{FOM}}{\text{AEP}} + \text{VOM}$$

Figure C.1 shows the projected costs over time for each category: high, medium, and low. The purple circle shows the value we use for our modeling efforts.

Figure C.1 Levelized Cost of Energy for Solid Oxide Fuel Cells Projected levelized cost of energy for power-only solid oxide fuel cells. Projections extend to 2050 based on the values found in Table C.2.

APPENDIX D
COPYRIGHT AND PERMISSIONS

Included for adherence to copyright and authorship permissions are: email correspondences and journal copyright permissions for Chapter 3: North Carolina Water Utility Builds Resilience with Distributed Energy Resources published by the Informs Journal on Applied Analytics and journal permissions from Optimization in Engineering for Figure 2.2 depicting the REopt system from [9].



Marketplace



Marketplace Permissions General Terms and Conditions

-
-
-
-

Last updated October 2022

URTKP IGT"PCVWTG"NKEGPUG
VGTOU"CPF"EQPFKVKQPU

Lwp"34."4245

Vjku"Ci tgg o gpv"dgvy ggp"Lc o gu" I t{ o gu*\$ [qw\$+"cpf"Urtkpi gt" Pcvwtg"\$Urtkpi gt" Pcvwtg\$+
eqpukuvu"qh" { qwt"nkegpug" fgvccknu"cpf"vjg"vgt o u"cpf"eqpfkvkqpu"rtqxkfgf"d{ "Urtkpi gt" Pcvwtg
cpf"Eqr { tki j v"Engctcepeg"Egpgvt0

Nkegpug" Pw o dgt 7788923423625

Nkegpug"fcvg Lwp"34."4245

Nkegpugf"Eqpv gpv"Rwdnku jgt Urtkpi gt" Pcvwtg

Nkegpugf"Eqpv gpv"Rwdnkecvkqp Qrvk o k | cvkqp"cpf"Gp i kpggtkpi

Nkegpugf"Eqpv gpv"Vkvng Qrvk o k | kpi " fguk i p"cpf"fkurcvej"qh" c"tgp g y cdng"gpgt i {
u{ uv g o " ykv j"eq o dkpgf" jgc v"cpf" r q y gt

Nkegpugf"Eqpv gpv"Cwv j qt Lwuug" Jkt y c"gv"cn

Nkegpugf"Eqpv gpv"Fcvg Lcp";."4244

V{ rg"qh"Wug Vjgukul Fkuugtvcvkqp

Tgswguvqt"v{ rg cecfg o kelwpxgtukv{ "qt"tgugcte j "kpukvwvg

Hqt o cv gngvtqpk

Rqtvkqp hki wtgulvcdngulknwuvtcvkqpu

Pw o dgt"qh"hki wtgulvcdngulknwuvtcvkqpu 3

Yknn" {qw"dg"vtcpuncvkpi A pq

Ektewncvkqpl fkuvtkdwwkqp 3"/"4;

Cwvjqt"qh"vjku"Urtkpi gt" Pcvwtg eqpv gpv pq

Vkvng Qrvk o cñ" Fgukip" cpf" Fkurvej" qh" J { dtkf" Eq/ i gpgtcvkqp" Oketqi tkf" U { uvg o u" y kvj" Tguknkgpeg Eqpukfgtcvkqpu

Kpuvkvwvkqp" pc o g Eqnqtcfq" Uejqqñ" qh" Okpgu

Gzrgev g" rtgugpv cvkqp" fcvg Lwp"4245

Qtfgt" tghgtgpeg" pw o dgt 965765:

Rqtkvqpu Hkiwtg"4

Lc o gu" I t { o gu 4499" Dtkuvqn" Uv

Tgswguvqt" Nqecvkqp NQWKUXKNNG. "EQ" : 2249 Wpkvgf" Uvcvgu Cvp<" Lc o gu" I t { o gu

Vqvcn 2022" WUF

Vgt o u" cpf" Eqpfkvkqpu

Urtkpi gt" Pcvwtg" Ewuvq o gt" Ugtxkeg" Egpvtg" I o d J" Vgt o u" cpf" Eqpfkvkqpu

Vjg" hqmqy kpi "vgt o u" cpf" eqpfkvkqpu *\$Vgt o u" cpf" Eqpfkvkqpu\$+ "vq i gv jgt" y kvj" vjg" vgt o u urgekhhkgf" kp" { qwt"] Tki j vuNkpm_ " eqpukvwvg" vjg" Nkegpug" *\$Nkegpug\$+ "dgv y ggp" { qw" cu Nkegpugg" cpf" Urtkpi gt" Pcvwtg" Ewuvq o gt" Ugtxkeg" Egpvtg" I o d J" cu" Nkegpuqt0" D { "enkemkpi) ceegr v) cpf" eq o rnvkpi " vjg" vtcpucev kqp" hqt" { qwt" wug" qh" vjg" o cvgtkcñ" *\$Nkegpugf" O cvgtkcñ\$+. { qw" eqphkt o " { qwt" ceegrvcpeg" qh" cpf" qdñk i cvkqp" vq" dg" dqwpf" d { "vjgug" Vgt o u" cpf Eqpfkvkqpu0

30" I tcpv" cpf" Ueqrg" qh" Nkegpug

30"30"V j g"Nkegpuqt" i tcpvu { qw" c" rgtuqpcn. "pqp/gzenwukxg. "pqp/vtcpuhgtcdng. "pqp/ uwdnkegpcudng. "tgxqecndng. "y qtnf/ y kfg" Nkegpug" vq" tgr tqfweg. "fkuvtkdvwg. "eq o o wpkecvg" vq v j g" rwdnke. " o cmg" cxckncdng. "dtqc fecuv. "nggevtqpkcem { "vtcpu o kv" qt" etgcvg" fgtkxcvkxg y qtmu" wukpi " v j g" Nkegpug" Ocvgtkcn" hqt" v j g" rwt rqug* u+ "ur gekhkgf" kp" { qwt" Tki j vuNkpm Nkegpeg" Fgvcknu" qpn { 0" Nkegpugu" ctg" i tcpvgf" hqt" v j g" urgekhe" wug" tgs wguvgf" kp" v j g" qt fgt cpf" hqt" pq" v j g" t" wug. "uwdlgev" vq" v j g" Vgt o u" cpf" Eqpfkvkqpu0" [qw" cempqy ngf i g" cpf ci tgg" v j cv" v j g" tki j vu" i tcpvgf" vq" { qw" wpfgt" v j ku" Nkegpug" f q" pqv" kpenwfg" v j g" tki j v" vq o qfk { . " g fkh. " vtcpuncvg. " kpenwfg" kp" eqnngevkxg" y qtmu. " qt" etgcvg" fgtkxcvkxg" y qtmu" qh" v j g Nkegpug" Ocvgtkcn" kp" y j qng" qt" kp" rctv" wpnguu" gz r tguun { " uvcvgf" kp" { qwt" Tki j vuNkpm Nkegpeg" Fgvcknu0" [qw" o c { " wug" v j g" Nkegpug" Ocvgtkcn" qpn { " cu" rgt o kvvgf" wpfgt" v j ku C i tgg o gpv" cpf" y knn" pqv" tgr tqfweg. "fkuvtkdvwg. "fkurnc { . " r gthqt o . " qt" v j g" t y kug" wug" qt gz r nqkv" cp { " Nkegpug" Ocvgtkcn" kp" cp { " y c { . " kp" y j qng" qt" kp" rctv. " gzegev" cu" gz r tguun { rgt o kvvgf" d { " v j ku" Nkegpug0

30"40" [qw" o c { " qpn { " wug" v j g" Nkegpug" Eqpvgpv" kp" v j g" o cppgt" cpf" vq" v j g" gzvvgp" rgt o kvvgf d { " v j g" Vgt o u" cpf" Eqpfkvkqpu. " d { " { qwt" Tki j vuNkpm" Nkegpeg" Fgvcknu" cpf" d { " cp { cr r nkecdng" nc y u0

30"50" C" ugrctcvg" nkegpug" o c { " dg" tgs wktgf" hqt" cp { " c f fkvkqpcn" wug" qh" v j g" Nkegpug" Ocvgtkcn. " g0 i 0" y jgtg" c" nkegpug" jcu" dggp" rwte j cugf" hqt" rtkpv" wug" qpn { . " ugrctcvg rgt o kuukqp" o wuv" dg" qdvckpgf" hqt" gnggevtqpk" tg/ wug0" Uk o knctn { . " c" Nkegpug" ku" qpn { " xcnkf" kp v j g" ncp i wc i g" ugngevgf" cpf" f qgu" pqv" cr rn { " hqt" g fkvkqpu" kp" v j g" ncp i wc i gu" wpnguu c f fkvkqpcn" vtcpuncvkqp" tki j vu" j cxg" dggp" i tcpvgf" ugrctcvgn { " kp" v j g" Nkegpug0

30"60" Cp { " eqpvgpv" y kv j kp" v j g" Nkegpug" Ocvgtkcn" v j cv" ku" qy pgf" d { " v j kt" rctvku" ku gz r tguun { " gzenwfgf" htq o " v j g" Nkegpug0

30"70" Tki j vu" hqt" c f fkvkqpcn" tgwugu" uwe j " cu" ewuvq o " g fkvkqpu. " eq o r wvgtl o qdkng cr r nkecvkqpu. " hkn o " qt" VX" tgwugu" cp flqt" cp { " qv j g" t" fgtkxcvkxg" tki j vu" tgs wguvu" tgs wktg c f fkvkqpcn" rgt o kuukqp" cpf" o c { " dg" uwdlgev" vq" cp" c f fkvkqpcn" hgg0" Rngcug" cr rn { " vq [lqwtpcn rgt o kuukqpu B urtkp i gtpcvwtg0eq o](#) " qt" [dqqm rgt o kuukqpu B urtkp i gtpcvwtg0eq o](#) " hqt v j g" tki j vu0

40" Tgugtxcvkqp" qh" Tki j vu

Nkegpuqt" tguxtxgu" cmm" tki j vu" pqv" gz r tguun { " i tcpvgf" vq" { qw" wpfgt" v j ku" Nkegpug0" [qw cempqy ngf i g" cpf" ci tgg" v j cv" pqv j kp i " kp" v j ku" Nkegpug" nk o kvu" qt" tguvtkevu" Nkegpuqt" u" tki j vu" kp qt" wug" qh" v j g" Nkegpug" Ocvgtkcn" kp" cp { " y c { 0" P gkv j g" t" v j ku" Nkegpug. " pqt" cp { " cev. " q o kuukqp. " qt uvcvg o gpv" d { " Nkegpuqt" qt" { qw. " eqpxg { u" cp { " q y pgtu j kr" tki j v" vq" { qw" kp" cp { " Nkegpug" Ocvgtkcn. " qt" vq" cp { " gng o gpv" qt" rqtvkqp" v j g" t gq h0" Cu" dgy v ggp" Nkegpuqt" cpf" { qw. " Nkegpuqt qy pu" cpf" tgvckpu" cmm" tki j v. " vkvng. " cpf" kpvgtguv" kp" cpf" vq" v j g" Nkegpug" Ocvgtkcn" uwdlgev" vq" v j g nkegpug" i tcpvgf" kp" Ugevq" 3030" [qwt" rgt o kuukqp" vq" wug" v j g" Nkegpug" Ocvgtkcn" ku" gz r tguun { eqpfkvkqpgf" qp" { qw" pqv" k o rcktkp i " Nkegpuqt" u" qt" v j g" cr r nkecdng" eqr { tki j v" q y pgt" u" tki j vu" kp v j g" Nkegpug" Ocvgtkcn" kp" cp { " y c { 0

50" Tguvtkevqpu" qp" wug

50"30" Okpqt" g fkvkpi" rtkxkng i gu" ctg" cmmqy gf" hqt" c f crvcvkqpu" hqt" uv { nkuvke" rwt rqugu" qt hqt o cvkpi" rwt rqugu" r tqxkfgf" uwe j " cnvgtcvkqpu" f q" pqv" cnvgt" v j g" qtk i kpcn" o gcpkpi" qt kpvpgvkqp" qh" v j g" Nkegpug" Ocvgtkcn" cpf" v j g" pgy" hk i wtg* u+ " ctg" uvkmm" ceewtcvg" cpf tgr tguvgpvcvkxg" qh" v j g" Nkegpug" Ocvgtkcn0" Cp { " qv j g" t" e j cp i gu" kpenwfkpi" " dwv" pqv" nk o kvg f vq. " etq r r kpi. " c f crvkpi. " cpf lqt" q o kvkpi" o cvgtkcn" v j cv" chhgev" v j g" o gcpkpi. " kpvpgvkqp" qt o qtcn" tki j vu" qh" v j g" cwv j qt* u+ " ctg" uvtkev { " r tqj kdkvg f0

50"40" [qw" o wuv"pqv" wug"cp{ "Nkegpugf" Ocvgtkcn"cu" rctv"qh"cp{ "fgukip"qt"vtc fgo ctm0

50"50"Nkegpugf" Ocvgtkcn" o c{ "dg" wugf"kp" Qrgp" Ceeguu" Rwdnkecvkqpu" *QCR+. "dvw" cp{ "uwej
tgwug" o wuv" kpenwfg" c" engct" cempqyngfi o gpv"qh" vjku" rgt o kuukqp" xkukdng" cv" vjg" uc o g" vk o g
cu" vjg" hk i wtgulvcdngulkmwuwvtcvkqp" qt" cdvutcev" cpf" y jkej" o wuv" kp fkecvg" vjcv" vjg" Nkegpugf
Ocvgtkcn" ku" pqv" rctv" qh" vjg" i qxgtpki" "QC" nkegpug" dw" jcu" dggp" tgrtqfwegf" ykvj
rgt o kuukqp0" Vjku" o c{ "dg" kp fkecvg" ceeqtfkpi" vq" cp{ "uvcpfctf" tghgtgpeki" u{ uvg o "dvw
o wuv" kpenwfg" cv" c" o kpk o w o ") DqqmlLqwtpcn" vkvng. "Cwvjqt. "Lqwtpcn" Pc o g" *kh" cr rnkecdng+.
Xqno w o g" *kh" cr rnkecdng+. "Rwdnkujgt. [gct. "tgrtqfwegf" ykvj" rgt o kuukqp" htq o "UPEUE0

60"UVO "Rgt o kuukqp" I wkfgnkpgu

60"30" Cp" cnvgtpcvxg" ueqrg" qh" nkegpug" o c{ "cr rn{ "vq" uk i pcvqtkgu" qh" vjg" UVO "Rgt o kuukqpu
I wkfgnkpgu" *\$UVO" RI \$+ "cu" c o g p f g f" htq o "vk o g" vq" vk o g" cpf" o c f g" cxckncdng" cv
[jvvruxll y y y0uv o /cuuqe0qt i lkpvgngewcn/rtqrgtv{|rgt o kuukqpu|rgt o kuukqpu/ i wkfgnkpgu|0](#)

60"40" Hqt" eqpvpgv" tgwug" tgs wugu" vjcv" swcnkh{ "hqt" rgt o kuukqp" w p f g t" vjg" UVO "RI ." cp f
y jkej" o c{ "dg" wr fcvgf" htq o "vk o g" vq" vk o g. "vjg" UVO "RI " uwrgtugf" vjg" vgt o u" cp f
eqpfkvkqpu" eqpvckpgf" kp" vjku" Nkegpug0

60"50" Kh" c" Nkegpug" jcu" dggp" i tcpvgf" w p f g t" vjg" UVO "RI ." dwv" vjg" UVO "RI" pq" nqpi gt
cr rn{ "cv" vjg" vk o g" qh" rwdnkecvkqp. "hwtvjgt" rgt o kuukqp" o wuv" dg" uqw i jv" htq o "vjg
Tki jvu jqnfgt0" Eqpvcev" [lqwtpcn rgt o kuukqpu B urtkp i gtpcvwtg0eq o](#) "qt
[dqqm rgt o kuukqpu B urtkp i gtpcvwtg0eq o](#) "hqt" vjgug" tki jvu0

70" Fwtcvkqp" qh" Nkegpug

70"30" Wpnguu" qv jgt y kug" kp fkecvg f" qp" { qwt" Nkegpug. "c" Nkegpug" ku" xcnkf" htq o "vjg" fcvg" qh
r wte jcu g" *\$Nkegpug" Fcvg\$+ "wpvkn" vjg" gp f" qh" vjg" tngxcpv" rgtkq f" kp" vjg" dngy" vcdng<

Tgwug"kp" c" o g fkecn eq o o wpkecvkqpu" rtqlgev	Tgwug"wr" vq" fkuvtkdwkqp" qt" vk o g" rgtkq f" kp fkecvg f" kp Nkegpug
Tgwug"kp" c fkuugtvcvkqplv jguku	Nkhgvk o g" qh" vjguku
Tgwug"kp" c lqwtpcnl o c i c kpg	Nkhgvk o g" qh" lqwtpcnl o c i c kpg
Tgwug"kp" c" dqqmlvgzvdqqm	Nkhgvk o g" qh" g fkvkqp
Tgwug"qp" c" y gdukv g	3" { gct" wpnguu" qv jgt y kug" urgekhhg f" kp" vjg" Nkegpug
Tgwug"kp" c rtgugpvcvkqplunk f g mkvl rquvgt	Nkhgvk o g" qh" rtgugpvcvkqplunk f g" mkvl rquvgt0" Pqv g< rwdnkecvkqp" y jgvjgt" gngvtqpk" qt" kp" rtkpv" qh rtgugpvcvkqplunk f g" mkvl rquvgt" o c{ "tgs wktg" hwtvjgt rgt o kuukqp0
Tgwug"kp" eqphgtgpeg rtqeggfki u	Nkhgvk o g" qh" eqphgtgpeg" rtqeggfki u
Tgwug"kp" cp" cppwcn" tgr qtv	Nkhgvk o g" qh" cppwcn" tgr qtv
Tgwug"kp" vtckpki lE OG o cvgtkcnu	Tgwug"wr" vq" fkuvtkdwkqp" qt" vk o g" rgtkq f" kp fkecvg f" kp Nkegpug
Tgwug"kp" pgy u o g fkc	Nkhgvk o g" qh" pgy u o g fkc
Tgwug"kp eqwtug r cemplencuutqq o o cvgtkcnu	Tgwug"wr" vq" fkuvtkdwkqp" cp f lqt" vk o g" rgtkq f kp fkecvg f" kp" nkegpug

80"Cempqyngfigogpv

80"30"Vjg"Nkegpuqt"u"rgtokuukqp"owuv"dg"cempqyngfigfg"pgzv"vq"vjg"Nkegpugf"Ocvgtken
kp"rtkpv"kp"gngevtqpke"hqto."vjku"cempqyngfigogpv"owuv"dg"xkukdng"cv"vjg"ucog"vkog"cu
vjg"hkiwtgulvcdngulkmwuvctvkqpu"qt"cdvvtcev"cpf"owuv"dg"j"rgtnkpmgf"vq"vjg
lqwtpcndqqm)u"jqogrcig0

80"40"Cempqyngfigogpv"oc{"dg"rtqxfgf"ceeqtfkpi"vq"cp{"ucvpctf"tghgtgpekp
u{uvgo"cpf"cv"co"pkp"owo"ujqwnf"kpenwfg"\$Cwvjqt."CtvkenglDqqm"Vkvng."Lqwtpcn
pcogldqqm"kor"tkpv."xqnwog."rcig"pwodgt."{gct."Urtkpi"gt"Pcvwtg\$0

90"Twug"kp"cfkuugtvcvkqp"qt"vjguku

90"30"Yjgtg)tgwug"kp"cfkuugtvcvkqplvjguku"jcu"dggp"ugngevgf."vjg"hqnnqykipi"vgtou
cr rn{<"Rtkpv"tkijvu"qh"vjg"Xgtukqp"qh"Teqtf"ctg"rtqxfgf"hqto"gngevtqpke"tkijvu"hqto"wg
qpn{"qp"kpukvkvkqpcn"tgrqkvqt{"cu"fgkpgf"d{"vjg"Ujgt"rc"iwkfgnkpg
*[y y y0ujgt r c l c e 0 w m l t q o g q l](#)+ "cpf"qpn{"wr"vq"yjc"v"ku"tgswtg"fgf"d{"vjg"cyctfkpi
kpukvkvkqpl0

90"40"Hqt"vjgugu"rdnkujgf"wpfgt"cp"KUDP"qt"KUUP."ugrctcvg"rgtokuukqp"ku"tgswtgfg0
Rngcug"eqpvcev"[lqwtpcn rgtokuukqpu Burtkpi gtpcvwtg0eqo](#)"qt
[dqqm rgtokuukqpu Burtkpi gtpcvwtg0eqo](#)"hqto"vjgug"tkijvu0

90"50"Cwvjqtu"owuv"rtqrgtn{"ekvg"vjg"rdnkujgf"ocpwuetkrv"kp"vjgkt"vjguku"ceeqtfkpi"vq
ewttgpv"ekvcvkp"ucvpctfu"cpf"kpenwfg"vjg"hqnnqykipi"campqyngfigogpv<")*Reproduced
with permission from Springer Nature* 0

:0"Nkegpug"Hgg

[qw"owuv"rc{"vjg"hgg"ugv"hqtvj"kp"vjg"Nkegpug"Citggogpv"*vjg"\$Nkegpug"Hgg\$+0"Cmn
c"oqwpvu"rc{cdng"d{"{qw"wpfgt"vjku"Nkegpug"ctg"gzewukxg"qh"cp{"ucngu."wug."ykvjjqnfkpi.
xcnwg"cf"fgf"qt"uk"oknet"vczgu."ixgtpogpv"hgg"qt"ngxkgu"qt"qvjgt"cuuguogpvu0"Eqnngevkq
cpflqt"tg"okwvpeg"qh"uwej"vczgu"vq"vjg"tgngxcpv"vcz"cwvjqtkv{"ujcmm"dg"vjg"tgu"rppukdkkv{"qh
vjg"rctv{"yjq"jcu"vjg"ngicn"qdnkicvkqp"vq"fq"uq0

;0"Ycttcpv{"

;0"30"Vjg"Nkegpuqt"ycttcpvu"vjcv"kv"jcu."vq"vjg"dguv"qh"kvu"mpqyngfig."vjg"tkijvu"vq
nkegpug"tgwug"qh"vjg"Nkegpugf"Ocvgtken0 [qw"ctg"uqngn{"tgu"rppukdng"hqto"gpuwtkpi"vjcv
vjg"ocvgtken{"qw"yukj"vq"nkegpug"ku"qtkikpcn"vq"vjg"Nkegpuqt"cpf"fgu"pqv"ectt{"vjg
eqr{"tkijv"qh"cpqvjgt"gpkv{"qt"vjktf"rctv{"*cu"etgfkvgf"kp"vjg"rdnkujgf"xgtukqp+0
Kh"vjg"etgfkv"nkp"qp"cp{"rctv"qh"vjg"Nkegpugf"Ocvgtken"kp"fkcevgu"vjcv"kv"ycu"tgrtkpv"fgf"qt
cfcvrgf"ykvj"rgtokuukqp"htqo"cpqvjgt"uqwtg."vjgp"{"qw"ujqwnf"uggm"cf"fkvqpcn
rgtokuukqp"htqo"vjcv"uqwtg"vq"tgwug"vjg"ocvgtken0

;0"40"GZEGRV"HQT"VJG"GZRTGUU"YCTTCPV["UVCVGF"JGTGKP"CPF"VQ"VJG
GZVGPV"RGTO"KVVG"FD["CRRNKECDNG"NCY."NKEGPUQT"RTQXKFGU"VJG
NKEGPUGF"OCVGTKEN"\$CU"KU"\$CPF"OCMGU"PO"QVJGT"TGRTGUGPVCVKQP
QT"YCTTCPV[0"NKEGPUQT"GZRTGUUN["FKUENCKOU"CP["NKCDKNKV["HQT
CP["ENCKO"CTKUKPI"HTQO"QT"QWV"QH"VJG"EQPVGPPV."KPENWFKPI"DWV
PQV"NKOKVGF"VQ"CP["GTTQTU."KPCEEWTCEKGU."QOKUUKQPU."QT"FGHGEVU
EQPVCKPGF"VJGTGKP."CPF"CP["KORNKGF"QT"GZRTGUU"YCTTCPV["CU"VQ
OGTEJCPVCDKNKV["QT"HKVP"GUU"HTQ"CRCTVKEWNCT"RWTRQUG0"KP"PO
GXGPV"UJCNN"NKEGPUQT"DG"NKCDNG"VQ["QW"QT"CP["QVJGT"RCTV["QT

CP ["QV J GT"RGTUQP"QT"HQT"CP ["URGEKCN."EQPUGSWGPKCN.
 KPEKFGPVKN."KPFKTEV."RWPVKXG."QT"GZGORNCT ["FCOC I GU.
 J Q Y GXGT"ECWUGF."CTKUKP I "QWV"QH"QT"KP"EQP PGEVKQP"YKV J "V J G
 FQ Y PNQCFKP I ."XKGYKP I "QT"WUG"QH"V J G"NKEGPUGF"OCVGTKCN
 TGI CTFNUGU"QH"V J G"HQTO"QH"CEVKQP." Y J GV J GT"HQT"DTGCE J "QH
 EQPVTCEV."DTGCE J "QH" YCTTCPV [."VQTV."PG I NK I GPEG.
 KPHTKP I GOGPV"QT"QV J GTYKUG"*KPENWFKP I ." YKV J QWV"NKOKVCVKQP.
 FCOC I GU"DCUGF"QP"NQUU"QH"RTQHKVU."FCVC."HKNGU."WUG."DWUKPGUU
 QRRQTVWPKV ["QT"ENCKOU"QH"V J KTF"RCTVKGU+."CPF" Y J GV J GT"QT" PQV
 V J G"RCTV [" J CU" DGGP"CFXKUGF"QH"V J G"RQUUKDKNKV ["QH"UWE J
 FCOC I GU"V J KU"NKOKVCVKQP"CRRNKGU" PQV YKV J UVCPFKP I "CP ["HCKNWTG
 QH"GUUGPVKCN"RWTRQUG"QH"CP ["NKOKVGF" TGOGF ["RTQXKFGF" J GTGKP0

320"Vgt o kpcvkqp"cpf"Ecpegnmckqp

320"30"Vjg"Nkegpug"cpf"cmn"tki jvu" i tcpvgf" jgtgwpfgt" yknn"eqpvkpwg"wpvkn"vjg"gpf"qh"vjg
 cr rnkcedng"rgtkqf"ujqyp"kp"Encwug"703"cdqyg0"Vjgtgchvgt."vjku"nkegpug"yknn"dg
 vgt o kpcvgf"cpf"cmn"tki jvu" i tcpvgf" jgtgwpfgt" yknn"egcug0

320"40"Nkegput"tgugt xgu"vjg"tki jv"vq"vgt o kpcvg"vjg"Nkegpug"kp"vjg"gxgpv"vjcv"rc { o gpv"ku
 pqv"tgegkxgf"kp"hwmm"qt"kh" { qw"dtgcej"vjg"vgt o u"qh"vjku"Nkegpug0

330" Ipgtca

330"30"Vjg"Nkegpug"cpf"vjg"tki jvu"cpf"qdnki cvkqpu"qh"vjg"rctvkgu" jgtgvq"ujcmn"dg
 eqpvtwgf."kpvgt rrtvgf"cpf"fgvgt o kpgf"kp"ceeqt fcepeg" ykvj"vjg"ncyu"qh"vjg"Hgfgtgn
 Tgrwdnke"qh" I gt o cp { " ykvj qwv"tghgtgpeg"vq"vjg"uvkrwncvkqpu"qh"vjg"EKU I "*Wpkvgf
 Pcvkqpu"Eqpxgpvkqp"qp"Eqpvtcevu"hqt"vjg"Kpvgtpcvkqpcn"Ucng"qh" I qqfu+"qt"vq" I gt o cp { "u
 ejqkeg/qh/ncy"rtkpek rng0

330"40"Vjg"rctvkgu"cempqy ngfi g"cpf"ci tgg"vjcv"cp { "eqpvtqxgtukgu"cpf"fkurwvgu"ctkupi
 qw"qh"vjku"Nkegpug"ujcmn"dg"fgkfgf"gzennwukxgn" { d { "vjg"eqwtvu"qh"qt"jcxkpi"lwtkufkevqpp
 hqt" J gkfgndgti." I gt o cp { ."cu"het"cu"ngi cmn { " rgt o kuukdng0

330"50"Vjku"Nkegpug"ku"uqngn { "hqt"Nkegput"u"cpf"Nkegpug"u" dgpghkv0"Kv"ku"pqv"hqt"vjg
 dgpghkv"qh"cp { "qvjgt" rgtuqp"qt"gpvk { 0

SwgukqpuA"Hqt"swgukqpu"qp"Eqr { tki jv"Engctcepeg"Egpgvt"ceeqwpvu"qt" y gdukvg"kuuwgu
 rngcug"eqpvcev"[urtkpi gtpcvwtguwr rqtv](#)**Beqr { tki jv**[leq o](#)"qt" - 3/ : 77/45 ; /5637"*vqnn"htgg"kp
 vjg"WU+"qt" - 3/ ; 9 : /868/49990"Hqt"swgukqpu"qp"Urtkpi gt" Pcvwtg"nkegpukpi" rngcug"xkukv
[jwruclly y y0urtkpi gtpcvwtg0leq o | i r | rctvpgtulki jvu/rgt o kuukqpu/vjktf/rctv { /fkvutkdwwkqp](#)

Qvjgt"Eqpfkvpkqp<

Xgtukqp"306"/"Fge"4244

SwgukqpuA"[ewuvq o gtectg](#)**Beqr { tki jv**[leq o](#)0

